Universität Ulm
Abteilung Angewandte Physiologie
Abteilungsleiter: Professor Lehmann-Horn

ON THE FUNCTIONAL CONSEQUENCES OF EPILEPSY-CAUSING MUTATIONS LOCATED IN ION CHANNELS

AND

THE ROLE OF CYTOPLASMIC PROTEIN REGIONS IN FAST AND SLOW INACTIVATION OF VOLTAGE-GATED SODIUM CHANNELS

Dissertation zur Erlangung des Doktorgrades der Humanbiologie der Medizinischen Fakultät der Universität Ulm

vorgelegt von:
Alexi Kirilov Alekov
Dobrich, Bulgarien

2002

Amtierender Dekan:	Prof. Dr. R. Marre
1. Berichterstatter:	PD Dr. H. Lerche
2. Berichterstatter:	Prof. Dr. O. Marti
Tag der Promotion:	22.11.2002

TABLE OF CONTENTS

1. INTRODUCTION 1
1.1. Voltage-gated cation channels 1
1.1.1. Voltage-gated sodium channels 4
1.1.1.1. Inactivation of the voltage-gated sodium channels 6
1.1.1.1.1. Fast inactivation 6
1.1.1.1.2. Slow inactivation 7
1.1.1.2. D4/S4-S5 loop 7
1.1.1.3. D4/S6 segment 8
1.1.2. *KCNQ2* and *KCNQ3* potassium channels 10
1.2. Epilepsy 11
1.2.1. Generalized Epilepsy with febrile seizures plus (*GEFS+)* 12
1.2.2. Benign familial neonatal convulsions (*BFNC)* 13
1.3. Aims 16

2. MATERIALS AND METHODS 17
2.1. Molecular and cell biology methods 17
2.1.1. Mutagenesis 17
2.1.2. Molecular biological methods 19
2.1.3. Cell biology methods 21
2.1.3.1. Cell culture and transfection of tsA201 cells 21
2.1.3.2. Oocyte preparation and injection 23
2.2. Electrophysiology 25
2.2.1. Reagents and solutions 25
2.2.2. General procedures 27
2.2.3. Two-electrode voltage-clamp on Xenopus Laevis oocytes 31
2.2.4. Whole cell and inside-out recordings from cells and oocytes 32
2.2.5. Voltage-clamp protocols and data analysis 35
2.2.5.1. Voltage-clamp protocols used to characterize *KCNQ2* potassium channels 35
2.2.5.2. Voltage-clamp protocols used to characterize sodium channels 36
2.2.5.3. Double mutant cycle analysis 40
2.2.5.4. Statistics 41

3. FUNCTIONAL CHARACTERIZATION OF A *BFNC* CAUSING MUTATION IN THE *KCNQ2* GENE 42
3.2. Activation and deactivation 43
3.3. Evaluation of the Role of the C-terminal part of the *KCNQ2* channel 44

4. FUNCTIONAL CHARACTERIZATION OF TWO MUTATIONS IN THE *SCN1A* GENE CAUSING *GEFS+* 45
4.1. Fast inactivation 45
4.2. Activation and deactivation 48
4.3. Slow inactivation 48
4.4. Effects of pH on R1460H mutation 50

5. ROLE OF D4/S4-S5 LOOP IN SODIUM CHANNEL FAST AND SLOW INACTIVATION 52
5.1. Assessment of a direct interaction of D4/S4-S5 with the inactivation particle 52
5.1.1. Activation and fast inactivation 52
5.1.2. Double mutant cycle analysis 54
5.2. Evaluation of the role of the D4/S4-S5 in slow inactivation 56
5.2.1. Activation and fast inactivation 56
5.2.2. Slow inactivation 58
5.2.2.1. Cumulative vs. conventional Protocols 58
5.2.2.2. Slow inactivation parameters 60

6. ROLE OF SEGMENT D4/S6 IN SODIUM CHANNEL INACTIVATION 62
6.1. Effect of the cysteine mutations and their modification by MTS-reagents 62
6.2. Effects of the size, charge and hydrophobicity of the introduced mutations and applied reagents.....65
6.2.1. Effects on fast inactivation 66
6.2.1.1. Persistent current I_{ss} 66
6.2.1.2. Voltage dependence of fast inactivation 69
6.2.1.3. Kinetic changes in fast inactivation 69
6.2.2. Activation and deactivation 70
6.2.3. Slow inactivation 71
6.3. Voltage dependence of the accessibility of positions F1586 and I1596 for modification by MTS reagents 73

7. DISCUSSION 75
7.1. Functional consequences of the epilepsy-causing *KCNQ2* mutation 75
7.2. Functional consequences of the mutations causing *GEFS+* 77
7.3. D4/S4-S5 80
7.3.1. D4/S4-S5 as a possible receptor site for the inactivation ball 80
7.3.2. Role of the D4/S4-S5 segment in slow sodium channel inactivation 81
7.4. Role of segment D4/S6 in the gating of sodium channels 82
7.4.1. D4/S6 and fast inactivation 82
7.4.2. D4/S6 and slow inactivation 83
7.4.3. Accessibility of the C-terminal part of D4/S6 84

8. SUMMARY 88
9. LITERATURE 90

INDEX OF FIGURES

Figure

1. Secondary structure of voltage-gated cation channels 2
2. Gating transitions in voltage-gated cation channels 3
3. Proposed phylogenetic tree for mammalian voltage-gated sodium channel subunits. 5
4. Amino acid sequence comparison of the D2/S4 and D4/S4 segment of various sodium channel α-subunits 13
5. Clinical and genetic data of the *BFNC* family 14
6. The *Xenopus Laevis* oocytes expression system 24
7. Scheme of a common electrophysiological setup 27
8. One electrode continuous voltage clamp method (whole cell patch clamp) 30
9. Conventional Two-Electrode Voltage Clamp 31
10. Patch configurations, represented schematically 33
11. Current density for expressed WT and mutant *KCNQ2* channels. 42
12. Activation parameters for expressed WT and mutant *KCNQ2* channels. 43
13. Representative whole cell sodium current families for WT and mutation causing *GEFS+* 46
14. Fast inactivation of for WT and mutation causing *GEFS+* 47
15. Activation parameters for WT and mutation causing *GEFS+* 49
16. Voltage dependence of the deactivation time constant for WT and mutation causing *GEFS+* 50
17. Parameters of slow inactivation for WT and mutation causing *GEFS+* 51
18. Normalized representative current traces for mutations in D4/S4-S5 53
19. Fast inactivation of mutations in D4/S4-S5 54
20. Double mutant cycles showing possible interactions between mutations in the D4/S4-S5 loop and the proposed inactivation ball. 56
21. Activation and fast inactivation of L1482C/A mutations 57
22. Cumulative vs. Conventional protocols for mesuring slow inactivation 59
23. Slow inactivation parameters for mutations in D4/S4-S5. 60
24. Representative raw current traces of WT and different cysteine mutations in IV/S6 63
25. Activation and fast inactivation parameters of IV/S6 mutations 64
26. Reaction of the double mutant FI/CC with different thiol reagents tested in inside-out patches 65
27. Representative raw current traces of WT and various other combinations of double mutations in positions F1586 and I1596 66
28. Persistent Na^+ current relative to the peak current for all mutations in D4/S6 68
29. Summarized activation and fast inactivation parameters for mutations in D4/S6 69
30. Voltage dependence of the deactivation time constant for mutations in D4/S6 70
31. Parameters of slow inactivation for mutations in D4/S6 72
32. Voltage dependence of the reaction of the double mutant FI/CC with MTSES which was added to the pipette solution. 74

INDEX OF TABLES

Table

1. Mutagenesis methods for the investigated sodium channel mutations 18

2. Fit parameters of steady-state fast inactivation for mutations in D4/S4-S5.....53

3. Fit parameters of fast inactivation and calculated rate constants for mutations in D4/S4-S5 55

LIST OF ABBREVIATIONS

3-D	Three dimensional
BFNC	Benign familial neonatal convulsions
cDNA	Complementary deoxyribonucleic acid
cRNA	Complementary ribonucleic acid
D1 – D4	1-4 Transmembrane domains in voltage-gated sodium or calcium channel α-subunit
DEPC	Diethyl-pyrocarbonate
DMSO	Dimethylsulfoxid
DNA	Desoxyribonucleic acid
EDTA	Ethylenediamine tetra-acetic acid
EGTA	Ethylenediamine tetra-acetic acid
EEG	Electro-encephalogram
FI	Fast inactivation
G	Conductance
GEFS+	Generalized epilepsy with febrile seizures plus
G_{max}	Maximal conductance
HEBS	HEPES buffered saline
HEPES	N-2-Hydroxyethylpiperazine-N'-2-ethanesulfonic acid
HyperPP	Hyperkalemic periodic paralysis
HypoPP	Hypokalemic periodic paralysis
I	Current amplitude

I_{max}	Maximal current amplitude
k	Slope factor of the Boltzmann function
KCNQ1-5	Human voltage-gated potassium channel KQT-like type 1-5 gene
KcsA	Bacterial potassium channel from *Streptomyces Lividans*
K_vLQT1	*KCNQ1* (see above)
LQT-syndrome	Syndrome associated with a prolonged cardiac QT-interval
M1(M2)	Transmembrane segment 1(2) in the KcsA potassium channel
MC	Myotonia congenita
MEM	Modified Eagle´s Medium
minK	Minimal potassium channel
MS222	3-Aminobenzoic acid ethyl ester methanesulfonate salt
MTSEA	2-Aminoethyl methanethiosulfonate, hydrobromide
MTSES	Sodium (2-sulfonatoethyl)methanethiosulfonate
MTSET	[2-(Trimethylammonium)ethyl] methanethiosulfonate bromide
MTS-reagents	Methanethiosulfonate reagents
$Na_v1.1$-1.9, Na_x	Voltage-gated sodium channel α-subunit isoforms
P	probability
PAM	Potassium-aggravated myotonia
PBS	Phosphate buffered saline
PC	Paramyotonia congenita
PCR	Polymerase chain reaction

RNA	Ribonucleic acid
S1 – S6	Transmembrane segments inside each domain in voltage-gated sodium (calcium or potassium) channel α-subunit
SCN1A-11A	Voltage-gated sodium channel α-subunit genes: 1-11
SI	Slow inactivation
TEA	Tetraethylammonium
U	Unit
V	Voltage
$V_{1/2}$	Half-maximal voltage of activation / inactivation
V_{rev}	Reversal potential
WT	Wild type

1. INTRODUCTION

Ion channels are membrane-spanning proteins that form hydrophilic pores with a specific selectivity to particular ions. They provide the basis for excitability in nerve and muscle cells. In neurons, they permit the generation, transmission and procession of signals. In heart and skeletal muscle, they regulate excitability and transform the action potential in mechanical contraction. In addition, ion channels are involved in a broad range of cell regulatory processes – e.g. secretion and volume regulation. A great number of ion channel genes have been identified and cloned during the last two decades and several hereditary diseases have been linked to mutations in genes encoding ion channels (Lehmann-Horn and Jurkat-Rott, 1999). Molecular electrophysiological investigation of these so-called channelopathies elucidate the pathophysiology of these rare diseases and help to understand disease-causing mechanisms in other, more common disorders with similar symptoms. Furthermore, insight into the molecular basis of these disorders allows a more rational approach to therapy. On the other hand, disease-causing mutations point to functional important parts of the protein and help to understand ion channel gating on a molecular level.

1.1. VOLTAGE-GATED CATION CHANNELS

The gating of most ion channels is regulated by different specific mechanisms, which change their permeation properties: membrane potential – voltage-gated ion channels, specific chemical signals such as Ca^{2+} or synaptic transmitters – ligand-gated ion channels, changes in the membrane conformation - mechanosensitive or volumesensitive ion channels etc. Voltage-gated cation channels are responsible for the generation and propagation of action potentials. They are built of several subunits - a main, pore-forming α-subunit and one or more smaller

subunits with modifying properties, called β, γ, or δ. The α-subunits have a common tetrameric structure with four domains (D1-D4) of six transmembrane segments each (S1-S6) with a specialized pore region (fig. 1). Whereas potassium channels form tetramers of four identical domains, the main molecule of the Na^+ and Ca^{2+} channels is one large subunit. The pore of the voltage-gated cation channels is formed by the loops, connecting segments S5 and S6 and the sixths transmembrane segments of the four domains. The S4 segments contain four to eight positively charged residues conferring voltage dependence to the channel protein (for a review see Bezanilla, 2000; Catterall, 2000).

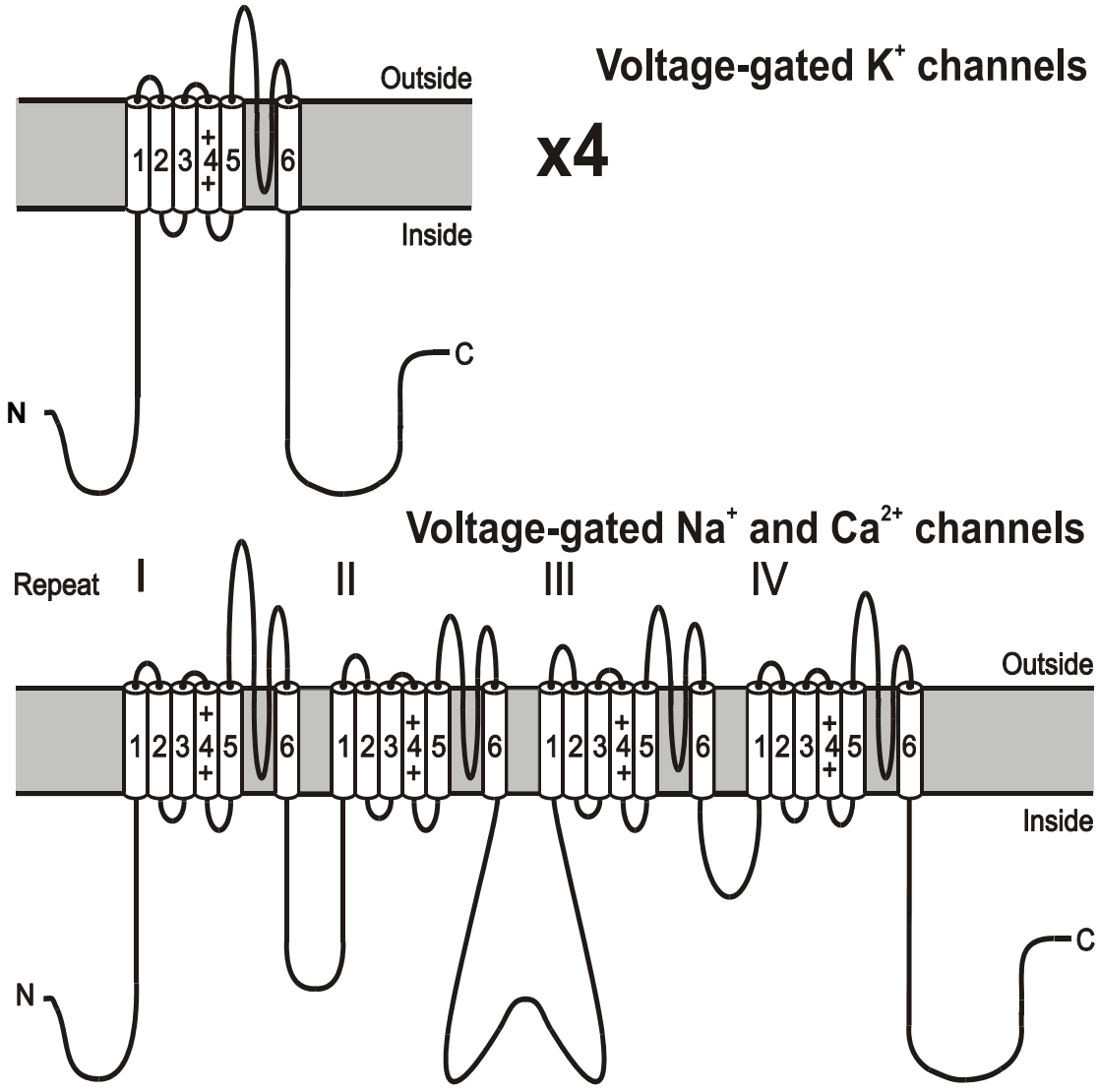

Figure 1. Secondary structure of voltage-gated cation channels.

At the resting membrane potential (-60 to –90 mV) the channels usually reside in the closed state and are not permeable for ions (fig. 2). Upon depolarization they open their gate and can conduct ions – a process called activation. This is triggered by the movement of the voltage sensors. Some of the channels, after opening of the activation gate, can close another existing gate upon ongoing depolarization – a process called inactivation. The inactivated channels need some time at hyperpolarized potentials before they can be activated again. During this refractory period the channels recover from the inactivated state. Voltage-gated ion channels can have more inactivated states which are kinetically distinct. Upon hyperpolarization the opened activation gate closes in a process called deactivation. In general, voltage-gated ion channels are characterized by at least one open (O) and one closed (C) state and may have one or more inactivated (I) states (fig. 2A).

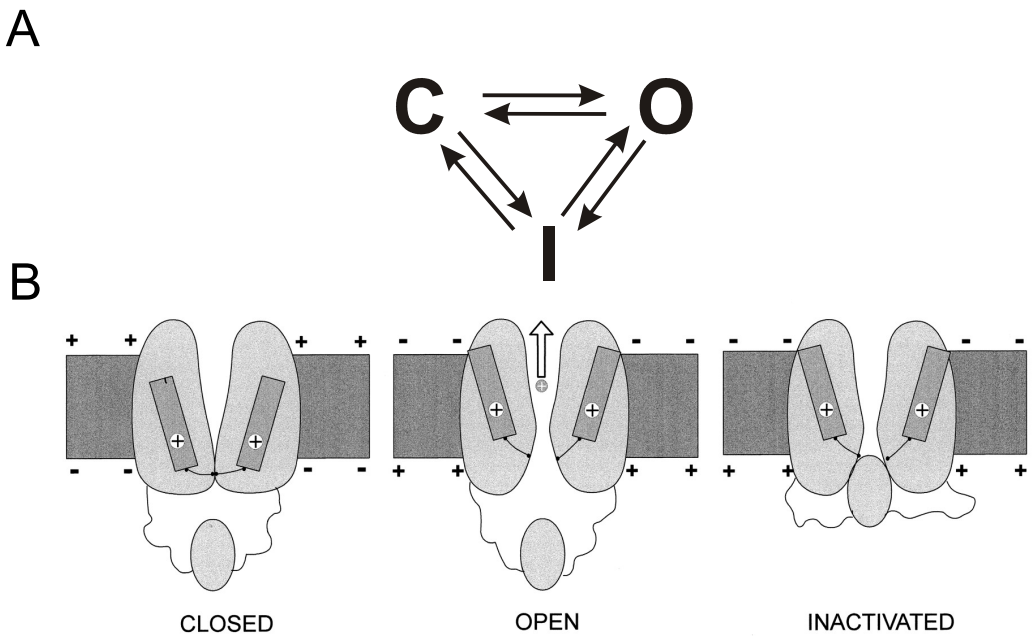

Figure 2. Gating transitions in voltage-gated cation channels. **(A)** Schematic representation of the main conformational states of voltage-gated channels and the transitions between them. **(B)** Mechanistic view of channel gating (Bezanilla , 2000).

1.1.1. Voltage-gated sodium channels

Voltage-gated sodium channels are the primary molecules responsible for the rising phase and the first repolarizing part of action potentials in electrically excitable cells. They consist of one pore forming *α*-subunit that is associated with accessory β-subunits in some tissues (brain and muscle)(Catterall *et al.*, 1994; Isom *et al.*, 1994 and 2001; Goldin, 2001). The sodium channel α-subunit is a large transmembrane protein (ca. 260 kDa) (see fig.1). There are several genes encoding different α-subunits (*SCN1A-11A*) that are expressed specifically in different tissues, e.g.: skeletal muscle (*SCN4A*), heart muscle (*SCN5A*) and brain (*SCN1A, SCN2A, SCN3A, SCN8A*). The proteins encoded by these genes have been named in many different ways, depending on expression pattern, origin, function etc. Recently, a systematic nomenclature for sodium channels has been proposed (fig. 3) (Goldin *et al.*, 2000).

In 1990, Fontaine *et al.* cloned portions of the adult human muscle sodium channel α-subunit gene and localized it to chromosome 17. The amino acid sequence of the human skeletal muscle sodium channel gene *SCN4A* has been identified in 1992 by Wang *et al.* The protein consists of 1836 amino acid residues. Until now more than 20 mutations in the $hNa_v1.4$ sodium channel have been related to four different muscle diseases: hyper –and -hypokalemic periodic paralysis (hyperPP, hypoPP), potassium aggravated myotonia (PAM) and paramyotonia congenita (PC). In 1993, Rüdel *et al.* suggested the term sodium channel disease to encompass the different allelic syndromes caused by *SCN4A* mutations.

By fluorescence in situ hybridization, Malo *et al.* (1994) mapped the *SCN1A* gene to chromosome 2q24 and only recently Escayg *et al.* (2000) could determine the coding sequence of the human *SCN1A* gene. Until now, 13 mutations segregating

with two different forms of epilepsy have been identified in the human $hNA_v1.1$ (Lerche *et al.*, 2001).

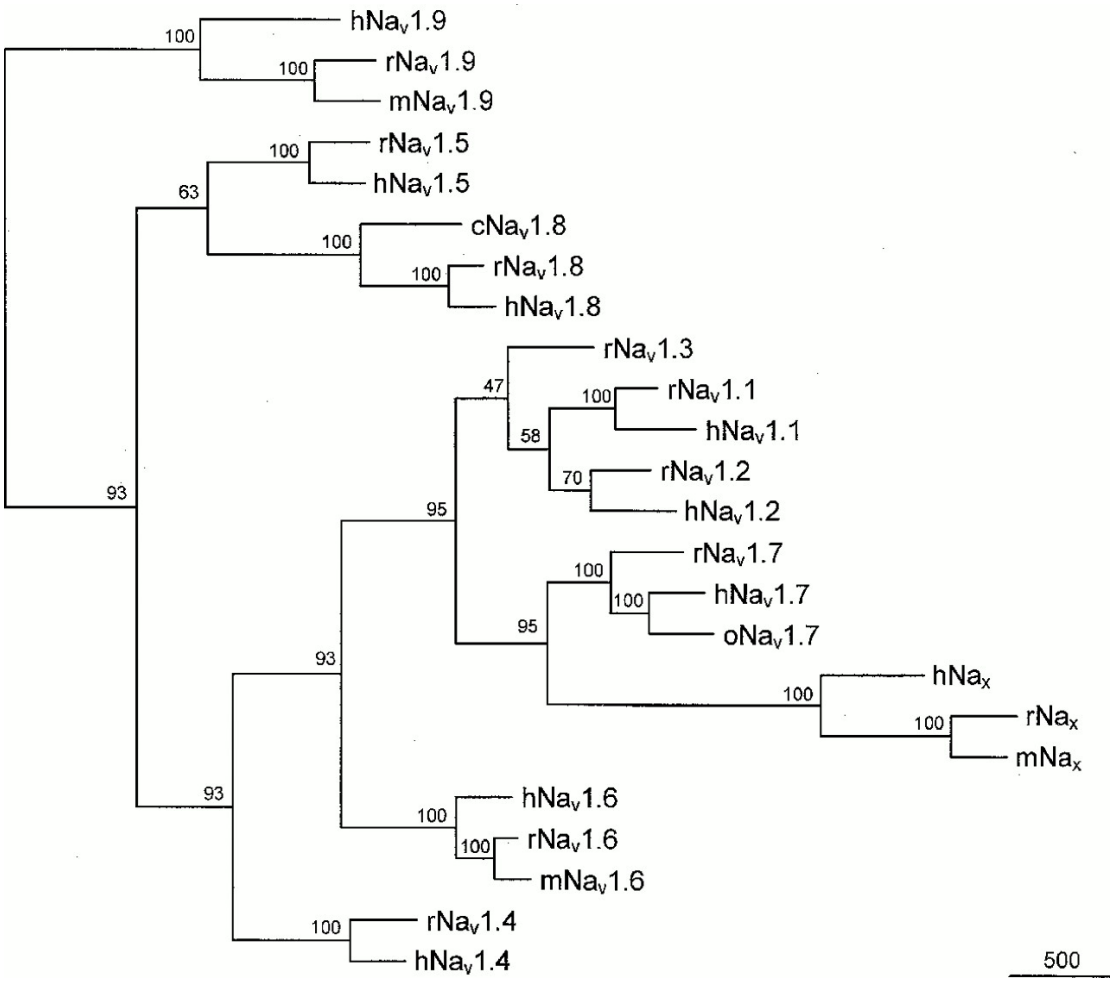

Figure 3. Proposed phylogenetic tree for mammalian voltage-gated sodium channel subunits. Sequences. The numbers at the nodes indicate the bootstrap values for 100 replications. The scale bar represents 500 substitutions. The species of origin is indicated as follows: h = Homo sapiens (human), r = *Rattus norvegicus* (rat), m = *Mus musculus* (mouse), c = *Canis familiaris* (dog), o = *Oryctolagus cuniculus* (rabbit) (Goldin et al., 2001).

1.1.1.1. Inactivation of the voltage-gated sodium channels

1.1.1.1.1. Fast inactivation

Voltage-gated sodium channels have several inactivated states, which are kinetically distinct. Fast inactivation (FI) occurs during the first milliseconds after membrane depolarization. Fast inactivation is believed to function in a so-called "hinged-lid" manner: a hydrophobic particle is occluding the pore from the intracellular side of the membrane (see fig. 2B). Armstrong and Bezanilla first proposed the ball and chain hypothesis in 1977. Later studies identified the intracellular linker between D3 and D4 as the inactivation domain: antibodies directed against the D3-D4 linker completely abolish fast inactivation (Vassilev *et al.*, 1998 and 1999), inactivation is absent in channels in which this linker is deleted (Stühmer *et al.*, 1989), and deletions or mutations in the D3-D4 linker slow or destroy inactivation (Patton *et al.*, 1992). A hydrophobic cluster of three amino acids, IFM (residues 1310-1312 in $hNa_v1.4$) (Kellenberger *et al.*, 1997a and 1997b), has been identified as a motif critical for inactivation. Substitution of these three residues with glutamine completely abolishes inactivation (West *et al.*, 1992), and inactivation can be restored by the addition of short peptides containing the IFM motif (Eaholtz *et al.*, 1994, 1998 and 1999). The hinged-lid model implies a particular binding site for the inactivation particle, but this proposed binding site still has not been identified. Mutations in several regions of the sodium channel molecule such as the S4-S5 loops in D3 and D4 and the transmembrane segment S6 in D4 exhibit prominent effects on fast inactivation gating (see below) and could contribute to a receptor site for the inactivation ball within the intracellular mouth of the channel protein.

The voltage sensitivity of fast inactivation is changed by mutations in the voltage sensors in all four domains (Kontis and Goldin, 1997), although voltage sensors in

D3 and D4 seem to be more important (Chen *et al.*, 1996; Yang *et al.*, 1997; Sheets *et al.*, 1999; Kuhn and Greeff, 1999; Cha *et al.*, 1999).

1.1.1.1.2. Slow inactivation

The slow inactivation process of voltage-gated sodium channels acts on a time scale of hundreds of milliseconds to seconds. Slow inactivation (SI) is voltage dependent and mutations in all four voltage sensors can affect its gating (Kontis and Goldin, 1997). Several regions like the pore (Balser *et al.*, 1996), the voltage sensors (Mitrovic *et al.*, 2000; Struyk *et al.*, 2000), S4-S5 loops (Cummins *et al.*, 1996; Hayward *et al.*, 1997), S5 (Bendahhou *et al.*, 1999) and S6 (Hayward *et al.*, 1997) segments are important for regular function of slow inactivation. This diversity makes speculations about the possible molecular mechanism of slow inactivation very difficult. One valuable hypothesis is that slow inactivation is mediated by a tight closure of the outer mouth of the pore. Benitah *et al.* (1999) have identified slow inactivation-associated movements near the outer part of the selectivity filter, and have identified a residue in the pore region, W402, which appears to be involved in the early steps of slow inactivation. This hypothesis is supported by the fact, that external Na^+ ions, but not internal Na^+ ions, inhibit the development of slow inactivation (Townsend and Horn, 1997). In addition C-type inactivation of *Shaker* K^+ channels, in many ways analogous to slow inactivation of Na^+ channels, involves a constriction of the outer mouth of the pore (Liu *et al.*, 1996; Loots and Isacoff, 1998).

1.1.1.2. D4/S4-S5 loop

The particular role of the D4/S4-S5 loop for the inactivation gating of voltage-gated Na^+ channels has been investigated extensively but is still not clarified. In structurally homologous K^+ channels, the ball and chain model for fast inactivation

has been verified conclusively. The ball is probably formed by 20 amino acids at the N-terminal cytoplasmic end of the channel protein (Hoshi *et al.,* 1990). Several studies showed possible participation of the S4-S5 loop of the K^+ channel in the binding of the inactivation ball (Isakoff *et al.,* 1991, Holmgren *et al.,* 1996) and recent study explicitly demonstrated such binding (Zhou *et al.*, 2001a). A similar role can be proposed for the S4-S5 loops in the voltage-gated sodium channel. Outward movement of D4/S4 could initiate a conformational change of D4/S4-S5 and other regions leading to the formation of a receptor site for the inactivation particle thereby coupling fast inactivation to activation (Mitrovic *et al.*, 1996; Lerche *et al.*, 1997; Filatov *et al.*, 1998; Tang *et al.*, 1998; McPhee *et al.*, 1998). Additionally, an interdependent action with regard to fast inactivation has been shown for mutations in the D3/S4-S5 loop and the proposed inactivation ball (Smith and Goldin, 1997).

1.1.1.3. D4/S6 segment

Recently, two crystallographic studies provided intrinsic information about the pore organization of the bacterial *KcsA* potassium channel (Doyle *et al.*, 1998; Zhou *et al.*, 2001b). Phylogenic and structural studies provide evidences for similarities between *KcsA* and the family of the voltage-gated cation channels. (MacKinnon, 1998; Minor *et al.*, 1999). Lipkind and Fozzard (2000) used comparative molecular modeling to propose a structure of the Na^+ channel pore, based on the data from the *KcsA* channel, which is in good agreement with previous electrophysiological data. In the *KcsA* potassium channel the M2 transmembrane segments of four neighboring subunits (which would correspond to the S6 segments of voltage-gated K^+, Na^+ and Ca^+ channels) are lining the cytoplasmic part of the pore. These segments show regular α-helical organization and form an inverted tepee, which encloses a water-filled symmetrical conducting pathway. The structural

assumptions, mentioned above have been confirmed by the low-resolution 3D structure of the sodium channel protein demonstrated by Sato *et al.* (2001).

There are three main evidences for the importance of D4/S6 segments for fast inactivation gating in Na^+ channels:

A) A receptor site for local anesthetic, antiarrythmic and anticonvulsant drugs binding to and blocking Na^+ channels is located in D4/S6 (Ragsdale *et al.*, 1994; Ragsdale *et al.*1996; Wang *et al.*, 1997). These drugs are blocking voltage-gated sodium channels in a state-dependant manner. Local anesthetics and functionally related drugs act from the cytoplasmatic side of the Na^+ channel to inhibit current and immobilize gating charge (Hille, 1966, Cahalan and Almers, 1979). Some local anesthetics, like lidocaine, stabilize the inactivated state (Hille, 1977, Bean *et al.*, 1983), whereas other components, like N-methylstrychnine, prevent inactivation suggesting that local anesthetics and related drugs interact with regions of the Na+ channel that are important for fast inactivation.

B) Mutations in the S6 segments of the $hNa_v1.4$ channel cause different types of myotonia (Wang et al, 1999; Green *et al.*, 1998; Heine *et al.*, 1993; Cannon and Strittmater, 1993; Mitrovic *et al.*, 1994). All these mutations are associated with defects in fast inactivation.

C) A combination of 3 mutations VIL1774-76AAA in the $rNa_v1.2a$ (corresponding to IIL1596-98AAA in the $hNa_v1.4$) or a combination of 2 other mutations F1764A/V1774A (corresponding to F1586A/I1596A in $hNa_v1.4$) at the intracellular end of the S6 transmembrane segment abolish fast inactivation by introducing a persistent sodium current of about 85% (McPhee *et al.*, 1994 and 1995).

1.1.2. *KCNQ2* and *KCNQ3* potassium channels

Potassium channels are the most diverse class of ion channels. This diversity is enhanced by splice variants and by formation of heteromeric channels. Until now mutations in more than ten potassium channel genes have been found which are related to human hereditary diseases (Lehmann-Horn and Jurkat-Rott, 1999; Cooper *et al.*, 2001). Interestingly, four of these genes encode potassium channels of the *KCNQ* family - the so-called group of the KQT-like potassium channels – *KCNQ1* to *KCNQ5* (Jentsch, 2000).

KCNQ1 (*KvLQT1*) was the first identified channel from the *KCNQ*-family (Wang *et al.*, 1996). It is localized on chromosome 11 and is selectively expressed in heart muscle. Mutations in the *KCNQ1* gene cause long QT (LQT) syndrome type 1 (Romano-Ward syndrome) and Jervell and Lange-Nielsen syndrome.

The *KCNQ2* potassium channel gene was isolated and mapped to chromosome 20q13.3 by two independent groups (Singh *et al.*, 1998; Biervert *et al.*, 1998). At the same time Charlier *et al.* identified the *KCNQ3* gene and mapped it to chromosome 8. These channels activate slowly and do not inactivate. *KCNQ2* and *KCNQ3* channel subunits can co-assemble to form a channel with essentially identical biophysical and pharmacological properties as the native M-current - a slowly activating and deactivating potassium current inhibited by muscarin (therefore M-current) that plays a critical role in determining the subthreshold electroexcitability of neurons as well as the responsiveness to synaptic inputs (Wang *et al.*, 1998). The co-assembly of *KCNQ2* and *KCNQ3* potassium channels leads to an increased current amplitude that is explained by enhancement in there surface expression (Schwake *et al.*, 2000). The two potassium channel subunits are colocalized in a somatodendritic pattern on pyramidal and polymorphic neurons in the human cortex and hippocampus. Immunoreactivity for *KCNQ2* but

not *KCNQ3* is prominent in some terminal fields, suggesting a presynaptic role for a distinct subgroup of M-channels in the regulation of action potential and neurotransmitter release (Cooper *et al.*, 2000).

1.2. EPILEPSY

Epileptic seizures are behavioral attacks resulting from the synchronized and excessive activity of large groups of central neurons. Symptoms vary widely, depending on the brain region that participates in the abnormal electrical activity. They may include alterations or loss of consciousness, sustained or rhythmic muscle contraction, stereotyped gestural movements, and visual or somatosensory hallucinations. The primary seizure types are generalized seizures, which involve the entire brain from the outset, and partial (focal) seizures, which begin in a localized brain region. Classification of epilepsy syndromes combines information on seizure type, age at onset, etiology, clinical course, and electro-encephalographic (EEG) findings (Comm. Classif. Terminol. Int. League Against Epilepsy, 1989). Idiopathic epilepsy lacks antecedent disease or injury to the central nervous system and is of presumed genetic origin. The current classifications are not well correlated with genetic causes, since the same mutations can produce different syndromes in different individuals, and a single syndrome can be generated by mutations in more than one gene. Epilepsy is present in approximately 3% of the general population and is more frequent during childhood (Hauser *et al.*, 1996). A strong genetic influence has been confirmed during the past few years by mapping and isolation of more than 40 genes responsible for monogenic epilepsy in human families and mouse models (Lerche *et al.*, 2001; Meisler *et al.*, 2001)

1.2.1. Generalized Epilepsy with febrile seizures plus (*GEFS+)*

Febrile seizures affect approximately 3-5% of children under 6 years of age and are by far the most common seizure disorder. A small portion of children with febrile seizures later develops ongoing epilepsy with afebrile seizures. Most cases of febrile seizures have a complex inheritance, but rare families show apparent autosomal dominant inheritance. *GEFS+* is a dominant disorder, characterized by highly variable phenotypes combining febrile and afebrile seizures, such as generalized tonic-clonic, absence, tonic, atonic and in rare cases partial seizures with a variable degree of severity (Scheffer and Bercovic, 1997; Singh *et al.*, 1999).

Linkage of the *GEFS+* phenotype to chromosome 2q21 was first described in two large families of French origin (Moulard *et al.*, 1999 and Baulac *et al.*, 1999). Further analysis revealed two mutations in the neuronal *α*-subunit gene, *SCN1A*, on chromosome 2 (*GEFS+* type 2: Escayg *et al.*, 2000). The mutations are located in the voltage sensors of the neuronal sodium channel *α*-subunit, which are highly conserved in different genes and species (fig. 4). Afebrile seizures were observed in 5 of the 11 individuals from the first family, carrying the Thr875Met mutation in the voltage sensor S4 in domain D2, compared with 11 of 12 individuals from the second family carrying the Arg1648His mutation in the voltage sensor S4 in D4. The latter mutation thus appears to have a more severe clinical phenotype (Escayg *et al.*, 2000).

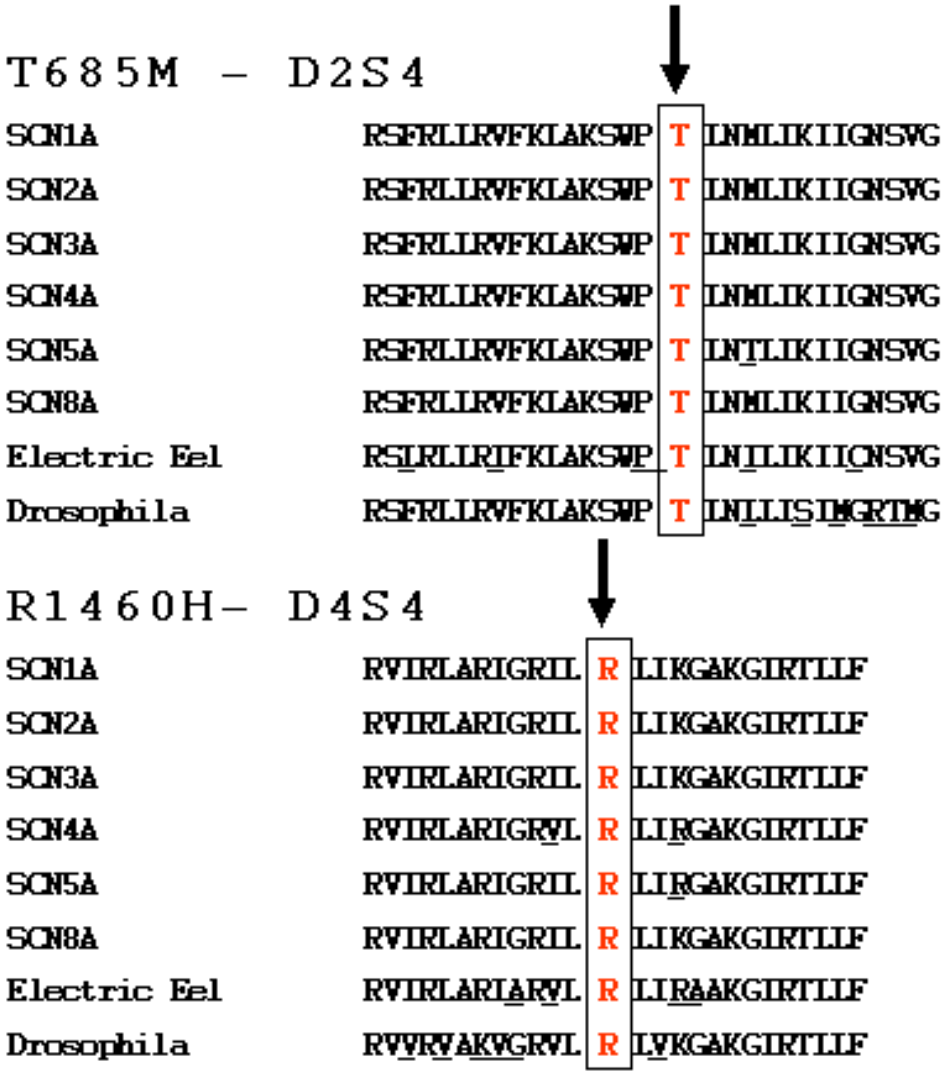

Figure 4. Amino acid sequence comparison of the D2/S4 and D4/S4 segment of various sodium channel α-subunits derived from different genes. Sequence changes are highlighted by underlining. Residues T875 and R1648 (*hNa$_v$1.1* numbering) corresponding toT685 and R1460 (*hNa$_v$1.4* numbering) are marked by an arrow.

1.2.2. Benign familial neonatal convulsions (*BFNC)*

Benign familial neonatal convulsions (*BFNC*) is a rare dominantly inherited epileptic syndrome. The penetrance of *BFNC* is as high as 85 %. BFNC is an often-cited model for “idiopathic epilepsy”. The affected individuals are epileptic, but have no other neurological deficits or other organ involvement. Recurrent, brief generalized seizures begin in the first days of life and cease after 1-3 months.

Infants otherwise grow and develop normally. The neurological examination, interictal EEGs and development of these children are usually normal. However affected persons carry a 10-16% risk of developing epileptic seizures again later in life.

A large four-generation Sicilian pedigree was described and a novel mutation in the *KCNQ2* gene on chromosome 20q13.3 was found (fig. 5A). Initial analysis of

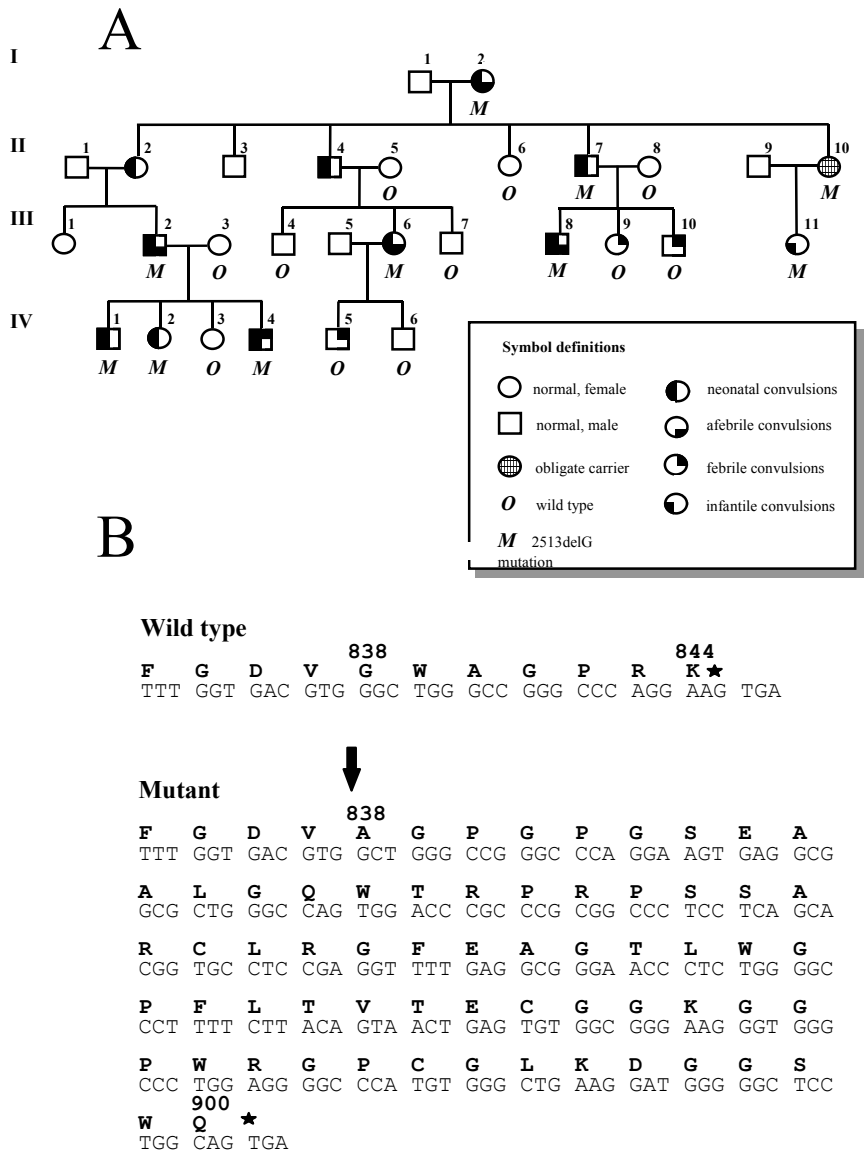

Figure 5. Clinical and genetic data of the *BFNC* family. **(A)** Pedigree of the Sicilian *BFNC* family; legend (M = heterozygous for the 2513delG mutation in exon 16, 0 = homozy-gous for the wild type). **(B)** Partial nucleotide and deduced amino acid sequence of the wild type and mutant *KCNQ2* gene. The 1 bp deletion causes a frame shift at codon 838 (indicated by an arrow), subsequently abolishing the stop codon at position 845 and adding 56 codons to the 3' end.

the index family (individuals III-2-3 and IV-1-4) suggested linkage to the known locus on 20q13.3. Mutation screening and sequencing revealed a 1bp deletion mutation (G2513 in codon 838), located close to the end of the open reading frame. The subsequent frame shift alters the 3´ end of the *KCNQ2* gene product, resulting in an extension of the channel protein by 56 amino acids (fig. 5B).

1.3. AIMS

The present work is divided into two parts:

The aim of the first part is the heterologous expression and functional characterization of the aforementioned mutations in the *SCN1A* (T685M and R1460H) and *KCNQ2* (2513delG) genes. The genetic data clearly link these mutations to the two forms of epilepsy *GEFS+* and *BFNC* and the electrophysiological characterization is intended to provide a detailed view of the molecular mechanism of the disease. In addition, the functional studies can supply information about the biophysical properties of the investigated channels.

The molecular mechanisms of the sodium channel fast and slow inactivation are only partly understood. Structure-functional studies of different regions of the sodium channel, involved in these processes could help to understand better the mechanisms underlying fast and slow inactivation. The major scope of the second part of this work is a detailed evaluation of the role of the D4/S6 segment and some aspects of the D4/S4-S5 loop in sodium channel fast and slow inactivation by introducing and studying artificial mutations in both regions.

2. MATERIALS AND METHODS

2.1. MOLECULAR AND CELL BIOLOGY METHODS

2.1.1. Mutagenesis

Mutagenesis and cloning procedures were performed by other coworkers in our laboratory. Therefore only a short description of the procedures is provided.

For DNA amplification commercial midi or miniprep kits of QIAGEN (QIAGEN GmbH, Germany) were used and the recommended procedures were followed. Restriction digestions, followed by sequencing, were used to verify the mutagenesis procedures.

2.1.1.1. *KCNQ2* channel mutagenesis

A construct of the *KCNQ2* encoding sequence inserted in the pTLN expression vector (Biervert *et al*., 1998) was kindly provided from Prof. Jentsch and used for mutagenesis procedures, RNA synthesis and expression.

The 1 bp deletion 2513delG (see Introduction) was introduced into the expression construct using the Gene Editor *in vitro* site-directed mutagenesis system (Promega Corporation, Madison, WI, USA). The coding nucleotides for the additional 56 amino acids (not presented in the original construct) were cloned by PCR from human genomic DNA and additionally inserted in the vector.

To generate a channel truncated at the site of the frame shift, a second mutation was made introducing a stop codon at position 838 using the same mutagenesis system.

2.1.1.2. Sodium channel mutagenesis

Constructs of the coding sequence of the $Na_v1.4$ sodium channel inserted in the pRc/CMV plasmid vector (George *et al*., 1992) or the pSP64 vector were kindly provided by Dr. Al George. The constructs are suited for expression in mammalian cells by transfection of cDNA and for expression *Xenopus Laevis* oocytes by injection of cRNA. Site-directed mutagenesis was performed and the mutant clones were reassembled in both vectors for further expression (pRc/CMV for transfection in the mammalian tsA201 cell line and SP6 for cRNA injection in *Xenopus Laevis* oocytes). The used mutagenesis strategies for the different mutations are listed in table 1.

Table 1. Mutagenesis methods for the investigated sodium channel mutations

Mutation	**Mutagenesis method**
T685M mutant	QuickChange™ mutagenesis kit (Stratagene, La Jolla, CA, USA)
R1460H	PCR based strategy
L1482A; L1482C	Altered Sites system™ using the plasmid vector pSELECT (Promega Corporation)
F1586C; F1586A; I1596C; I1596A; F1586C/I1596A; F1586A/I1596C; F1586A/I1596A; F1586C/I1596C; F1586R/I1596R; F1586E/I1596E;	QuickChange™ mutagenesis kit or PCR based strategy

2.1.2. Molecular biological methods

2.1.2.1. In vitro RNA synthesis

For all RNA procedures an autoclaved diethyl-pyrocarbonate-water (0.1% DEPC, Sigma) was used in order to prevent RNAse activity. All reagents and materials were kept on ice. The commercial kits mMessage^{TM} mRNA Machine kit (Ambion) or SP6 CAP-Scribe Kit (Boehringer) were used and the recommended procedures were followed. In brief, the linearized plasmid DNA was incubated for 2 hours with the transcription buffer, the rybonucleotyde mix and the enzyme mix at 37°C.

Additionally 1µl RNAse-free DNAse type I (2U/µl) was added and the mixture was incubated for 15 more minutes at 37°C to remove DNA. The probe was extracted with the phenol/chloroform method and precipitated with isopropanol. After washing with 100% and 70% ethanol the RNA was dried for 5 min at 37°C and resuspended in 10 or 20µl DEPC water. RNA preparations were analyzed on an agarose gel and spectroscopically.

2.1.2.2. Restriction digestions

Restriction enzymes were applied to linearize plasmid DNA for in vitro cRNA synthesis. All restriction enzymes were used according to the manuals of the suppliers. Usually a 1 ml Eppendorf tube with 2µl DNA (around 2 µg), 1 µl 10x restriction buffer and 10U of the restriction enzyme was filled up to 10 µl with autoclaved distilled water and incubated for 1 to 2 hours at 37°C.

2.1.2.3. Agarose gel electrophoresis

To estimate quality and quantity of the nucleic acid probes, agarose gel electrophoresis was performed using 1% agarose gel (Sambrook *et al.*, 1989). Agarose (Sigma-Aldrich) was boiled in TEA buffer (40 mM Tris-Acetate (Merck), 1mM EDTA (Merck), pH 8.0). Preceding RNA gel electrophoresis, the electrophoresis chamber was treated with 1% H_2O_2 for 30 min to minimize RNA-ase activity and a fresh gel was prepared. After cooling down to approximately 50-60°C, 0.1µg/ml Ethidium-bromide was added for further fluorescence visualization. Horizontal gel was prepared in a plastic chamber. The chamber was filled with TEA buffer, the DNA or RNA samples together with appropriate marker were loaded in the gel pockets and 60 to 90 Volt were was applied. The electrophoresis process was stopped after one hour and the separated bands were visualized by UV light.

2.1.2.4. Spectroscopic measurement of nucleic acid concentration

To determine the concentration of the DNA and RNA probes the extinction A_{260} at 260 nm optical wavelength was measured on an automated spectrophotometer (Ultrospec 3000, Amersham Pharmacia Biotech, Freiburg, Germany). Appropriate nucleic acid dilution was prepared to obtain an extinction coefficient between 0 and 1. Optical density of 1 corresponds to a concentration of 50µg/ml for DNA probes. A qualitative test was done by measuring the ratio A_{260}/A_{280} (extinction coefficients at 260 and 280 nm wavelength). A ratio between 1.6 and 2 was considered to indicate purified DNA.

2.1.3. Cell biology methods

2.1.3.1. Cell culture and transfection of tsA201 cells

2.1.3.1.1. Cell passaging

Cultured tsA201 cells were used for heterologous expression of sodium channels and their functional characterization with the whole cell patch clamp technique. Standard cell culture procedures for adherent cell lines were applied: cells were maintained in 25ml sterile flasks (Integra Bioscience or Greiner, Frickenhausen) in 50% Dulbeco´s MEM + 50% HAMS nutrition mixture (GIBCO Brl, Paisley, Scotland or PAA Laboratories, Linz, Austria) supplemented with 10% inactivated fetal calf serum (PAA Laboratories, Linz, Austria) in controlled 5% CO_2 atmosphere at 37°C (Cell incubator IG 150, Jouan, Unterhachingen, Germany). Cells were passaged regularly every 3 days. Before splitting, cells were gently washed with Ca^{2+} and Mg^{+} free PBS solution (PAA Laboratories, Linz, Austria) to stabilize the pH of the medium and to attenuate the following resuspension by weakening the cell-cell and cell-dish connections. Resuspension was achieved by pipetting the cells up and down several times with a 5ml plastic pipette (Greiner, Frickenhausen, Germany). Cells were distributed in flasks supplemented with fresh medium in the ratio one to three. Microscopical observations and inspections were carried out periodically. Cells were used for transfections until passage 25.

2.1.3.1.2. Freezing and thawing

Cells from 2 flasks were mixed with an equal volume of cold, freshly prepared cell-freezing medium (10% DMSO (Sigma-Aldrich) in DMEM (GIBCO Brl)) in a freezing vial. The vials were placed in a styropor box and stored for 1 to 2 days at -70°C before they were transferred to liquid nitrogen for long-term storage. When a new

batch of cells was needed, a probe was thawed as quickly as possible (at 37°C or by hand) and immediately transferred to cold medium, centrifuged for 5 minutes at 300 g and resuspended in complete medium for cultivation.

2.1.3.1.3. Transient cell transfection

Transient cell transfection was performed by the standard calcium-phosphate method (Graham and Van der Eb, 1973; Wigler *et al*., 1978). This method uses the ability of the calcium-phosphate precipitates to penetrate the cell membrane with the bound DNA and to deliver the DNA into the cytoplasm. Sterile 6 cm dishes (Greiner, Flickenhausen, Germany) filled with 5 ml cell culture medium and a cell density of around 40% were prepared the day before transfection. For most experiments, 5 to 10µg of cDNA encoding the WT or mutant α-subunit sodium channel was cotransfected in a 4:1 ratio with a plasmid containing CD8 cDNA in order to recognize transfected cells using microbeads with CD8-antibodies. In some experiments (see results section), the DNA encoding the β_1 sodium channel subunit was cotransfected in a 3:1 ratio to increase surface expression (Isom *et al*., 1994). The whole amount of cDNA was mixed with 250µl sterile $CaCl_2$ solution and added dropwise to 250µl 2xHEBS solution (in mM: 170 NaCl, 40 HEPES, 2 KCl, 10 Dextrose, 1.4 Na_2HPO_4). After 20 min incubation at room temperature the mixture was added to the cells, supplemented with fresh cell culture medium. Transfection was stopped after 6-8 hours by gently washing the cells with PBS and resuspending like mentioned before. Different amounts of the suspension (from 100µl up to 1ml) were distributed in 3.5cm cell culture dishes for further electrophysiological experiments.

2.1.3.2. Oocyte preparation and injection

The use of *Xenopus Laevis* oocytes as an expression system for ion channels was first described by Miledi *et al*. (1983) and since then has become a standard technique for investigation of ion channels. Oocytes are especially suitable for electrophysiological recordings, since they have only a few endogenous channels, and faithfully express foreign RNA that has been injected.

2.1.3.2.1. Frog surgery

Adult *Xenopus laevis* frogs with a length of at least 9 cm (fig 6A) were anesthetized in 1l 0.5% Tricaine water solution (3-aminobenzoic acid ethyl ester methanesulfonate salt (MS222), Sigma-Aldrich, Munich, Germany) for about 15-20 min. The frog was put on ice on his back after achieving the necessary anesthetic grade checked by the loss of the righting response and the loss of response to painful stimuli. Extremities and head were covered with ice in order to prolong the effect of the anesthetic and to prevent excessive bleeding. The surgical area and all surgical instruments were sterilized with 70% ethanol solution. Instruments were kept on a sterile wrap during the procedure. Skin, muscle fascia and muscle tissue were cut at a length of 1cm. Pieces of ovaries (about 200 oocytes) could be removed through this opening with forceps and scissors. The wound was closed with absorbable sutures (Serafit, Serag-Wiessner, Naila, Germany).

2.1.3.2.2. Defolliculation and selection

Before defolliculation oocytes were extensively washed with OR2 medium (in mM: 82.5 NaCl, 2 KCl, 1 $MgCl_2$, 5 HEPES, pH 7.4). Defolliculation was achieved by treatment with 2mg/ml collagenase (type CLS III, Biochrom KG) solution in OR2 Ca^{2+}

free medium (Masui, 1967). Usually 2 hours of gently shaking at room temperature were enough to defolliculate the oocytes completely without damaging the viteline membrane. Defolliculated oocytes were stored in L-15 medium (Sigma Aldrich, Munich, Germany) supplemented with 50mg/ml gentamicin sulfate (Biochrom KG, Berlin, Germany) at 18°C in low temperature aseptic incubator (VWR Scientific, West Chester, USA). Medium was changed every day. Before injection selection was done for healthy stage V and VI oocytes (Dascal, 1987) (fig. 6B).

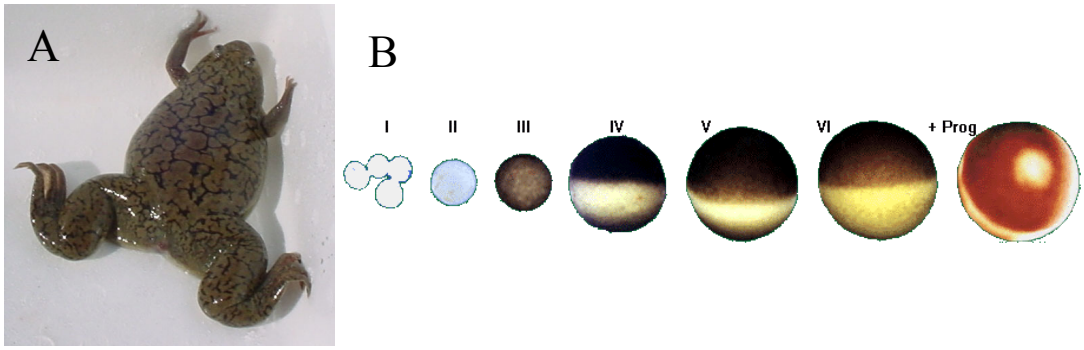

Figure 6. The *Xenopus Laevis* oocytes expression system. **(A)** Adult female *Xenopus Laevis* frog. **(B)** Developmental states of *Xenopus Laevis* oocytes: healthy stage V and VI oocytes can be recognized by their size and by the clear differentiation of the animal and vegetal poles.

2.1.3.2.3. Oocyte microinjection

In vitro synthesized RNA can be injected and expressed in *Xenopus laevis* oocytes (Gurdon *et al*., 1971). Borosilicate glass pipettes (1.14 OD, 0.53 ID; Drummond Scientific, Broomall, USA) were pulled on a two stage horizontal DMZ Universal puller (Zeitz Instruments, Augsburg, Germany). The tips of the pipettes were broken under a StereoZoom 3 microscope (Bausch&Lomb, Dornach, Germany) to obtain optimal diameter and sharpness (around 20 µm tip diameter). Pipettes were filled with red-colored heavy mineral oil (Sigma-Aldrich, Munich, Germany) and were mounted in the head-stage of a NANOJECT Auto-Nanoliter Injector (Drummond Scientific, Broomall, USA). The pipette tip was filled with 2µl RNA. Oocytes were

lined up on a plastic grid previously sterilized with 70% ethanol and covered with culture medium. 40 to 120nl undiluted RNA were injected in the vegetal pole of a single oocyte (Nieuwkoop, 1977). After injection oocytes were stored in groups of 20 peaces in 6 well plates (Greiner, Frickenhausen, Germany) and incubated at 18°C. The amount of the injected RNA correlated well with expression levels, i.e. current size was dependent on the expression rate. With a concentration of 0.5 to 1 µg RNA/µl, the amount of RNA injected ranged from 20 to 120ng RNA per oocyte.

In order to compare current amplitudes of *KCNQ2* WT and mutant channels, RNA preparations yielding equal bands on a gel, thus having approximately the same density, were injected on the same day into the same charge of oocytes and measured in parallel on days 2-4 after injection.

In order to increase current density and stabilize gating (Isom *et al*., 1993), sodium channel α-subunit encoding RNA was co injected with RNA encoding the β_1 sodium channel subunit in the ratio 1:3.

2.2. ELECTROPHYSIOLOGY

2.2.1. Reagents and solutions

2.2.1.1. Solutions for voltage-clamp measurements

All reagents were ordered from Sigma-Aldrich (Deisenhofen, Germany) or Amercham Bioscience (Freiburg, Germany). The used solutions are listed below in mM.

***KCNQ2* potassium channels:**

Standard bath solution for two electrode voltage-clamp (Frog Ringer)

115 NaCl, 2.5 KCl, 1.8 CaCl2, 10 Hepes, pH 7.4 (NaOH)

Standard pipette solution for two electrode voltage-clamp - 3000 KCl

Sodium channels:

Standard bath solution for two electrode voltage-clamp (Frog Ringer)

115 NaCl, 2.5 KCl, 1.8 CaCl2, 10 Hepes, pH 7.4 (NaOH)

Standard pipette solution for two electrode voltage-clamp - 3000 KCl

Standard bath solution for whole-cell patch-clamp–

150 NaCl, 2 KCl, 1.5 $CaCl_2$, 1 $MgCl_2$, 10 Hepes, pH 7.4 (CsOH)

Standard pipette solution for whole-cell patch-clamp

105 CsF, 35 NaCl, 10 EGTA, 10 Hepes, pH 7.4 (CsOH)

For the macropatch recordings from oocytes, the above bath and pipette solutions were reversed.

2.2.1.2. Methanethiosulfonate reagents

Methanethiosulfonate (MTS) reagents have active sulfhydryl groups which covalently bind to exposed cysteines in proteins via disulfide bonds. The MTSES ((2-sulfonato ethyl)methanethiosulfonate), MTSET (2-(Trimethylammonium) ethyl methanethiosulfonate Bromide) and MTSEA ((2-Aminoethyl)methane thiosulfonate Hydrobromide) reagents were purchased from Toronto Research Chemicals (Toronto, Canada) and used in the present experiments.

Small potions of stock solution were prepared in water (usually 100 time the desired end concentration) and stored at –20°C. Immediately prior application, the stock was defreezed and diluted in the bath or pipette solution in the desired concentration.

2.2.2. General procedures

Most of the current knowledge about ion channels in cell membranes derived from experiments using voltage clamp. The method allows ion flow across a cell membrane to be measured as electric current while the membrane potential is held under experimental control with a feedback amplifier. The method was developed by Cole (1949) and Hodgkin *et al*. (1952). Since that time many variants of the technique have evolved and voltage clamp measurements have been extended to a vide range of tissues. A common electrophysiology setup is shown on figure 7.

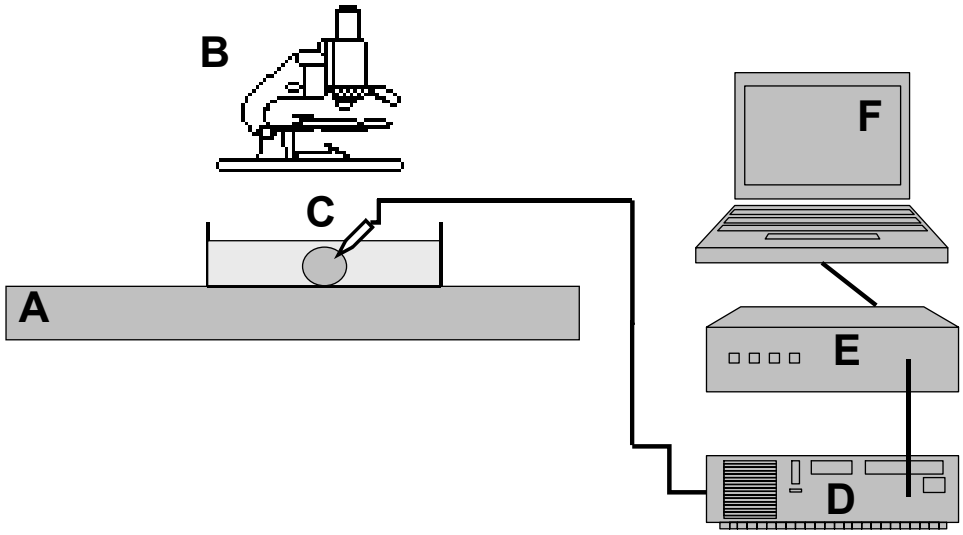

Figure 7. Scheme of a common electrophysiological setup. The probe is placed on a massive antivibration table **A** under an optical microscope **B**. The glass microelectrode **C** is connected to a feedback amplifier **D**. The amplified and filtered signal is digitized by the AD converter **E**. The digitized signal is visualized and stored on a PC **F** running specific software.

2.2.2.1. Electrical and mechanical isolation

The recording chamber, the microscope and the micromanipulators were placed on an anti-vibration table – a heavy granite plate placed on active (pneumatic) support for the patch clamp setup and passive (tampons) support for the two electrode voltage clamp measurements. A faraday cage was build around the experimental setup and all metal parts near the head-stage were grounded, using the virtual ground input of the amplifier.

2.2.2.2. Glass electrodes

Glass microelectrodes were pulled on a horizontal two stage DMZ Universal Puller (Zeitz Instruments, Augsburg, Germany) from thin wall borosilicate glass pipettes with filament (1.5 mm OD, 1.17 mm ID; Clark Electromrdical Instruments, Reading, UK or Science Products, Hofheim, Germany). The microelectrodes for patch-clamp recordings were fire polished. The resistance of the whole-cell patch clamp electrodes ranged between 0.8 and 1.5 MΩ. The electrodes for the macropatch recordings from oocytes had a tip resistance of 0.5 to 0.8 MΩ. The electrode tips were coated with Sigmacote (Chlorinated organopolysiloxane in heptane; Sigma-Aldrich, Munich, Germany). Sharp glass electrodes for two-electrode voltage clamp (TEVC) were pulled in a way to minimize the access resistance while minimizing cell damage – 0.5 to 1MΩ with the standard 3M KCl electrode solution.

2.2.2.3. Ag/AgCl electrodes

Ag/AgCl electrodes were prepared by chemically chlorating silver wire peaces (l=5cm, d=300µm, Science Products, Hoffheim, Germany) in Fe_2Cl_3 solution.

2.2.2.4. Digitizing, recording and analysis

In all experimental configuration the voltage clamp amplifier output was digitized by a DIGIDATA 1200 AD/DA converter (Axon Instruments, Union City, USA), connected to a personal computer (PC 486) running Clampex 6.0 (Axon Instruments, Union City, USA) acquisition software under Microsoft DOS 6.2 (Microsoft Corp. Redmond, USA). The current responses to the voltage stimuli were recorded on the hard drive and additionally a hard copy record was done for every protocol. Analysis was done on a PC using combination of Clampfit (Axon), Origin (Microcal, Northampton, USA) and Excel (Microsoft) software.

2.2.2.5. Capacitance cancellation and series resistance compensation

Fig. 8 shows a simplified circuit of a cell with capacitance C_M and membrane resistance R_M. Voltage clamp is performed by an amplifier with amplification μ through an electrode with resistance R_S. Application of a square voltage impulse results in capacitance current, which can be described by the simple equation $I_{IN} = \frac{R_S x C_M}{\mu}$. This current can interfere with the currents flowing trough ion channels and additionally can lead to saturation of the amplifiers of the recording circuits. Cancellation of this capacitive current is achieved by supplying the command stimulus with the additional current, required to charge the cell directly to the desired value.

The resistance R_S, which is in series with the membrane resistance is a main source of voltage error in voltage clamp experiments. Such error is called series resistance error. When a current I flows across the membrane the resistance R_S leads to a discrepancy between the measured membrane potential V_M (controlled by the

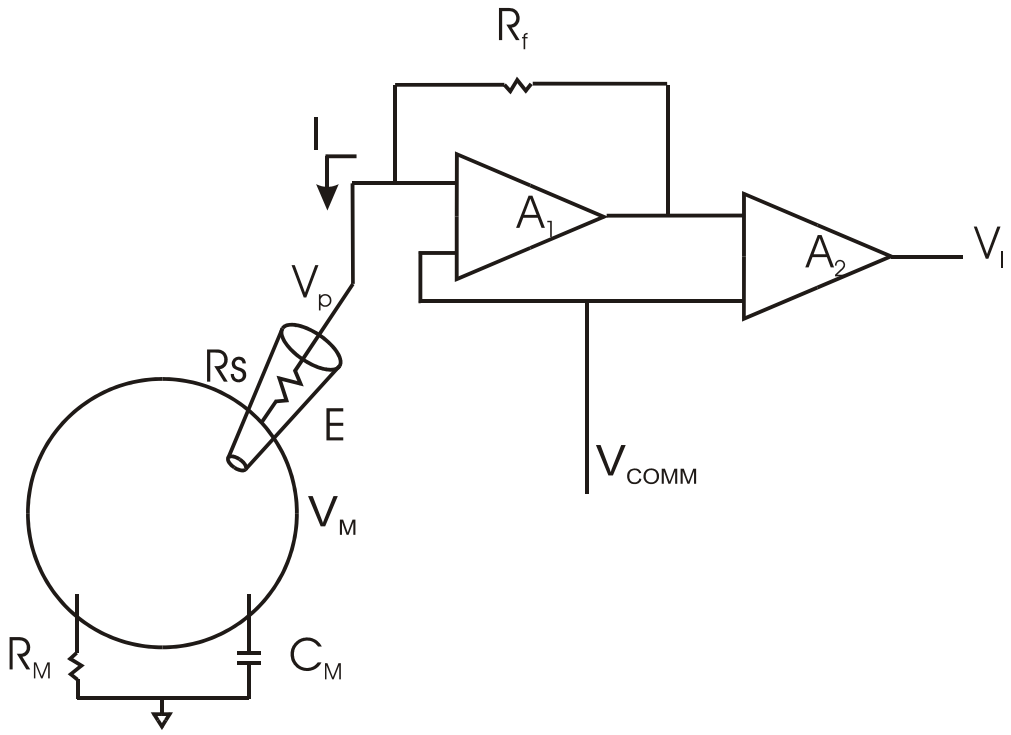

Figure 8. One electrode continuous voltage clamp method (whole cell patch clamp). The voltage at the top of the pipette V_P is the sum of the the membrane potential V_M, which is controlled by the circuit, and the current-induced voltage drop across the pipette.The operational amplifier 1 (A_1) is configured as a current to voltage converter. The differential amplifier 2 (A_2) substracts the pipette potential (V_P) to generate the current output (V_I).

amplifier) and the true potential difference across the membrane, V_T. The size of the error is *IxRs*. Compensation of the series resistance error is achieved by adding to the command signal a voltage signal proportional to the membrane current, which is scaled appropriately.

The circuits present in the voltage clamp amplifiers were used for capacitance cancellation and series resistance compensation. In experiments, where two-electrode voltage-clamp was used, the gain of the amplifier was maximized and additionally the maximal series resistance compensation was applied, according to the user manual of the manufacturer. In whole cell experiments, compensation of

more than 70% of the series resistance was used, which corresponds to a maximal voltage error of 4 mV for current sizes ranging from 1 to 15 nA.

2.2.3. Two-electrode voltage-clamp on *Xenopus Laevis* oocytes

2.2.3.1. Experimental setup

Fig. 9 shows a schematic diagram for the two electrode voltage clamp (TEVC) circuit. The oocyte is penetrated with two microelectrodes, one to record voltage (*E_1*) and the other to pass current (*E_2*). The main disadvantage of the TEVC is the relative slow response due to the high value of the capacitance of the oocyte membrane.

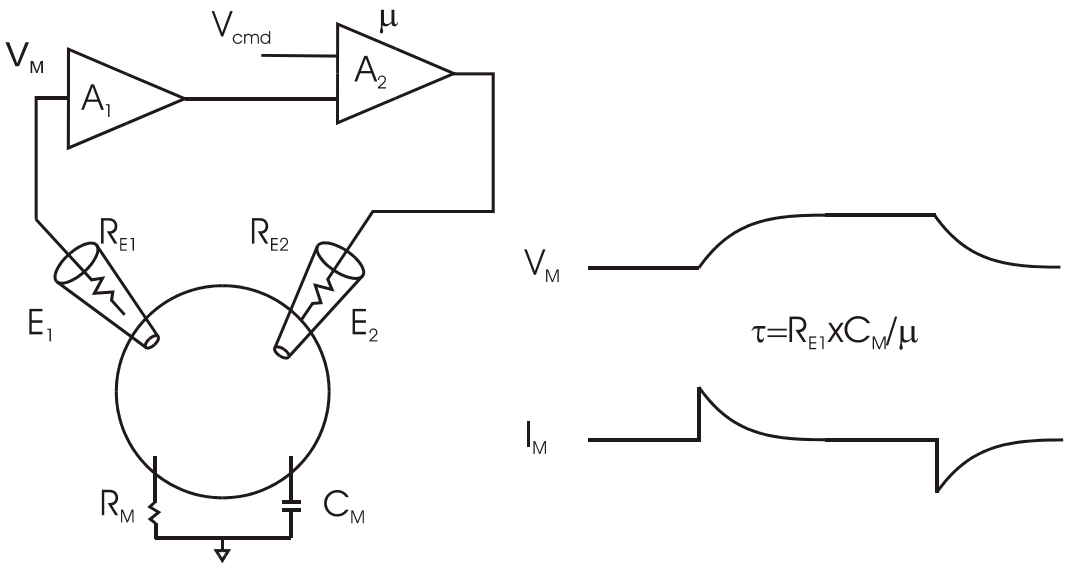

Figure 9. Conventional Two-Electrode Voltage Clamp. **(A)** The membrane potential (V_M) is recorded by a unity-gain buffer amplifier (A_1) connected to the voltage-recording microelectrode (E_1). V_M is compared to the command potential (V_{CMD}) in a high-gain differential amplifier (A_2; gain = μ). The output of A_2 is proportional to the difference ε between V_M and V_{CMD}. The voltage at the output of A_2 forces current to flow through the current-passing microelectrode (E_2) into the cell. The polarity of the gain in A_2 is such that the current in E_2 reduces ε. **(B)** Finite time is required to charge the cell capacitance. If μ was infinite, or if R_{E2} was zero, the response would approach the ideal case.

The Plexiglas recording chamber was placed under a stereo microscope (StereoZoom 3, Bausch&Lomb , Dornach, Germany). Head-stages and pipette holders (Axon Industries) were fixed on Leitz manipulators. The feedback amplifier TurboTec 01c (npi, Tamm, Germany) was used for all TEVC measurements.

2.2.3.2. Experimental procedures

The voltage electrode was wrapped in aluminum foil in order to reduce the capacity coupling between current and voltage electrodes. In order to minimize the capacity C_M (see fig. 9), the recording chamber was filled with solution just enough to cover the oocyte. The cell was fixed on a grid in the recording chamber. The tips of the two electrodes were inserted in the bath solution. Electrode potentials were compensated, while the amplifier was switched to current clamp mode. The voltage electrode was inserted in the oocyte and the resting membrane potential was measured. Only cells with a resting membrane potential more negative than –20 mV were measured. Series resistance and capacity compensation were performed, using the circuits present in the npi amplifier. According to the manufacturer's application notes, the gain of the amplifier was first maximized, and then the maximal percentage of series resistance compensation was applied.

2.2.4. Whole cell and inside-out recordings from cells and oocytes

2.2.4.1. Patch clamp technique

The "patch clamp" method was described first by Neher and Sakmann (1976) and later in an improved form by Hamill *et al*. (1981) (fig. 8). A mechanically stable contact with very high resistance (> 1GΩ) between the cell membrane and a glass microelectrode is achieved by applying negative pressure ("cell attached"

configuration, fig. 10). This allows low noise recordings and also resolution of single channels. Several configurations are used in the patch clamp method:

cell-attached (fig. 10B);

whole cell (fig. 10D);

cell free – inside-out and outside-out (fig 10C,E).

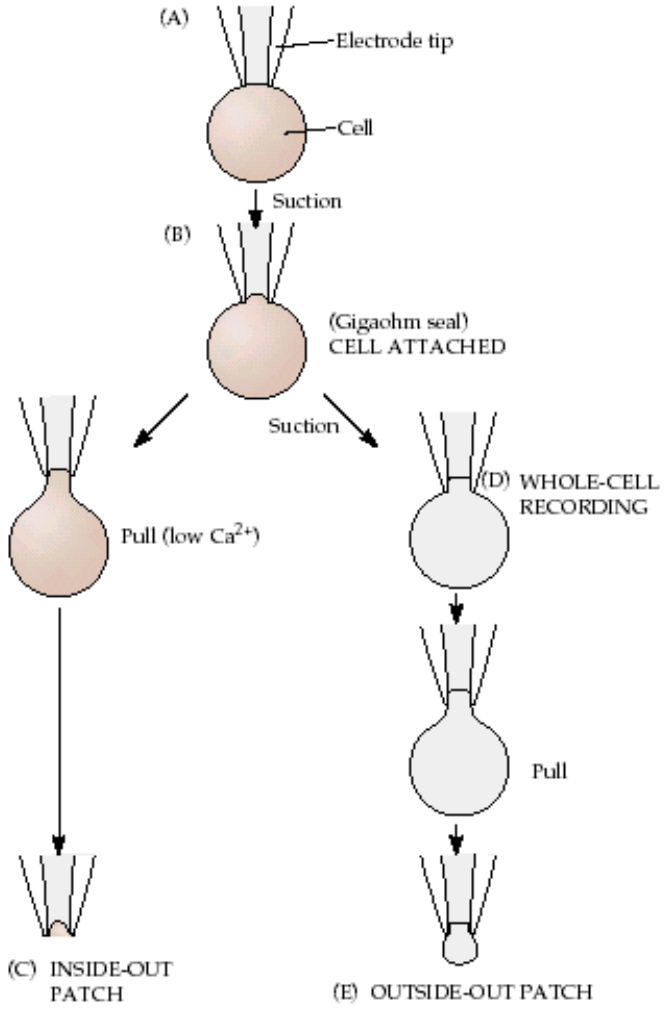

Figure 10. Patch configurations, represented schematically. The electrode forms a seal on contact with the cell membrane **(A)**, which is converted to a gigaohm seal by gentle suction **(B)**. Records may then be made from the patch of membrane within the electrode tip (cell-attached patch). Pulling away from the cell results in the formation of a cell-free vesicle, whose outer membrane can then be ruptured to form an inside-out patch **(C)**. Alternatively, the membrane within the electrode tip may be ruptured by further suction to obtain a whole-cell recording **(D)** or, by pulling, to obtain an outside-out patch **(E)**.

2.2.4.2. Experimental setup

The EPC 7 amplifier (List Medical, Darmstadt, Germany) was used to perform continuous single electrode voltage clamp in the whole-cell and the inside-out configurations. A 3-kHz 8-pole low-pass continuous Bessel filter (KF9006, Zeitz Instruments, Augsburg, Germany) was used to pre-filter the signal from the cell. The amplifier head-stage was mounted on a hydraulic micromanipulator (Narishige Scientific Instruments, Tokyo, Japan) and fixed on an inverted stereo microscope Axiovert 10 (Zeiss , Germany).

2.2.4.3. Experimental Procedures

2.2.4.3.1. Whole cell measurements from transiently transfected tsA201 cells

Cell culture dishes of 3.5 cm diameter were used as a recording chamber. In order to recognize transfected cells, they were incubated with 0.3 µl per dish CD8-antibody coated beads, 1 µg/µl (Dynabeads M-450, Dynal, Oslo, Norway) for 2-3 minutes prior measuring. Usually more than 80% of the cells, marked with beads showed recordable sodium current. Whole-cell recording usually started ten minutes after breaking the cell membrane. This time is long enough to allow full exchange of the cell cytoplasm with the pipette solution. Non-transfected tsA201 cells can have endogenous sodium currents of usually less than 200 pA. Therefore, only transfected cells with sodium currents larger than 1 nA were taken for evaluation. Series resistance compensation was used and only recordings with a voltage error less than 4mV were evaluated.

2.2.4.3.2. Inside-out recording on *Xenopus laevis* oocytes

A small chamber with a volume of 150 µl was used for the inside-out recordings on oocytes. Solution exchanges for application of MTS reagents were performed as follows: 3 ml (20 times the volume of the recording chamber) were prepared and were added to the bath solution by a syringe and plastic tube fixed on the chamber. The excess solution was removed by a peristaltic pump. Usually a complete exchange was obtained in less than 30 seconds.

2.2.5. Voltage-clamp protocols and data analysis

2.2.5.1. Voltage-clamp protocols used to characterize *KCNQ2* potassium channels

2.2.5.1.1. Voltage dependence of activation

“Instantaneous current-voltage relations” (I-V curves) were recorded in order to determine the voltage dependence of activation of expressed *KCNQ* channels: oocytes were held at –80mV, 4-s long depolarizing pulses to different voltages were followed by a 500ms pulse at –30 mV to measure the tail current amplitude (see fig. 11). This amplitude is proportional to the number of the channels opened during the preceding pulse. The obtained activation curves (see fig. 12A) were normalized to the maximal amplitude and fitted to a standard Boltzmann function: $I/I_{max}(V) = 1/(1 + exp[(V-V_{0.5})/k])$, with I/I_{max} being the normalized potassium current amplitude, $V_{0.5}$ the voltage of half-maximal activation and k a slope factor.

2.2.5.1.2. Activation kinetics

The time constants of activation of *KCNQ2* potassium channels were obtained by fitting the rising part of the currents at various potentials by a first order exponential function.

2.2.5.1.3. Deactivation parameters

Tail current traces of WT and mutant *KCNQ2* channels were recorded after a 2-s depolarization to +20 mV at test potentials between –50 and –160 mV (see fig. 12C). The tail current decay was fit to a first order exponential function, yielding the deactivation time constant, τ_{deact}.

2.2.5.2. Voltage-clamp protocols used to characterize sodium channels

2.2.5.2.1. Voltage dependence of activation

The voltage dependence of activation for WT and mutant sodium channels was obtained by 25-ms depolarizing pulses to different potentials from a holding potential of –140 mV or –85 mV for the whole-cell measurements, –80 mV for the TEVC experiments and -120 mV for the inside-out recordings (see fig. 13). The exact holding potential is further specified in the results section. I-V curves were obtained by plotting the maximal current amplitude of every trace vs. voltage (see fig. 15C). After normalization they were fit to the following Boltzmann function multiplied by the unitary conductance: $I(V) = g * (V - V_{rev}) / [1 + \exp(V - V_{0.5}) / k]$. V_{rev} represents the reversal potential for the sodium ions and *g* is the unitary channel conductance. From these relation, the conductance-voltage curve (representing the activation gating) can be derived: $G / G_{\max} = 1 / [1 + \exp(V - V_{0.5}) / k]$.

2.2.5.2.2. Activation kinetics

The 10 to 90% rise time of the sodium currents at different potentials was determined in order to characterize activation kinetics of the WT and mutant sodium channels. Additionally, activation and inactivation of the sodium current traces were fit for some mutants to the Hodgkin-Huxley equation (m^4h, Hodgkin & Huxley, 1952):

$$I(t) = A * [1 - \exp(-(t - t_0) / \tau_m)]^4 * \{A_f * \exp(-(t - t_0) / \tau_f) + (1 - A_f) * \exp(-t / \tau_s) + C\},$$

where τ_f and τ_s are the resulting fast and slow time constants of inactivation, τ_m the activation time constant, A an amplitude factor, A_f the relative amplitude of the fast component, t the time after onset of the depolarization, t_0 the delay to activation of the channel and C a constant term (see fig 13 and 15B).

2.2.5.2.3. Deactivation parameters

In order to measure deactivation of WT and mutant sodium channels, a short depolarizing pulse (0.5 ms to –10 mV) was followed by the test pulse to the indicated potentials. The deactivation time constant, τ_{deact}, was obtained by a first order exponential fit to the tail current decay (see fig. 16).

2.2.5.2.4. Steady state fast inactivation

Steady-state inactivation was determined using a two step protocol: 300-ms-prepulses to the various potentials were followed by a short test pulse to –20 mV or –10 mV. The normalized peak current at this potential is proportional to the percentage of sodium channels that are still available for activation. The data points

were fit to a standard Boltzmann function: $I/I_{max}=1/(1+exp[(V-V_{0.5})/k_V])$, with $V_{0.5}$ being the voltage of half-maximal inactivation and k_V a slope factor (see fig. 14C).

2.2.5.2.5. Inactivation time constants and persistent current

Inactivation time constants (see fig. 14A) were obtained by fitting the sodium current decay to a second order exponential function plus a constant term *C*:

$$I(t) = A_f \exp[-(t-t_0)\tau_f] + A_s \exp[-(t-t_0)/\tau_S] + C\,.$$

The amplitude A_f of the fast time constant τ_f (or τ_h) contributes to more than 90% to the total current amplitude (except for the mutants which do not inactivate.

The persistent current (see fig. 21A) was obtained by using the following relation:

$$I_{SS} = C/(A_f + A_S + C)$$

In some cases the persistent current level was determined by the ratio of the sodium current at the end of 70-ms depolarizing test pulses to the peak current.

2.2.5.2.6. Recovery from fast inactivation

Recovery from fast inactivation was recorded from a holding potential of -100 mV. Cells were depolarised to 0 mV for 100 ms to inactivate all Na^+ channels and then repolarized to various recovery potentials for increasing durations. The time course of recovery from inactivation was best fit to a second order exponential function with an initial delay (see fig. 14B).

2.2.5.2.7. Steady state slow inactivation

Two different protocols were used to determine the voltage dependence of steady state slow inactivation (see fig. 22B): (A) “conventional protocol – 60-s pulses to various potentials were applied from a holding potential of –140 mV. Subsequently, 100-ms pulses to –100 mV were applied in order to allow cannels to recover from fast inactivation, followed by a test pulse to 0 mV was applied. A 40-s interval at –140 mV was chosen between these test sequences in order to allow complete recovery from slow inactivation; (B) “cumulative protocol” – 30-s prepulses from -130 mV to +30 mV were applied. Every pulse was followed by a 100 ms recovery pulse at 100 mV and a test pulse to 0 mV. No time was left for recovery from slow inactivation between the test sequences (see fig. 22B and C).

The data were fit to a standard Boltzmann function $I/I_{max}=1/(1+exp[(V-V_{0.5})/k_V])$.

2.2.5.2.8. Entry into slow inactivation

Cells were held at –100 mV, depolarized to various potentials for increasing durations, repolarized for 100 ms to –100 mV to let the channels recover from fast inactivation, and then depolarized again to –10 mV to determine the fraction of slow inactivated channels. No time was left for recovery from slow inactivation between the test sequences Experimental points were well fit with a first order exponential function to obtain the time constant of entry into the slow inactivated state (see fig. 17B).

2.2.5.2.9. Recovery from slow inactivation

Recovery from slow inactivation at various potentials was measured after 30 s conditioning pulse to 0 mV. Cells were held at the recovery potential and no time was left for recovery from slow inactivation between the test sequences. Experimental points were fit to a second order exponential function (see fig. 17C).

2.2.5.3. Double mutant cycle analysis

A possible way to demonstrate interactions between two protein regions is to estimate the energetic effects of mutations in both regions on the energetic landscape of the whole protein or to build the so-called double mutant cycles. Considering only the transitions between two states of the sodium channel (e.g. open and inactivated), one can write the following state diagram:

$$O \xleftrightarrow{Kon,Koff} I ,$$

where K_{on} and K_{off} are the forward and backward rate constants. K_{on} and K_{off} can be calculated using the equations $K_{on}=(1-I_{ss})/\tau_f$ and $K_{on}=I_{ss}/\tau_f$, where I_{ss} is the percentage of noninactivating current and τ_f is the time constant of fast inactivation (Starace *et al.*, 1993). The thermodynamic changes in the free energy during the transition can be calculated by using the equation $\Delta G=-RTln(K_{eq})$, where R is the universal gas constant, T is the absolute temperature, and $K_{eq}=(1-I_{ss})/I_{ss}$. – the steady-state distribution of sodium channels in the inactivated↔not-inactivated states.

Looking at a protein with two mutations (A and B) introduced separately at different sites and the double mutant (AB), the following considerations can be made. The change in the free energy (ΔG) for independent mutations should be a state (or

potential) function that depends only on the initial and final energy of the system and not on the path that is taken between the states. In this case, the four states of the system are WT, A, B, and the double mutant AB. The sum of $\Delta(\Delta G)$ in either direction around the cycle must be the same, so that $\Delta(\Delta G)$ from WT→A + A→AB must equal the sum of $\Delta(\Delta G)$ from WT→B + B→AB. If mutations A and B are acting independently, then the sum of $\Delta(\Delta G)$ from WT→A + WT→B should also equal the sum of $\Delta(\Delta G)$ from WT→B + B→AB. The opposite case suggests possible functional interactions between the two single mutants.

2.2.5.4. Statistics

All data are shown as means±standard error of the mean if not indicated otherwise. Independent Student´s T-test was used to test for statistically significant differences between WT and mutant channels.

3. FUNCTIONAL CHARACTERIZATION OF A BFNC-CAUSING MUTATION IN THE *KCNQ2* GENE

The 1bp deletion 2513delG (see Introduction) was introduced in the cDNA of *KCNQ2* by site-directed mutagenesis and both WT and mutant channels were expressed in *Xenopus laevis* oocytes. Potassium currents activated slowly at potentials more positive than –50 mV (fig 11A).

3.1. Current Amplitude

A striking difference between WT and mutant channels was seen in current amplitude: currents derived from 2513delG had on average less than 5% of the WT amplitude (0.16 ± 0.01 µA (n=16) vs. 3.8 ± 0.6 µA (n=13) at the end of a 4-s depolarizing test pulse to +10 mV, fig. 11A). Co-expression of WT and mutant channels yielded an average current amplitude of 1.3 ± 0.2 µA (n=12), not

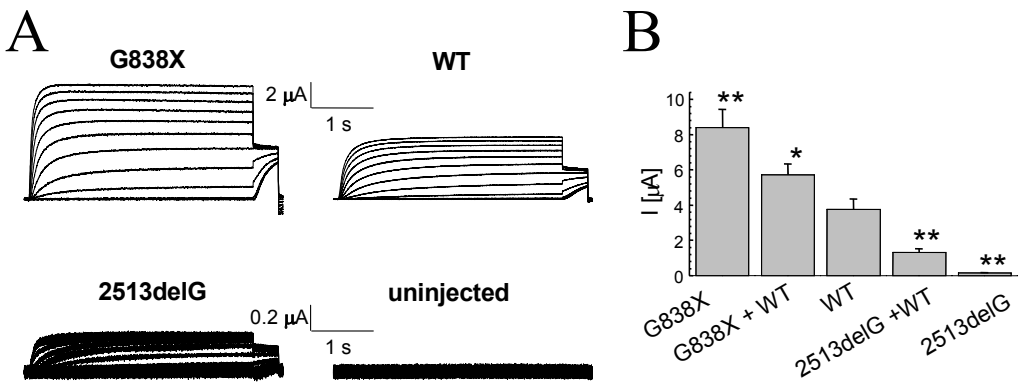

Figure 11. Current density for expressed WT and mutant channels. **(A)** Representative raw current traces at –80 to +20 mV as recorded from Xenopus laevis oocytes injected with either WT or mutant *KCNQ2* cRNA and from an uninjected oocyte. The scaling for 'G838X' and 'WT' is 10 fold bigger than for '2513delG' and 'uninjected'. **(B)** Current amplitudes determined at the end of a 4-s depolarizing test pulse to +10 mV for all three clones and a 1:1 mixture of each mutant with WT, when approximately the same total amount of cRNA was injected into each oocyte. Oocytes were injected and measured on the same day (see Materials and methods). Statistically significant differences to the WT are indicated as follows: * $p < 0.05$, ** $p < 0.001$, n = 12-16.

supporting a significant dominant negative effect of the mutation ($p > 0.05$)(fig. 11B).

3.2. Activation and deactivation

There was no significant change in the voltage dependence nor the kinetics of currents derived from 2513delG mutant channels when compared to the WT. The activation curve revealed a half-maximal activation $V_{0.5}$ at –41 ± 1 mV for the WT

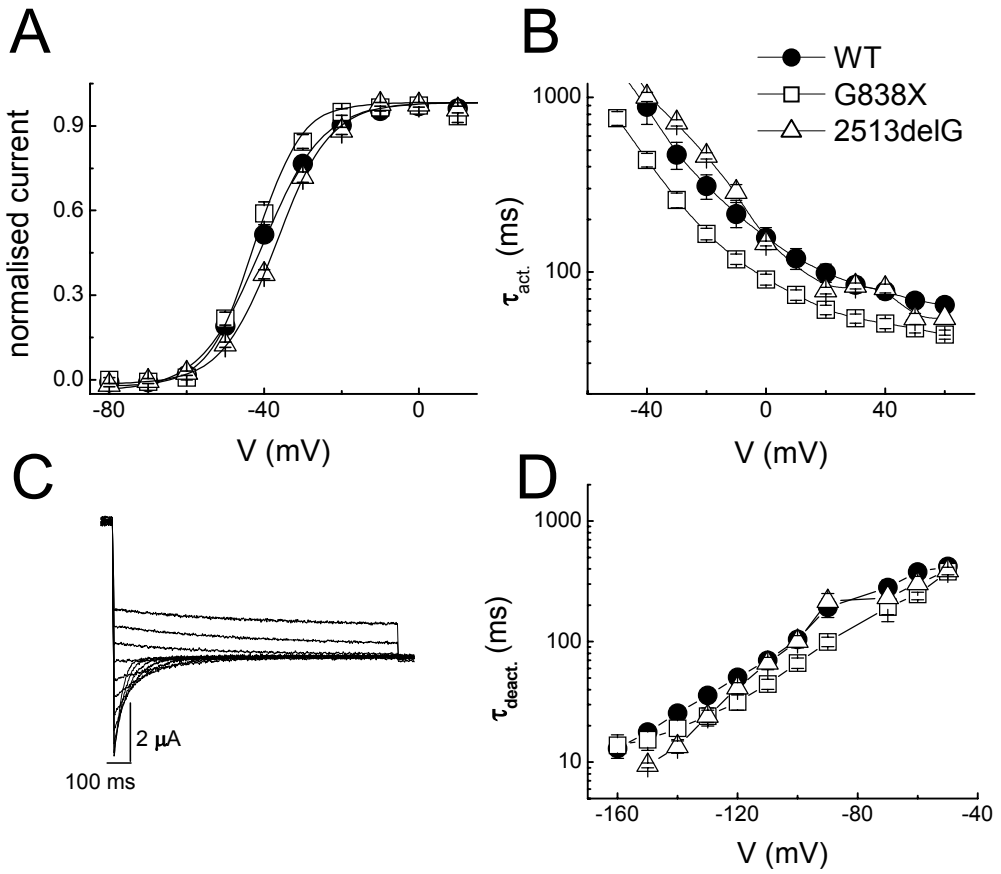

Figure 12. Activation parameters. **(A)** Activation curves for all three clones as obtained from tail current amplitudes at –30 mV. Parameters are as follows: $V_{0.5}$ = -41 ± 1 mV, -42 ± 1 mV, -37 ± 1 mV; k = 7.9 ± 0.5 mV, 5.9 ± 0.4 mV, 7.0 ± 0.2 mV for WT, G838X and 2513delG, respectively, n = 13-22. **(B)** Time constant of activation τ_{act}, n = 9-15. The difference between G838X and WT is statistically significant (e.g. at +10 mV: $\tau_{act.}$ = 74 ± 5 ms vs. 120 ± 16 ms, $p < 0.05$, n = 10, 12). **(C)** Tail current traces recorded after a 2-s depolarization to +20 mV at test potentials between –50 and –160 mV from an oocyte injected with WT cRNA. **(D)**. The deactivation time constant, $\tau_{deact.}$. The difference between G838X and WT, seen almost throughout the whole voltage range, was not statistically significant (e.g. at –100 mV $p = 0.0504$).

and –37 ± 1 mV for the mutant, respectively, n=13,22 (fig. 12A). Current activation was well fit to a first order exponential function yielding the time constant $\tau_{act.}$ (fig. 12B). Deactivation was measured at various test potentials after a 2-s activating pulse to +20 mV (fig. 12C). Tail currents were also well fit to a first order exponential throughout the whole voltage range, yielding the deactivation time constant $\tau_{deact.}$ (fig. 12D). The reversal potential, as derived from a tail current analysis, was not significantly changed (-74 ± 2 mV for the WT vs. –72 ± 2 mV for 2513delG), indicating that the pore properties of the channel were not affected by the mutation.

3.3. Evaluation of the Role of the C-terminal part of the *KCNQ2* channel

To evaluate if the additional 56 amino acids, or just the loss of the last seven regular residues caused the reduction in current amplitude of the 2513delG mutant channel, a second mutation with a stop codon at position 838 was constructed (‘G838X’). This mutation yielded potassium currents with a twofold increase in amplitude compared to the WT (8.4 ± 1.1 µA, n=12, fig. 11A and B). In addition, G838X slightly accelerated activation and deactivation throughout the whole voltage range, albeit the latter not significantly (Figs. 12B and D). The reversal potential was determined to –71 ± 2 mV, which is not significantly different from those of the two other clones. The data indicate, that it is the pathological extension of the mutant protein, and not the loss of the last seven regular C-terminal amino acids that produce the phenotype.

4. EXPRESSION AND FUNCTIONAL CHARACTERIZATION OF TWO MUTATIONS IN THE *SCN1A* GENE CAUSING GEFS+

To study the functional consequences of the two *SCN1A* mutations causing GEFS+ (Escayg et al., 2000), following mutations were introduced in the *SCN4A* gene predicting the following amino acid substitutions in $Na_v1.4$: T685M and R1460H corresponding to T875M and R1648H in $Na_v1.1$. WT and mutant channels were transiently expressed in tsA201 cells and electrophysiologically characterized. Families of whole cell currents for WT and mutant T685M and R1460H channels elicited by various depolarizing steps from a holding potential of –140 mV are shown in fig. 13. In order to look for differences in gating between WT and mutant channels that may explain the occurrence of epileptic seizures, the kinetics and voltage dependence of activation, deactivation and fast and slow inactivation were determined.

4.1. Fast inactivation

Comparison of the non-inactivating fraction of sodium channels (so-called “persistent current”) revealed no differences between WT and mutant channels (see fig. 13). The persistent current level was determined by the ratio of the sodium current at the end of 70ms depolarizing test pulses to the peak current: I_{ss}/I_{peak} at –20mV for WT vs. T685M and R1460H, respectively: 0.6±0.2% vs. 0.8±0.5% and 0.7±0.3%, n=7, 8, 16. For the R1460H mutation there was a small but significant slowing of fast inactivation at depolarized potentials and a marked decrease of its voltage dependence, while the T685M mutation showed no differences compared to the WT (fig. 14A). The loss of voltage dependence has already been described for other mutations in D4S4 and may indicate an

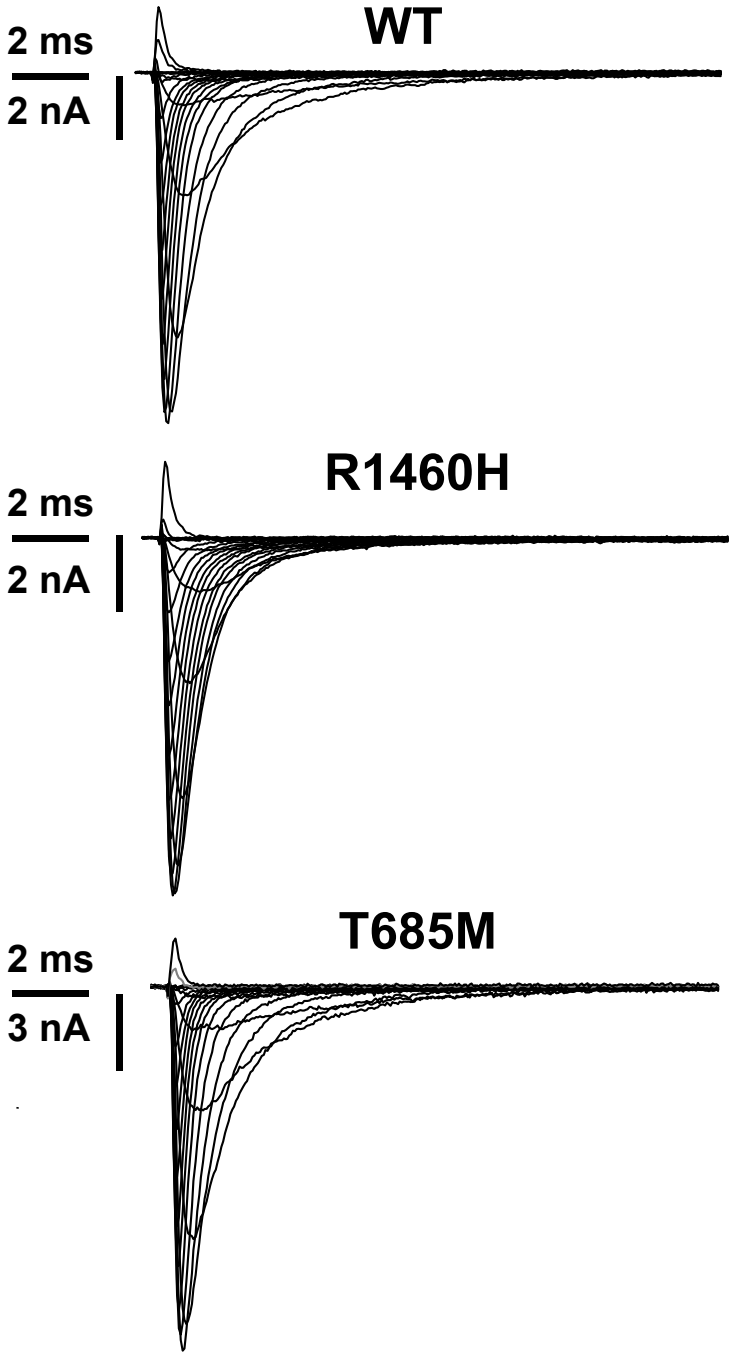

Figure 13. Representative whole cell sodium current families recorded from cells transfected with either WT or mutant channels.

uncoupling of inactivation from activation (Chahine et al,. 1994; Lerche et al., 1996; Mitrovic et al., 1999). The recovery from fast inactivation at –100, -120 and –140 mV after a 100 ms depolarizing pulse at 0 mV is shown in fig. 14B. For the T685M mutation the recovery was not changed, but for the R1460H mutation

τ_{rec} was decreased by about 3-fold at –100 mV. Steady state fast inactivation was shifted towards hyperpolarized potentials for both mutations (fig. 14C).

Both, the slowing of fast inactivation and the acceleration of its recovery in the

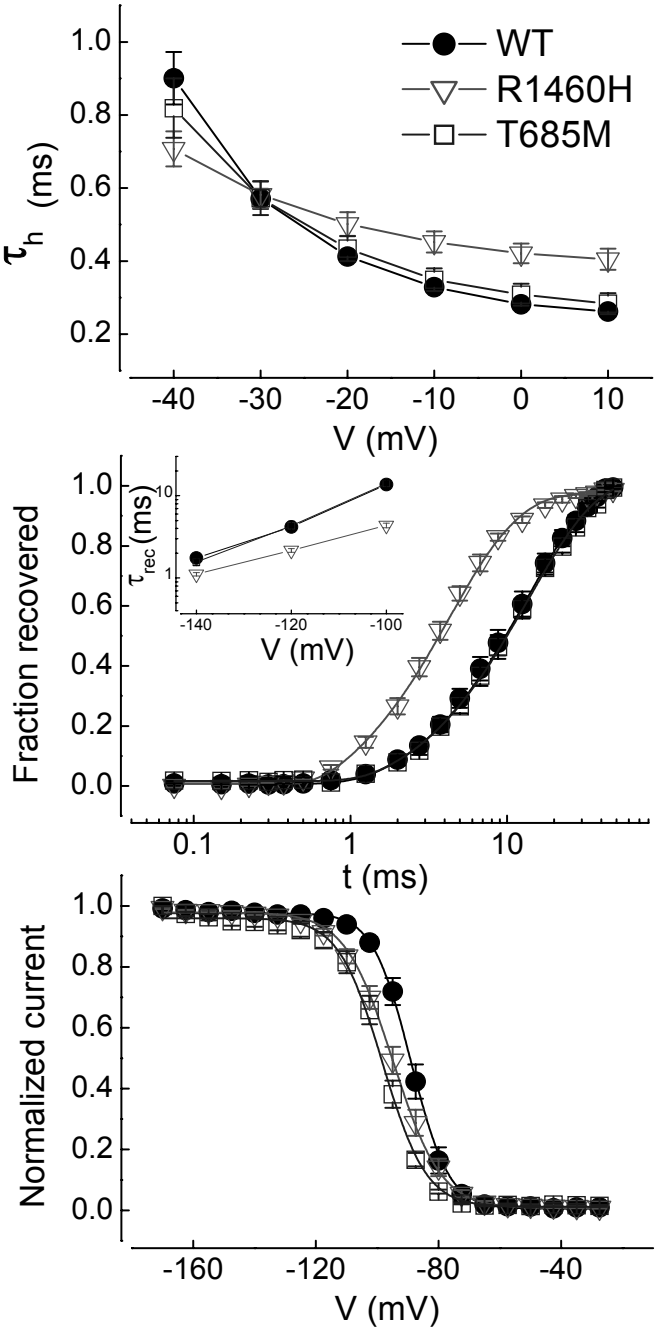

Figure 14. Fast inactivation. **(A)** Voltage dependence of the inactivation time constant, $\tau_{h.}$ Values at 0mV were 0.28±0.01 (WT, n=8) vs. 0.31±0.01ms (T685M, n=8) vs. 0.42±0.03ms (R1460H,n=14, p<0.001). **(B)** Time course of recovery at –100mV. Insert shows time constants at –100, -120 and –140mV. **(C)** Steady state fast inactivation. $V_{0.5}$: –98.3±1.3mV, n=9 ,p<0.001 and –96.0±1.6mV, n=16, p<0.02 vs. –89.0±1.4, n=7 for T685M and R1460H mutations vs. WT; k_V: 6.5±0.4mV, n=9 and 7.2±0.2mV,n=16, p<0.001 vs. 5.5±0.3, n=7 for the T685M and R1460H mutations vs. WT.

case of the R1460H mutation increase excitability as has been previously shown for *SCN4A* mutations causing myotonia. In contrast, the hyperpolarized shift in the steady-state inactivation curve is stabilizes the inactivated state and in this way would decrease membrane excitability.

4.2. Activation and deactivation

For better resolution of the activation and deactivation kinetics, measurements were performed at 14.5±0.5°C. For quantification of the activation time course, the 10-90% rise time was calculated. There was a significant acceleration of the activation time course for the T685M and R1460H mutant channels compared to WT between –52.5 and –30mV (fig. 15A). The currents of the T685M mutation were additionally fitted to a Hodgkin-Huxley function (m^4h, Hodgkin and Huxley, 1952) to determine the activation time constant τ_m (fig. 15B).

The voltage dependence of activation was not changed. The steady state activation curve of the R1460H mutation exhibited a slightly decreased slope (fig. 15C).

The time constants of deactivation τ_{deact} were almost identical for WT and the two investigated mutations (fig. 16).

4.3. Slow inactivation

Steady-state slow inactivation was shifted in the hyperpolarizing direction for both mutations: $V_{0.5}$ -70.9±1.5mV,n=6 vs. –90.1±2.1mV, n=5, $p<0.001$ and vs. –80.9±2.1mV, n=4, $p<0.02$ for WT, T685M and R1460H mutation respectively (fig. 17A). This markedly stabilization of the slow inactivated state indicated by the –20mV (T685) and –10mV (R1460H) shifts in the voltage dependence would decrease the effective number of excitable channels and this way decrease

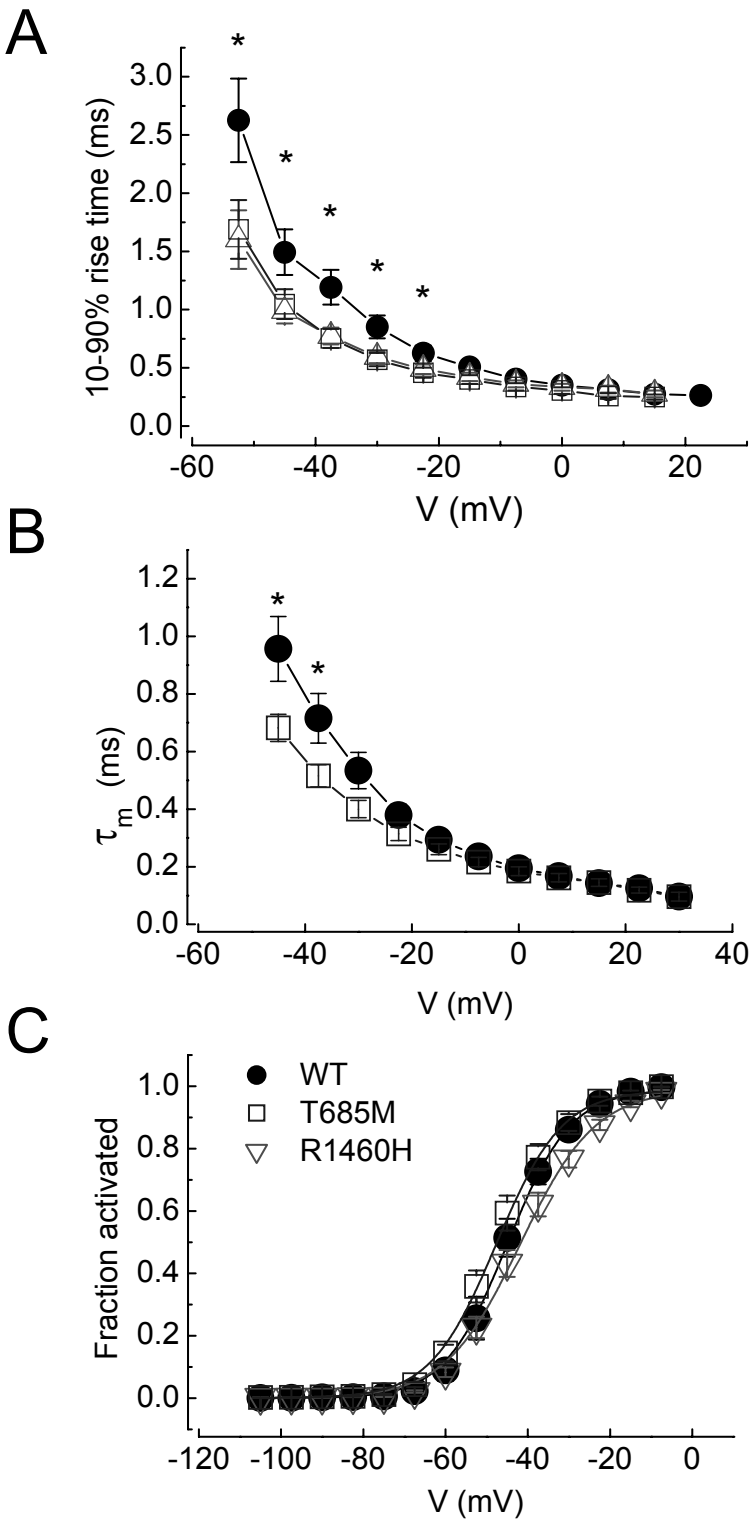

Figure 15. Activation parameters. **(A)** 10%-90% rise time of the sodium current as a function of test potential. The differences between –52.5 and –30mV among mutant and WT channels are statistically significant at $p<0.05$; n=8, 8, 7 for the T685M and R1460H mutations vs. WT, T=15°C. **(B)** τ_m, of the sodium current for the T685M mutations as a function of test potential at 15°C. **(C)** Voltage dependence of activation for WT and mutant sodium channels, obtained by 25ms depolarizing pulses to the indicated potentials from a holding potential of –140mV: $V_{0.5}$ was –47.6±2.1mV, n=11 and –44.4±2.1mV, n=6, vs. –45.3±1.9, n=7 for the T685M and R1460H mutations vs. WT; k_V was 6.7±0.3mV, n=11 and 7.8±0.2mV, n=6, $p<0.01$ vs. 6.2±0.3, n=7 for the T685M and R1460H mutations.

neuronal excitability. The entry into the slow inactivated state was not changed for the R1460H mutation but was 3 fold accelerated for the T685M mutation (fig 17B). The recovery from slow inactivation was significantly slowed for both mutants (fig 17C).

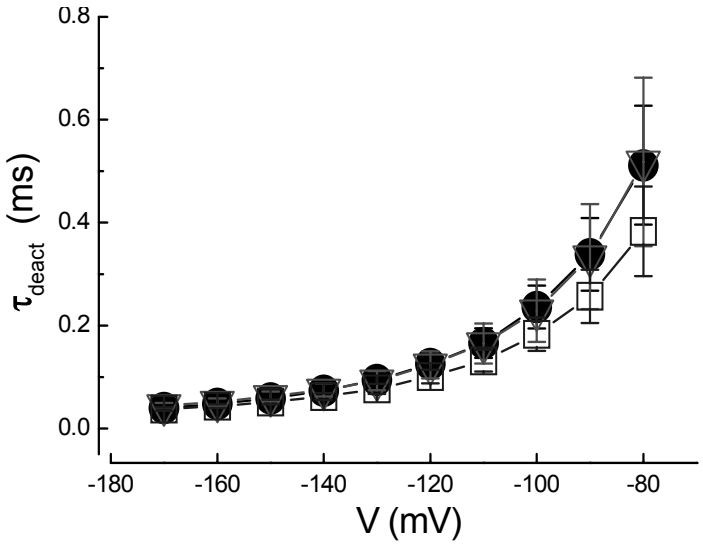

Figure 16. Voltage dependence of the deactivation time constant, τ_{deact}. Values at all potentials were not significantly different from WT, n=4, p>0.05, T=15°C.

4.4. Effects of pH on R1460H mutation

The protonation state of the amino acid histidine is dependent on the pH of the environment (Starace *et al.*, 1997; Bezanilla *et al.*, 2001). The pK of the histidine in an average protein environment is around 6.9. It has been shown for other arginine to histidine mutations in D2S4 and D4S4, that pH changes affect channel gating (Kuzmenkin *et al.*, 2002; Chahine *et al.*, 1994). R1460 is the fifth arginine in D4S4 and is exposed and accessible only from the intracellular side of the membrane (Yang et al. 1996). The gating of the R1460H mutation was examined at intracellular pH 6.2 and 8.5 in order to detect possible effects of pH. There were no changes in activation, deactivation, fast or slow inactivation. This indicates that functional alterations of the R1460H mutation are rather caused by steric effects than by charge neutralization.

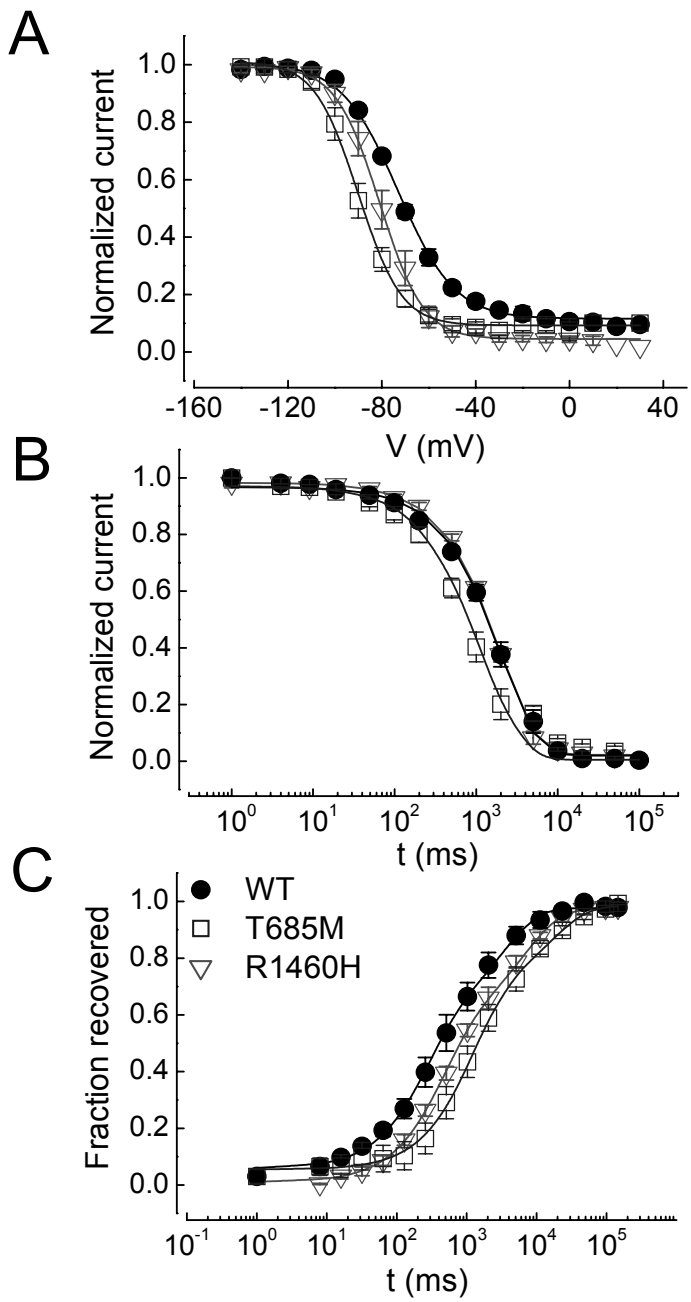

Figure 17. Parameters of slow inactivation. **(A)** Steady-state slow inactivation parameters. **(B)** Entry into slow inactivation at 0mV. Time constants were : 0.9±0.1s, n=5, p<0.001 and 1.9±0.3, n=3 vs. 2.2±0.1s, n=6 for the T685M and R1460H vs. WT. **(C)** Time constants and relative amplitudes of the recovery from slow inactivation at –100mV:

•Mutation	τ_{srec1}(s)	τ_{srec2}(s)	A_{1rel}%
•WT, n=5	0.38±0.06	9.0±3.4	58±2
•T685M, n=8	0.93±0.14, p<0.05	13.0±1.4	61±3
•R1460H, n=5	0.46±0.06, p<0.05	7.5±1.3s	56±4

5. ROLE OF THE D4/S4-S5 LOOP IN SODIUM CHANNEL FAST AND SLOW INACTIVATION

5.1. ASSESSMENT OF A DIRECT INTERACTION OF D4/S4-S5 WITH THE INACTIVATION PARTICLE IFM OF THE SODIUM CHANNEL

In order to examine a possible cooperativity between D4/S4-S5 and the inactivation particle of the Na^+ channel, two mutations in the human skeletal muscle sodium channel ($Na_V1.4$) located in the D4/S4-S5 loop (L1482C and F1473C) were combined with a mutation in the center of the proposed inactivation particle (F1311C). The position of the mutants was chosen according to results of our group from a previous study of the D4/S4-S5 loop (Lerche *et al*., 1997), where the L1482C and F1473C mutations showed significant increase of the non-inactivating sodium current. The WT, single and double mutants were heterologously expressed in *Xenopus Laevis* oocytes, they were electrophysiologically characterized using the TEVC technique, and double mutant cycle analysis was performed, using I_{ss} to calculate the change in the Gibbs energy $\Delta G=RTln(1-I_{ss}/I_{ss})$ (see Materials and methods, section 2.2.5.4.).

5.1.1. Activation and fast inactivation

Whole cell Na^+ currents for mutant and WT channels were elicited by voltage steps from a holding potential of –85 mV using 300-ms prepulses to –120 mV. The single mutants from the D4/S4-S5 loop did not change significantly the voltage dependence of activation (data not shown), which is in line with the previous study (Lerche *et al.,* 1997). Fast inactivation was impaired by all studied mutants (fig. 18). The F1473C/F1311C mutations had a more prominent effect on the time constant of fast inactivation, while the L1482C/F1311C mutant introduced the largest

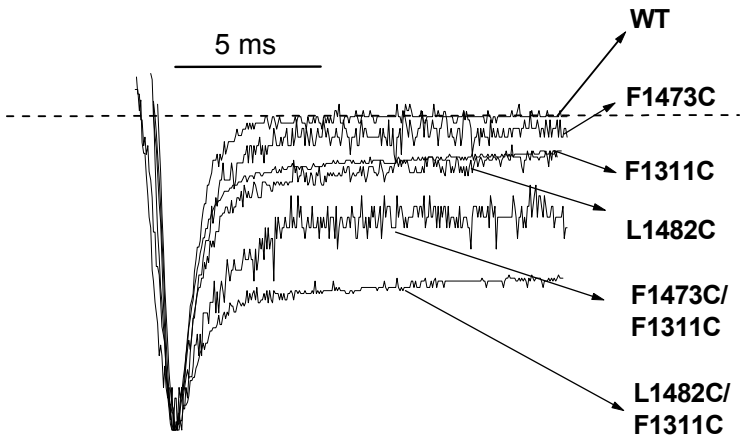

Figure 18. Normalized representative current traces obtained by depolarizing pulses to –7.5mV (peak current). The dashed line indicates the zero current.

persistent current. The voltage dependence of the fast inactivation was shifted to the left for all studied mutants, hence the fast inactivation state was destabilized (table 2, fig. 19A).

Table 2. Fit parameters of steady-state fast inactivation

	$V_{0.5}$ (mV)	K (mV)	C
WT, n=5	-59.2±2.3	5.2±0.4	0.02±0.02
F1311C, n=5	-43.4±2.7	4.9±0.4	0.10±0.04
F1473C, n=13	-51.2±0.8	4.7±0.1	0.05±0.01
F1473C/F1311C, n=5	-33.4±0.8	4.2±0.5	0.30±0.03
L1482C, n=5	-46.7±1.8	5.1±0.4	0.04±0.01
L1482C/F1311C, n=6	-38±1	6.8±0.7	0.36±0.03

The time constant of fast inactivation , τ_h, was significantly slowed for F1311C and both double mutants (fig. 19B, table 3). It's amplitude accounted for >80% of the total current amplitude, except for the two double mutants, where the non-inactivating component dominated (fig 19C). Recovery from fast inactivation was accelerated for all mutants except for F1473C. Values for recovery at –100 mV were: WT – 1.17±0.07ms, n=5; L1482C – 0.59±0.04 ms, n=7, p<0.0001; F1473C – 1.29±0.09 ms, n=11, p>0.1; F1473C/F1311C – 0.40±0.04 ms, n=11, p<0.0001; L1482C/F1311C – 0.80±0.09 ms, n=2, p<0.05 (fig. 19D).

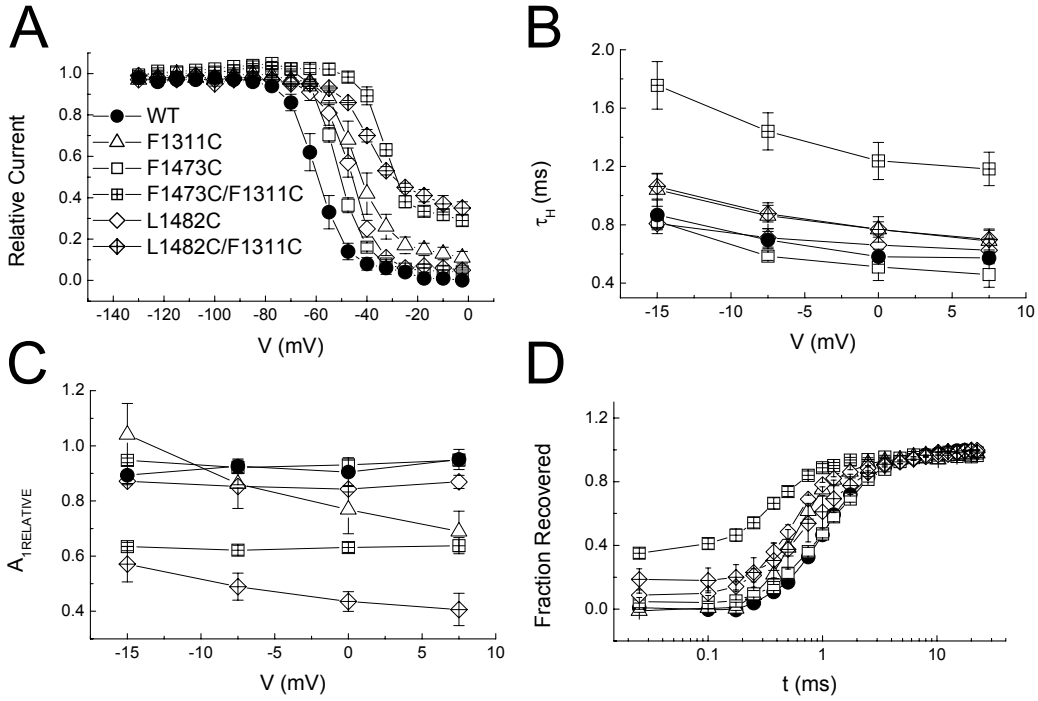

Figure 19. Fast inactivation. **(A)** Steady state fast inactivation. **(B)** Voltage dependence of the fast time constant τ_H. **(C)** Relative amplitude of the fast time constant $A_{1RELATIVE}$. **(D)** Time course of recovery from fast inactivation at –100mV after 100-ms depolarizing pulses to 0mV.

5.1.2. Double mutant cycle analysis

The persistent current for WT and each mutant was calculated using the ratio of the constant term from the fit of the current decay divided by the sum of the faster, slower and constant term component. These values were used to evaluate the

energetic effect of the mutations by the double mutant cycle analysis (see Materials and Methods). The obtained values are represented in table 3.

Table 3. ***Fit parameters of fast inactivation and calculated rate constants. Values for Kon, Koff. Keq and ⊿(G) are represented as mean±SD***

Mutation	τ_f (ms)	I_{ss}	K_{on} (s^{-1}) $K_{on}=(1-I_{ss})/\tau_f$	K_{off} (s^{-1}) $K_{off}=I_{ss}/\tau_f$	K_{eq} $K_{eq}=(1-I_{ss})/I_{ssf}$	ΔG (kJ/mol)
WT ,n=6	0.72±0.07	0.011±0.005	1500±200	15±6	220±70	-12.2±1.1
F1311C, n=5	0.9±0.1	0.11±0.01	100±100	127±15	8±1	-5.1±0.3
F1473C, n=5	0.46±0.06	0.011±0.001	2300±300	27±4	88±12	-10.9±0.3
F1473C/F1311C, n=8	1.4±0.1	0.29±0.02	530±70	210±13	2.5±0.2	-2.2±0.2
L1482C, n=5	0.73±0.09	0.057±0.005	1400±200	80±5	17±2	-6.9±0.3
L1482C/F1311C, n=5	0.89±0.06	0.38±0.04	730±80	430±50	1.8±0.2	-1.3±0.5

Mutant cycles were constructed for both double mutants. The differences *⊿(⊿G)* are considered to represent the coupling energies for the two mutations in each cycle (Carter *et al*.,1994). Both cycles resulted in small, but not significant coupling energies (fig. 20).

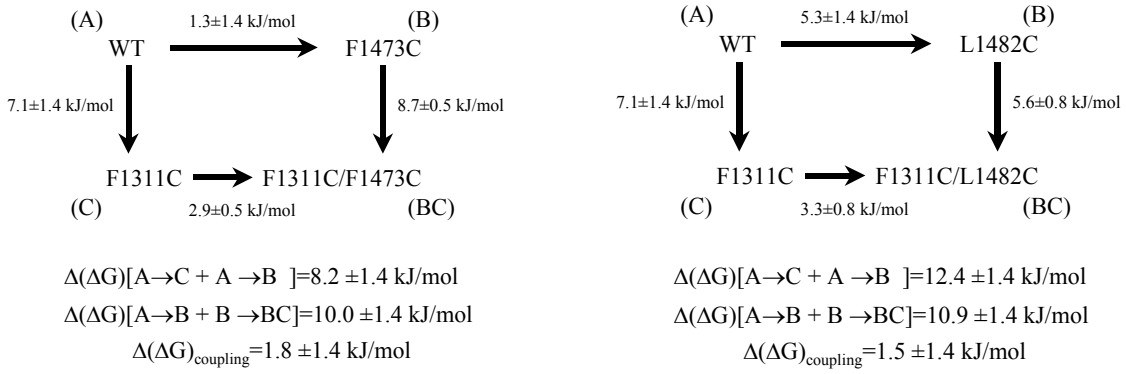

Figure 20. Double mutant cycles showing possible interactions between mutations in the D4/S45 loop and the proposed inactivation ball.

5.2. EVALUATION OF THE ROLE OF THE D4/S4-S5 IN SLOW INACTIVATION

A previous study of our group (Lerche *et al.,* 1997) suggested changes in slow inactivation due to mutations in the loop D4/S4-S5 of $Na_v1.4$. In order to evaluate these changes in more detail, the mutations L1482A and L1482C were expressed in tsA201 cells and the effects on channel gating were investigated.

5.2.1. Activation and fast inactivation

Whole cell Na^+ currents for mutant and WT channels were elicited by voltage steps from a holding potential of –85 mV using 300-ms-prepulses to –120 mV. Representative raw current traces for all three clones are shown in Fig. 21A. The time constant of fast inactivation , τ_h, was slightly but significantly increased for L1482A but not for L1482C channels in the range 0 to 52.5 mV (τ_h at 0 mV for WT, L1482C and L1482A, respectively: 0.42±0.03 ms, 0.50±0.03 ms and 0.79±0.06 ms, n=14,13 and 8, $p<0.000001$).

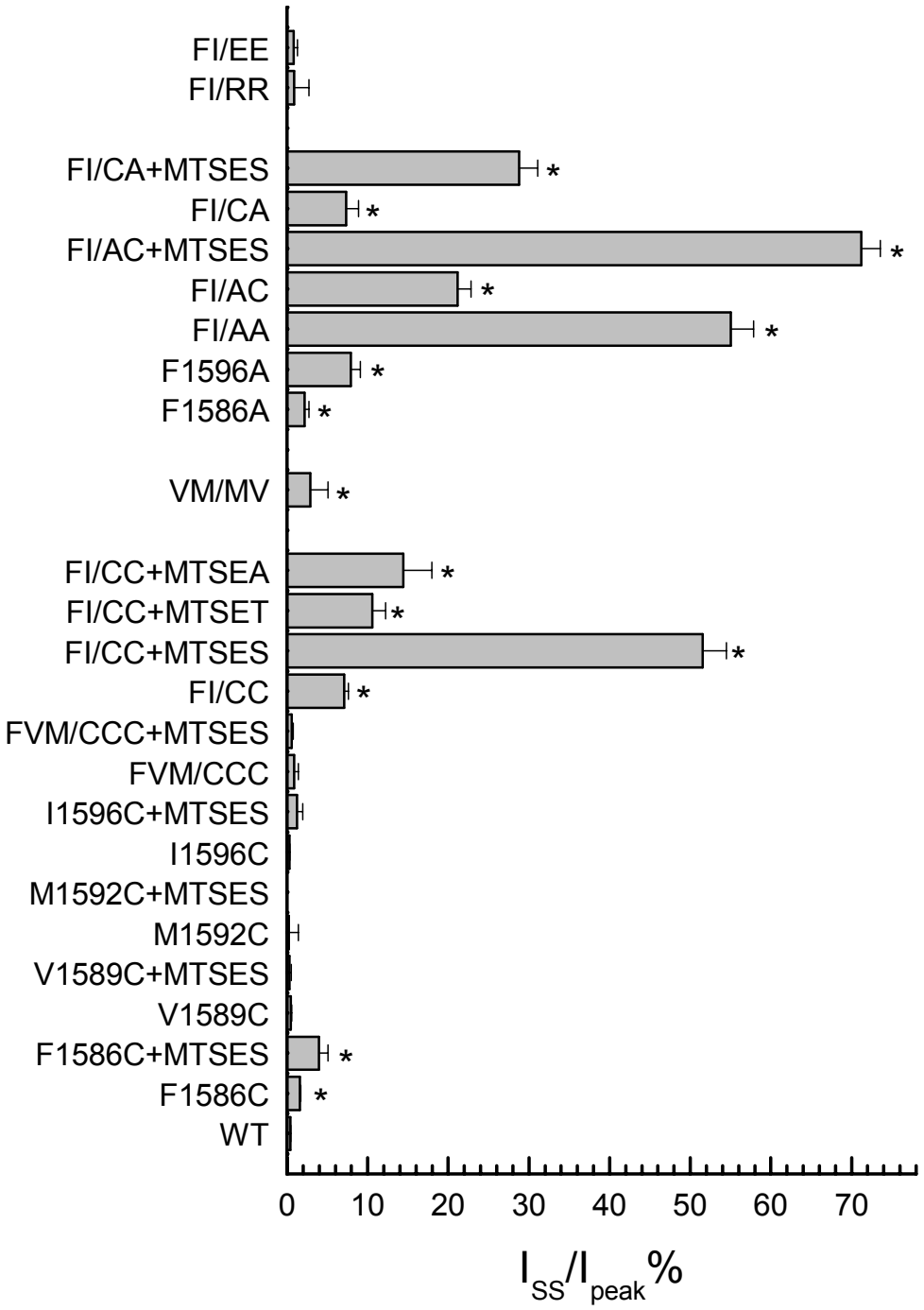

Figure 28. Persistent Na^+ current relative to the peak current determined 20 ms after onset of the depolarization for all mutations in IV/S6 examined in this study. Shown are means ± SEM. Significant differences are marked with an apteryx.

The most obvious difference between both mutants and WT was a considerable increase in persistent current: 1.5±0.3% (L1482C, n=13) and 5.1±0.9% (L1482A, n=8) of peak current, compared to 0.2±0.2% (n=14) for the WT ($p<0.001$). The

steady-state fast inactivation curve was slightly shifted in the depolarizing direction for L1482C but not L1482A channels and recovery from fast inactivation was accelerated for both clones (Figs. 21B, C). Thus, L1482A disrupts fast inactivation to a greater extend than L1482C. The shift in steady-state activation was not significant (Fig. 21B).

5.2.2. Slow inactivation

5.2.2.1. Cumulative vs. conventional Protocols

Recovery from fast and slow inactivation after a 3-s conditioning pulse to 0 mV revealed that a 100-ms period at –100 mV is sufficient to let the channels recover from FI without occurrence of significant recovery from SI (Fig. 22A). Thus, all protocols to record slow inactivation contain a 100-ms recovery pulse to –100 mV before each test pulse. To determine the parameters of slow inactivation, first a conventional pulse protocol for steady-state SI was compared with a cumulative one. Cumulative protocols reduce measuring time considerably, since the long pulses for full recovery from slow inactivation are not used (fig. 22B). There was almost no difference between the results obtained by the cumulative or conventional protocol (fig. 22C), thus cumulative protocols were used to compare mutant and WT channels.

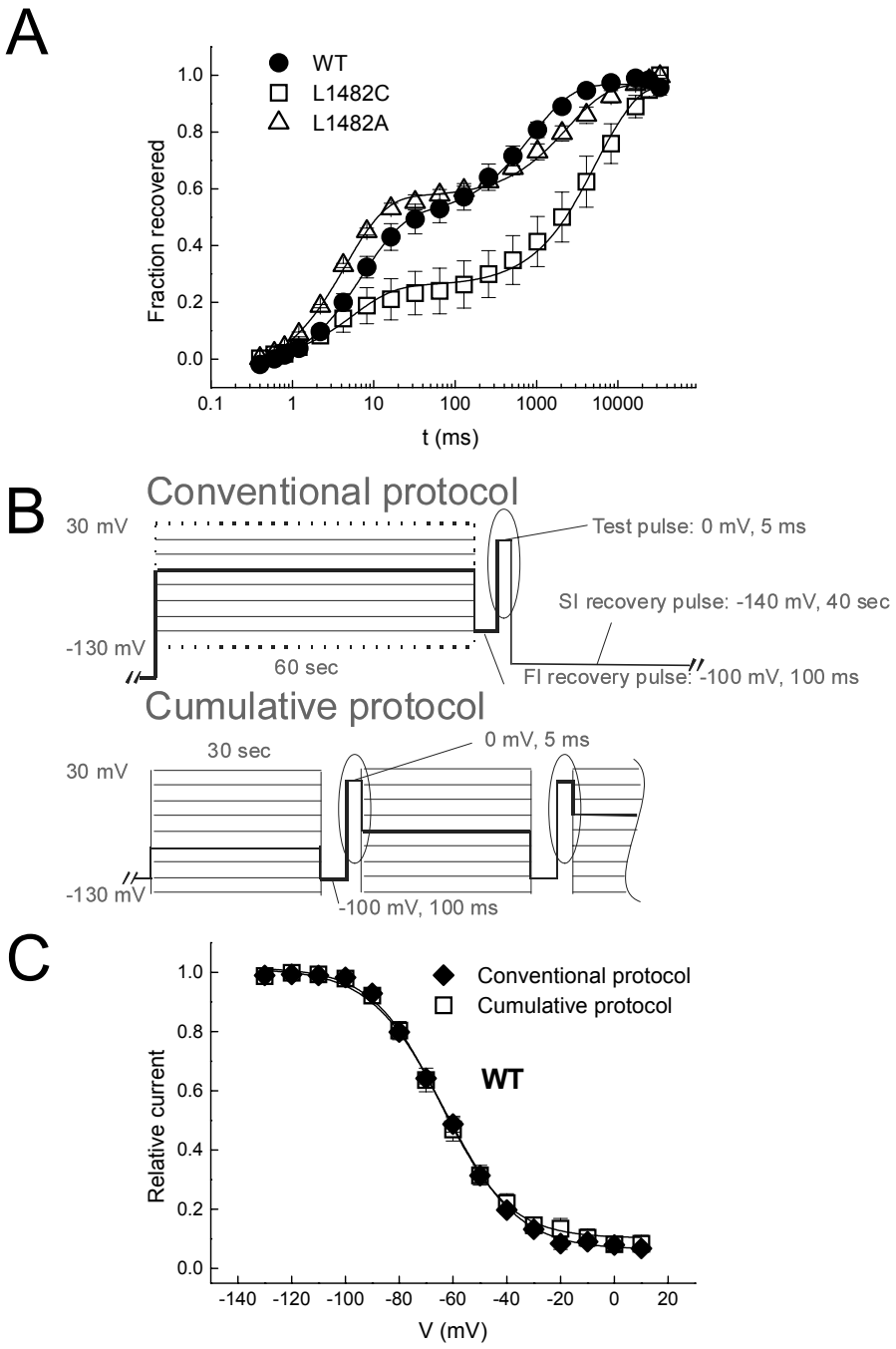

Figure 22. Cumulative vs. Conventional protocols. **(A)** Time course of recovery from fast and slow inactivation after a 3 s-conditioning pulse to 0 mV. Lines are fits to a second order exponential function for fast and slow inactivation, respectively. **(B)** Grafical representation of the conventional and cumulative protocols. **(C)** Steady state slow inactivation as measured by the conventional and cumulative protocol. Parameters were $V_{0.5}$: -62±2 vs. -64±3 mV; k_V: 13±1 vs. 12±1 mV ; n=7, 6 for the conventional and cumulative protocols, respectively.

5.2.2.2. Slow inactivation parameters

Steady-state slow inactivation was significantly different for both mutations (fig. 23A). The most obvious differences were a complete SI for the mutants, compared to 9±3% (at 0 mV) of WT channels that did not enter the slow inactivated state and a difference in slope of the availability curve. The midpoints of steady-state slow

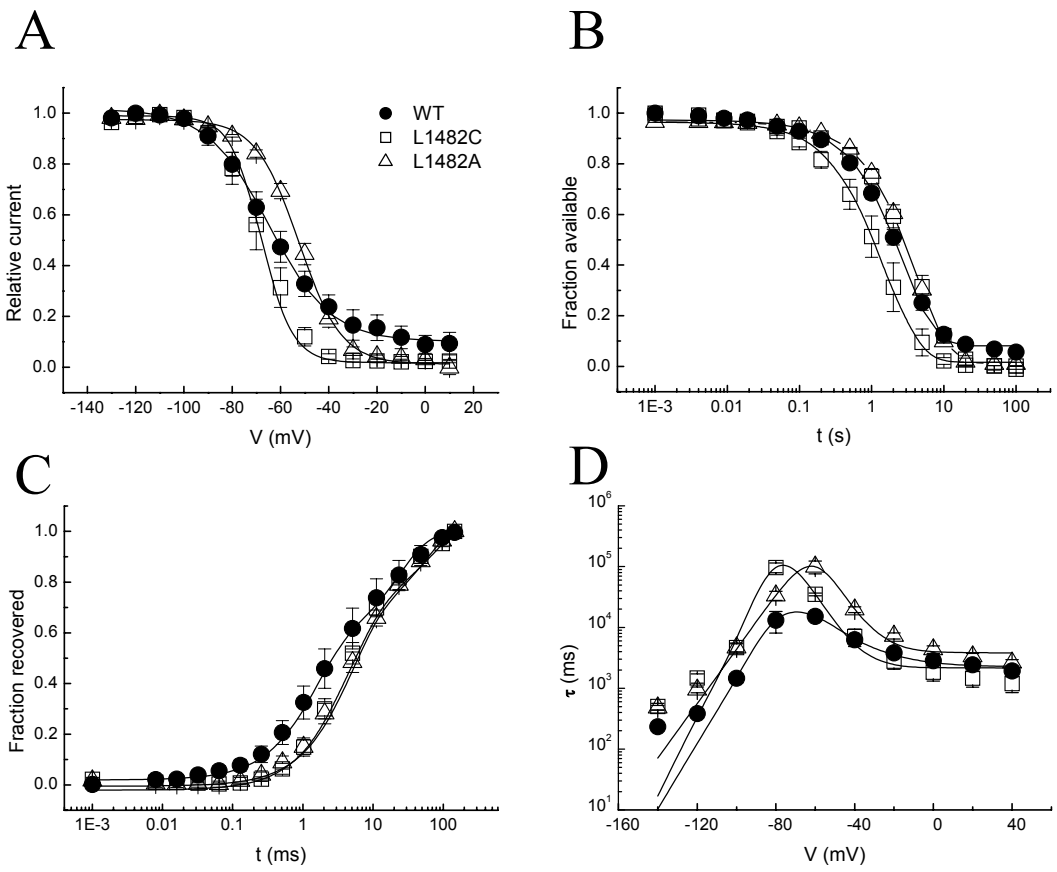

Figure 23. Slow inactivation parameters. **(A)** Steady state slow inactivation curve for WT, L1482C and L1482A channels, measured with the cumulative protocol. The values for WT vs. L1482C and L1482A are: $V_{0.5}$: -64±3 vs. -67±3 and -53±1 mV (p<0.01); $k_{0.5}$: 12.2±0.5 vs. 6.5±0.4 (p<0.000001) and 8.1±0.3 mV (p<0.0001); n=6,9,7. **(B)** Entry into slow inactivation at 0 mV. The time constants, τ_{sentry} for WT vs. L1482C and L1482A are: 2.8±0.2 vs. 1.8±0.5 and 4.4±0.6 s (p<0.05), n=8, 4, 6. **(C)** Recovery from slow inactivation measured at -100 mV. The time constants, τ_{srec} for WT vs. L1482C and L1482A are: τ_{srec1} = 1.5±0.2 vs. 4.7±0.7 (p<0.005) and 4.7±0.8 s (p<0.05); τ_{srec2} = 22.9±5.7 vs. 79±36 and 54±11 s. The relative amplitude of τ_{srec1}=57±6 vs. 70±2 and 66±2%, n=5, 7, 9 for WT vs. L1482C and L1482A. **(D)** Voltage dependence of time constants for entry (-60 to +40 mV) and recovery (-140 to -80 mV) of SI. The data are fit to a simple two-state kinetic model (slow inactivated, non slow inactivated) with rate constants being exponential functions of voltage: on rate $\beta=\beta_0/(1+exp(-(V-V_{0.5})/k_\beta))$, off rate $\alpha=\alpha_0 exp(-V/k_\alpha)$. Following parameters were obtained: WT: α_0=2.6x10^{-6}s^{-1}, k_α=8.0mV, β_0=0.44 s^{-1}, $V_{0.5}$=-29mV, k_β=16.8mV; L1482C: α_0=4.8x10^{-8}s^{-1}, k_α=6.7mV, β_0=0.46 s^{-1}, $V_{0.5}$=-36.9mV, k_β=8.4mV; L1482A: α_0=7.7x10^{-6}s^{-1}, k_α=9.7mV, β_0=0.26 s^{-1}, $V_{0.5}$=-27.0mV, k_β=8.9mV.

inactivation were shifted to the left for L1482C and to the right for L1482A channels. Entry into and recovery from the slow inactivated state were also determined with cumulative protocols. The time course of entry was significantly accelerated for L1482C but not for L1482A (Figs. 23B), whereas recovery from SI was significantly slowed for both mutations (Figs. 23C). The voltage dependence of entry into and recovery from SI could be well fit using a two-state Eyring model with exponential functions of voltage for entry and recovery (Fig. 23D). A discrepancy of the fit with the experimental data can be observed at potentials more negative than –100 mV. This can be explained by the fact, that the Eyring function used in the fit is considering linear dependence of the rate constants form the electric field. This assumption is not right at very hyperpolarized potentials because the weight of the higher terms (E^2, E^3 etc.) increases (Destexhe and Huguenard, 2000). Better results can be obtained by adding the higher terms to the fitting equation. The difficulty in such fitting procedures is that several possible solutions exist, thus making an unique solution impossible.

6. ROLE OF SEGMENT D4/S6 IN SODIUM CHANNEL INACTIVATION

To evaluate the role of the D4/S6 segment, the amino acids F1586, V1589, M1592 and I1596 in hSKM1 were substituted by cysteine, alanine or charged amino acids resulting in single, double or triple mutants. This aminoacids had been previously shown to be important for inactivation of voltage-gated sodium channels (see Introduction, section 1.1.1.4.). A simplified labeling for these mutations is used as follows: FI/CC stands for the double mutation F1586C/I1596C; FVM/CCC stands for the triple mutation F1586C/V1589C/M1592C etc. WT and mutant channels were transiently expressed in tsA201 cells or *Xenopus Laevis* oocytes and electrophysiologically characterized. Whole cell currents were elicited by various depolarizing steps from a holding potential of –85 mV. Inside-out macroscopic currents were recorded from a holding potential of -120 mV (see Materials and Methods).

6.1. Effect of the cysteine mutations and their modification by MTS-reagents

The first mutations to be studied were the single cysteines substitutions F1586C, V1589C, M1592C, I1596C, the double mutant FI/CC and the triple mutant FVM/CCC. In order to test accessibility of the engineered cysteines and modification of channel gating, the negatively charged MTSES (2.5 mM) and the positively charged MTSET (1 mM) and MTSEA (1 mM) reagents were applied intracellularly. Representative whole cell currents from some of the characterized mutations are shown in fig. 24. Mutation F1586C but not I1596C introduced a significant persistent current I_{ss} (values for WT, F1586C and I1596C respectively: 0.4±0.1%, n=6; 1.5±0.3, n=5, $p<0.0001$; 0.3±0.2, n=4). Application of MTS

reagents on the single cysteine mutants did not lead to an additional significant increase of the amount of noninactivating sodium current. The double mutant FI/CC introduced 7.1±0.5% persistent current (n=7) which raised to 51±3% (n=10) after application of MTSES. In contrast, the triple mutant FVM/CCC after MTSES only slowed the time course of inactivation two times without inducing a significant persistent current (values for τ_f for WT and FVM/CCC+MTSES respectively: 0.48±0.05 ms, n=5; 0.88±0.14 ms, n=4, p<0.05).

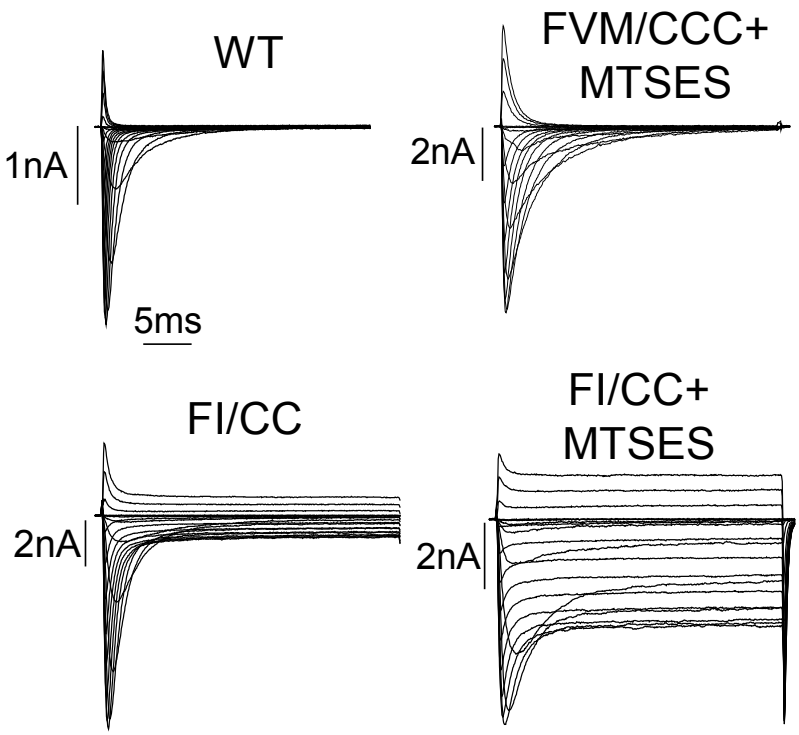

Figure 24. Representative raw current traces of WT and different cysteine mutations in IV/S6, in part after modification by MTSES.

The steady-state inactivation curve was not significantly changed. Only mutation FI/CC+MTSES shifted the voltage dependence of inactivation to more depolarized potentials (fig. 25A). The time course of fast inactivation was significantly slowed for mutants FI/CC+MTSES and FVM+MTSES and recovery from fast inactivation was significantly accelerated for mutations FI/CC, FI/CC+MTSES, FVM and FVM+MTSES (fig 25 B and C).

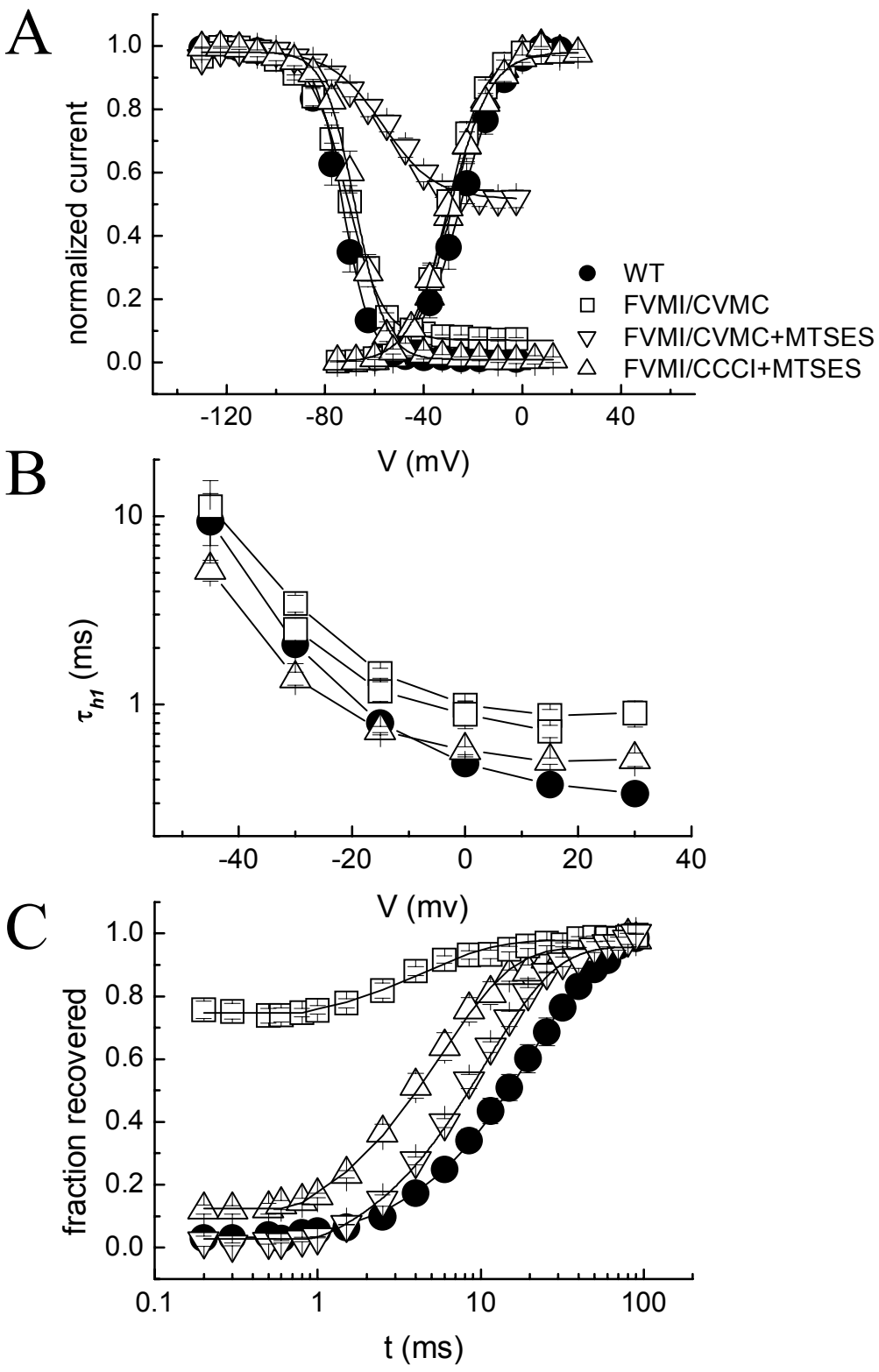

Figure 25. Activation and fast inactivation parameters of IV/S6 mutations. All values are shown as means ± SEM, n = 4-10. **(A)** Steady-state activation (open symbols) and inactivation (filled symbols) curves for the double and triple mutations indicated, before and after modification by MTSES. **(B)** Fast inactivation time constant, τ_h, as a function of voltage. Significant differences to WT were obtained by mutations FVM+MTSES and FI/CC+MTSES **(C)** Time course of recovery from inactivation at –100 mV. Significant differences to WT were obtained for all three mutations.

Interestingly, the positively charged MTS reagents (MTSET and MTSEA) did not change the I_{ss} of FI/CC but prevented further modification by MTSES (fig. 26). This finding demonstrates, that at lest one of the single mutants at position 1586 or 1596 could be modified by the positively charged reagents, but this modification did not result in destabilizing fast inactivation.

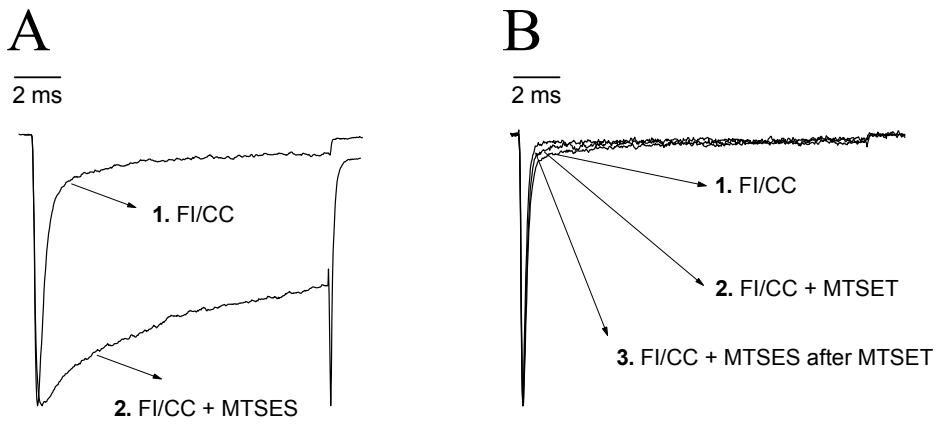

Figure 26. Reaction of the double mutant FI/CC with different thiol reagents tested in inside-out patches. **(A)** Representative recording of a macropatch before and after application of MTSES which induced a large persistent current. **(B)** In contrast, the reaction with MTSES was prevented by previous application of MTSET, which did not alter channel inactivation significantly.

6.2. Effects of the size, charge and hydrophobicity of the introduced mutations and applied reagents

To clarify the importance of positions 1586 and 1596 and the molecular mechanism underlying the observed effects on channel gating, additional mutations were constructed and studied following two main approaches:

A) Positive and negative charged amino acids were introduced at positions 1586 and 1596, resulting in the double mutations FI/RR and FI/EE.

B) To test the accessibility of both cysteines separately, we introduced alanine/cysteine double mutations (FI/CA, FI/AC, FI/AA), since we knew from a previous study using the rat brain sodium channel type IIa ($rNa_v1.2$) that a double

alanine mutation in these positions removes fast inactivation almost completely (McPhee *et al*., 1995) and since we could confirm this result in $hNa_v1.4$.

Representative whole cell families of some of the investigated mutations are shown in fig 27.

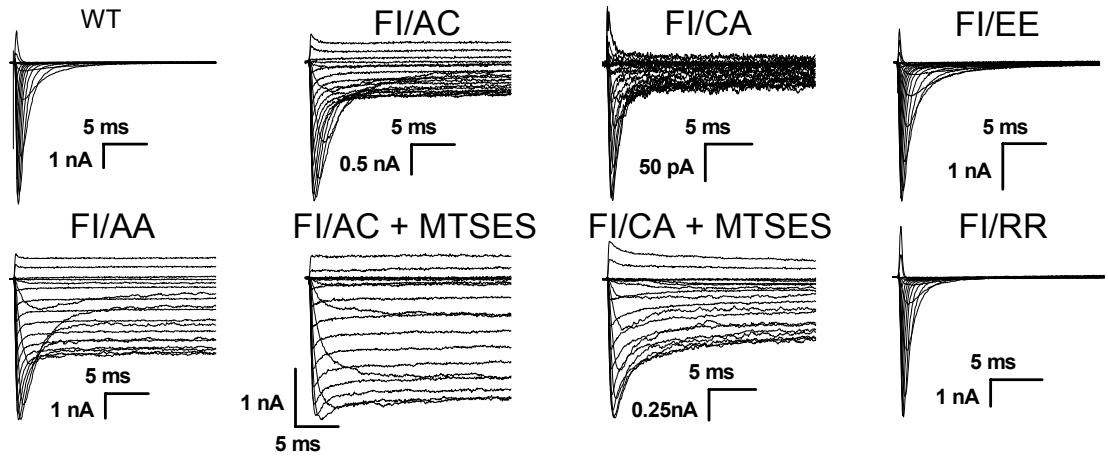

Figure 27. Representative raw current traces of WT and various other combinations of double mutations in positions F1586 and I1596.

6.2.1. Effects on fast inactivation

6.2.1.1. Persistent current I_{ss}

Many of the studied mutations induced a significant increase in the amount of non-inactivating current. The results are summarized in fig. 28. Both FI/AC and FI/CA could be further modified by MTSES (see also fig. 27), showing the functional importance of both amino acids for fast inactivation. The largest effect was observed for the FI/AC mutation after application of MTSES, the double mutant FI/AA and the double mutant FI/CC after application of MTSES. The double mutant FI/CA showed very poor expression in tsA201 cells and was expressed in *Xenopus Laevis* oocytes for evaluation. It could be modified by 1mM MTSES and exhibited a noninactivating current of 58±8%, n=2. This value can be compared to the values obtained from mutations expressed in tsA201 cells because the

persistent current of FI/CA in *Xenopus Laevis* oocytes was similar to that measured when the mutant was expressed in cells (data not shown). Additionally, the values of the persistent current for FI/CC and FI/CC+MTSES were also comparable when these mutations were expressed in cells and oocytes.

As mutations introducing two positive (FI/RR) or two negative charges (FI/EE) did not lead to a significant increase of the persistent current I_{SS}, the negative charge of MTSES when applied to FI/CC cannot be responsible for the observed removal of fast inactivation. The size of the side chain is also not crucial at these positions, since the two alanines of FI/AA almost completely abolished fast inactivation as did the large MTSES, but not the even larger MTSET. Both hydrophobic (FI/AA) and hydrophilic (FI/CC+MTSES) side chains had the largest effect on fast inactivation so that hydrophobicity is neither decisive for the observed effects.

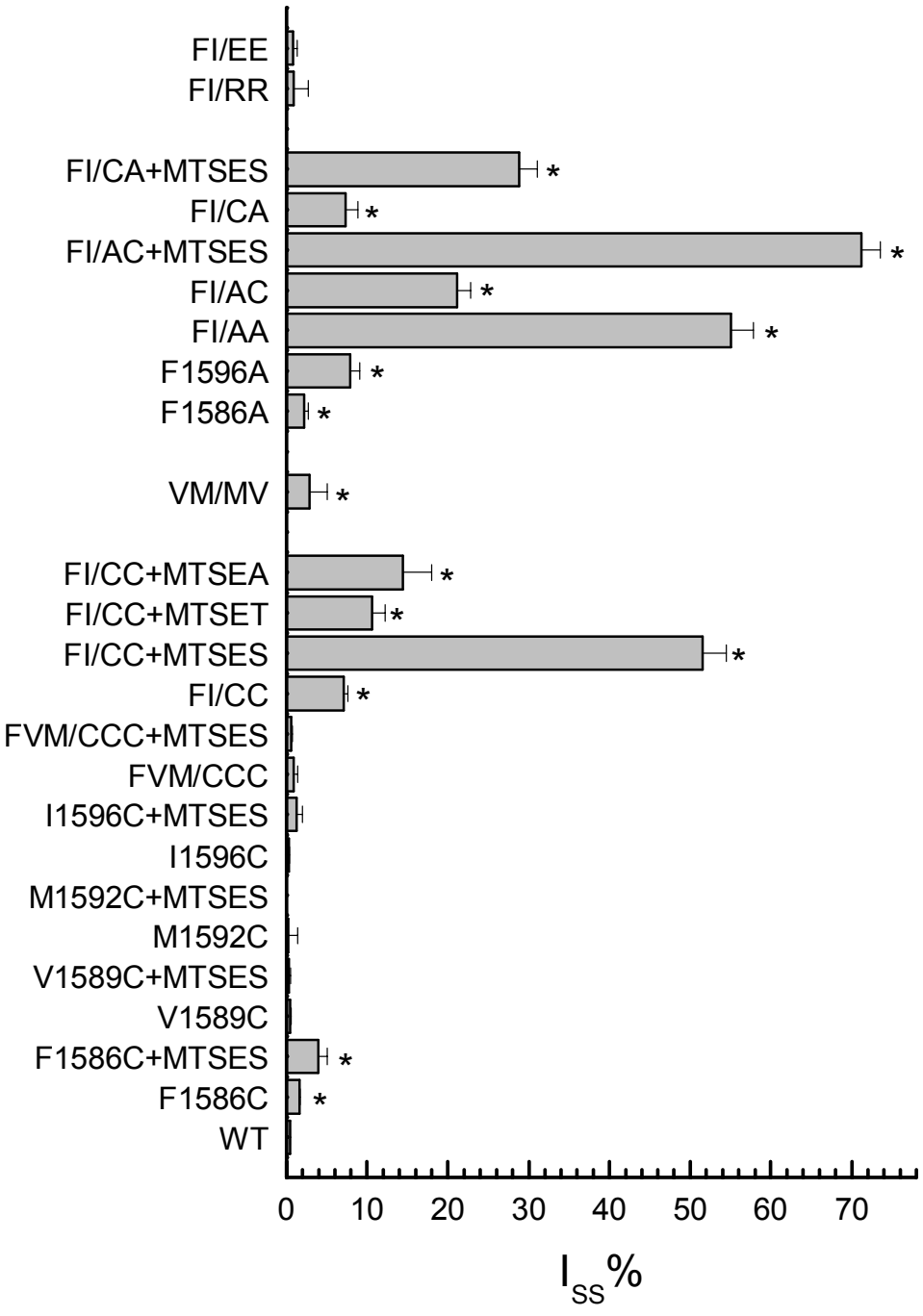

Figure 28. Persistent Na^+ current relative to the peak current determined from fit of depolarizing current traces (25ms to 0mV) for all mutations in IV/S6 examined in this study. Shown are means ± SEM. Significant differences are marked with an asteryx.

6.2.1.2. Voltage dependence of fast inactivation

The majority of the investigated mutations changed the voltage dependence of fast inactivation. Voltage shifts of the steady-state fast inactivation curve are represented in fig. 29B. Only the FI/CA mutation shifted the voltage dependence of inactivation in the hyperpolarizing direction. The main part of the mutants introduced depolarizing shifts.

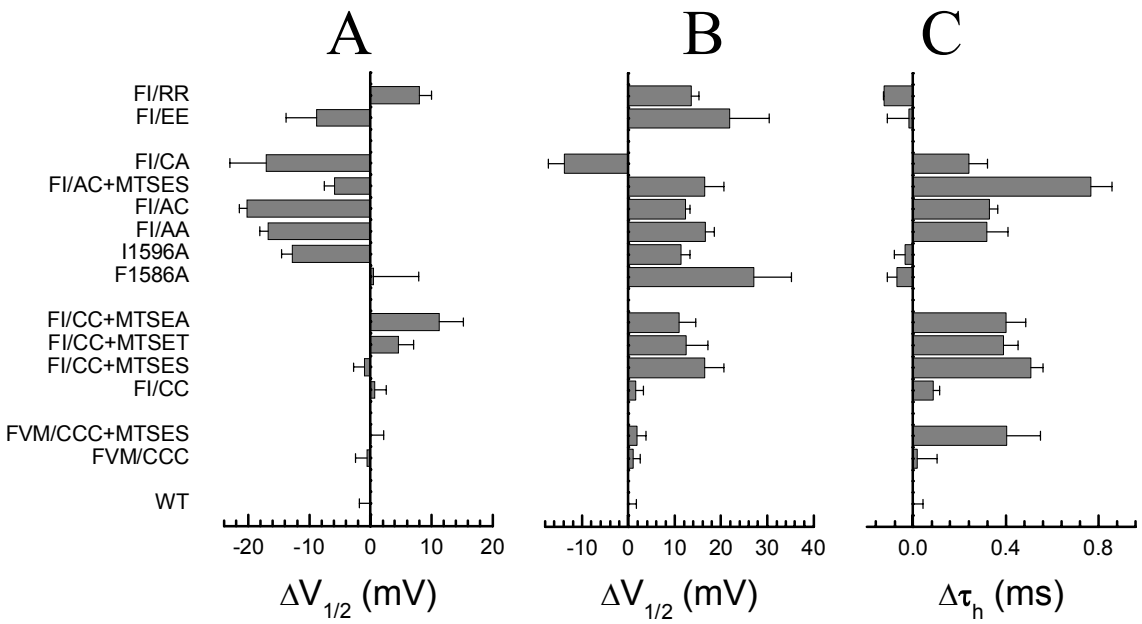

Figure 29. Summarized activation and fast inactivation parameters for some of the investigated mutations. The bars represent difference between the value for the mutations and the value for WT respectively. Shown are means ± SEM. **(A)** Changes in the voltage dependence of activation for some of the mutant sodium channels compared to WT. For WT $V_{0.5}$=-29±2mV, n=6. **(B)** Changes in the voltage dependence of fast inactivation for some of the mutant sodium channels compared to WT. For WT $V_{0.5}$=-74±2mV, n=8. **(C)** Changes in the time constant of fast inactivation for some of the mutant sodium channels compared to WT. For WT τ_f=0.48±0.04ms. n=5.

6.2.1.3. Kinetic changes in fast inactivation

The time constant of inactivation was increased for the majority of the mutants (fig 29C). The largest effects were observed while studying the double mutants, especially FI/AA, FI/AC, FI/AC + MTSES modification, FI/CA and the triple mutant

FVM/CCC after modification with MTSES (values for τ_h respectively: 0.80±0.09 ms, n=5, p<0.05; 0.81±0.03 ms, n=10, p<0.0001; 1.2±0.1 ms, n=6, p<0.0001; 0.72±0.03 ms, n=3, p<0.05; 0.88±0.14 ms, n=4, p<0.05).

Many of the investigated mutations drastically destabilized the fast inactivated state by significantly increasing the amount of persistent current, slowing the time course of fast inactivation and accelerating recovery from fast inactivation, demonstrating the importance of the region for the regulation of fast inactivation.

6.2.2. Activation and deactivation

Most of the investigated mutations drastically shifted the voltage dependence of activation in the hyperpolarizing direction but the introduction of positive charges at positions 1586 and 1596 (FI/RR and FI/CC+MTSET or MTSEA) led to the opposite effect (fig. 29A).

Deactivation kinetics were obtained from fits of the time course of tail currents at different voltages. Deactivation was markedly slowed (up to 4-fold) for mutants FI/CC, FI/AC and FI/CA+MTSES, as well as for FI/AA (fig 30). Values at -125 mV

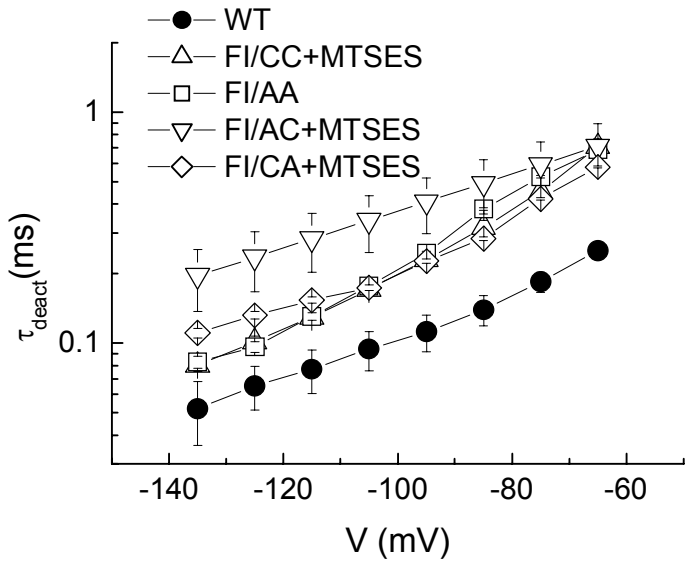

Figure 30. Voltage dependence of the deactivation time constant, τ_{deact} as measured by the decay of the tail currents at different potentials. Values are presented as mean±SEM, n=3-6.

were as follows: WT- 0.07±0.02 ms, n=3; FI/CC+MTSES: 0.101±0.005, n=8, p<0.05; FI/AA- 0.096±0.005, n=3, p>0.05; FI/AC+MTSES- 0.23±0.06, n=3, p<0.05; FI/CA+MTSES- 0.132±0.005, n=3, p<0.05.

Both findings, the large shifts in the voltage dependence caused by the introduced mutations and the slowing of the deactivation kinetics, demonstrate that D4/S6 also plays an important role for activation gating of the sodium channels.

6.2.3. Slow inactivation

Slow inactivation was evaluated for WT and for the double mutants. Entry into the slow inactivated state was extremely slowed for the FI/AC mutant after modification by MTSES (fig 31A). Recovery from slow inactivation was accelerated for all other double mutants except the FI/CC mutant after MTSES application (fig 31B). The steady-state slow inactivation curve was significantly shifted in the hyperpolarizing direction for mutants FI/AA and FI/AC and to more depolarized potentials for mutants FI/CC and FI/AC+MTSES (fig 31C). To study whether the observed left shift in FI/AC and FI/AA is caused only by the single mutant F1586A, we evaluated slow inactivation also for the single mutants F1586A and I1596A. The steady-state slow inactivation was shifted to more hyperpolarized potentials for I1596A (-72.3±2.2 mV, n=5, p<0.05), but not for F1586A (-63±2.2 mV, n=3), compared to WT (-60±4 mV, n=3). Obviously, the common left shift of the inactivation curve for FI/AC and FI/AA was not due to the introduced F1586A mutation.

The observed large effects demonstrate the intrinsic involvement of segment D4/S6 in the slow inactivation process.

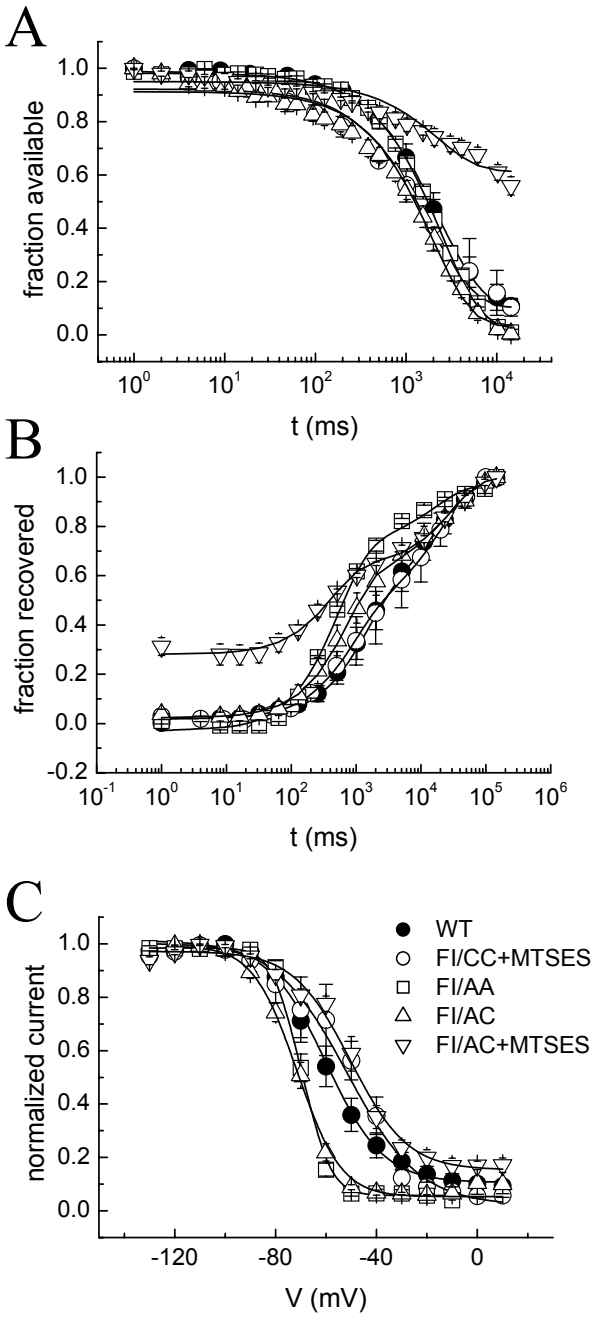

Figure 31. Parameters of slow inactivation. **(A)** Entry into slow inactivation at 0mV. Time constants were : 2.4±1.1s, n=2 (FI/CC+MTSES); 2.5±0.1, n=4 (FI/AA); 2.0±0.2, n=5 (FI/AC) and 4.3±0.3s, n=3, p<0.05 (FI/AC+MTSES) vs. 2.4±0.6s, n=2 for WT. **(B)** Time constants and relative amplitudes of the recovery from slow inactivation at –120mV:

•Mutation	τ_{srec1}(s)	τ_{srec2}(s)	A_{1rel}%
•WT, n=5	1.4±0.16	24.4±3.4	56±2
•FI/CC+MTSES, n=2	0.942±0.08, p<0.05	22.0±2.4	46±10
•FI/AA, n=3	0.76±0.04, p<0.05	17.7±4.5s	76±2
•FI/AC, n=5	0.80±0.20, p<0.05	30±8s	59±4
•FI/AC+MTSES, n=3	0.42±0.02, p<0.0005	30±7s	36±4

•**(C)** Steady-state slow inactivation parameters. $V_{0.5}$ was as follows: $V_{0.5}$: -60±5mV, n=3 (WT); -50±5mV, n=2 (FI/CC+MTSES); -70±1mV, n=4 (FI/AA); -71±2mV, n=8, p<0.05 (FI/AC); -49±2mV, n=5 (FI/AC+MTSES).

6.3. Voltage dependence of the accessibility of positions F1586 and I1596 for modification by MTS reagents

In order to investigate a possible state dependence of the modification of FI/CC by MTSES, the reaction rates at different holding potentials were determined (fig 32A, the pulse protocol is explained in the legend). The reaction with MTSES was drastically slowed at depolarized potentials indicating that at least one of the two cysteines is not accessible when the channel is inactivated. Comparing the calculated reaction rates with the normalized steady-state fast and slow inactivation curves revealed the same voltage dependence for modification/accessibility and both types of inactivation (fig. 32B). To distinguish whether this voltage dependence in accessibility is caused by fast or slow inactivation, the modification rates were measured using 100-ms depolarizing pulses at different frequencies (0.2 to 5 Hz) and a higher concentration of MTSES (10 mM) to accelerate the reaction rates. These protocols increased the time spend in the fast inactivated state by 10 times without inducing significant slow inactivation. The calculated reaction rates did not differ significantly from each other (fig. 32C) demonstrating that the accessibility of the C-terminal part of D4/S6 is not influenced by fast inactivation and therefore must be modulated by the slow inactivation process.

Additionally, the modification rate of FI/AC mutation by MTSES was measured at holding potentials -120 mV and -60 mV. The steady-state slow inactivation curve for mutation FI/AC is shifted in the hyperpolarizing direction (see fig. 31C) thus making measurements at potentials more positive than -60 mV impossible. The double mutant showed fast modification (with time constant τ<1s). Because of this, the reaction kinetics could not be resolved, but no difference between the modification rates at both potentials was observed. The greatly increased accessibility and the lack of difference between the modification at -120 mV and -60 mV suggest that only position 1586 is protected when sodium channels are in the slow inactivated state.

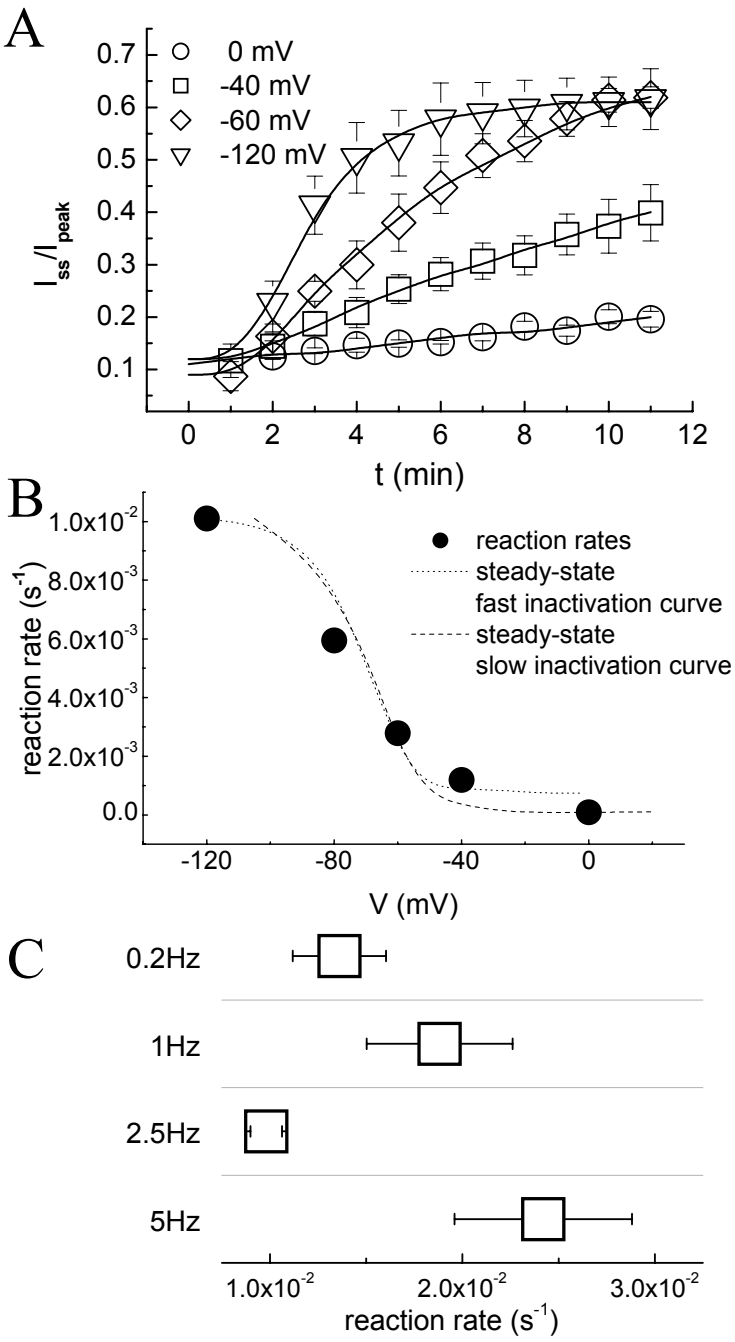

Figure 32. Voltage dependence of the reaction of the double mutant FI/CC with MTSES which was added to the pipette solution. (**A)** Increase of the persistent Na^+ current with time as a measure of the reaction rate with MTSES (2.5 mM). Cells were held at the potentials indicated, hyperpolarized for 750 ms to –140 mV to let them recover sufficiently from fast and slow inactivation and then depolarized to 0 mV to determine the persistent current every minute. Lines are fits to a first order exponential function yielding the reaction rate as the inverse of the time constant. (**B)** Reaction rates as determined in A as a function of voltage. The voltage dependences of both fast and slow inactivation for FI/CC in the absence of MTSES are similar (shown as lines as indicated). **(C)** Reaction rate of FI/CC with MTSES (10 mM) for a different voltage protocol. Depolarizing voltage steps to 0 mV with a length of 100 ms which did not allow slow but fast inactivation of the channel were applied at different frequencies as indicated. The reaction rates did not differ significantly from each other.

7. DISKUSSION

7.1. FUNCTIONAL CONSEQUENCES OF A EPILEPSY CAUSING *KCNQ2* MUTATION

KCNQ2 encodes a delayed rectifier potassium channel which is activated upon depolarization of the cell membrane and therefore contributes to the repolarizing phase of the action potential. A reduction of this current impairs repolarization leading to a hyperexcitability of the cell membrane, which can explain the pathogenesis of seizures in BFNC, especially since *KCNQ2* is expressed in most regions of the brain (Biervert *et al*. 1998, Yang *et al*. 1998). The same pathomechanism seems to be valid for mutations in the *KCNQ1-4* genes, linked to inherited cardiac arrhythmia in the long QT syndrome, BFNC or congenital deafness. Mutations that have been functionally characterized thus far substantially reduce the resulting potassium current (Chouabe *et al*., 1997; Wollnik *et al*., 1997; Biervert *et al*., 1998; Schröder *et al*., 1998; Kubisch *et al*., 1999). Additional evidence for the induction of seizures by reduced potassium current comes from studies with potassium channel blockers in brain slices. Dendrotoxin, 4-aminopyridine and tetraethylammonium, classical blockers of various types of potassium channels, all produce epileptic activity (Velluti *et al*. 1987, Rutecki *et al*. 1987, 1990).

Since our results suggest normal pore properties (potassium reversal potential is not changed), it is unlikely that this mutation affects single channel conductance. Channel gating is also unaffected, indicating that the mutated part does not interact with functionally important regions of the channel protein.

Potassium channel subunits coassemble to tetramers but a significant dominant negative effect of the mutation was not observed. Thus, WT channel function should not significantly be suppressed by a coassembly of mutant and WT subunits. Haploinsufficiency should therefore produce the phenotype.

Schwake *et al*. (2000) demonstrated a similar current reduction to be associated with reduced surface expression of mutant channels. A mutation in *KCNQ1* causing the Jervell and Lange-Nielson syndrome disrupt assembly of *KCNQ1* channels (Schmitt *et al*., 2000). Experimental data of our group using chimeras between *KCNQ1, KCNQ2* and *KCNQ3* channels show that the interaction of *KCNQ2* and *KCNQ3* channels is mediated by the C-terminus (Lerche *et al*., 2000b; Maljevic *et al*., 2001). Hence, the most valuable explanation for the observed functional consequences of the 2513delG mutation is a disturbed coassembly to tetramers leading to a reduced surface expression of the *KCNQ2/KCNQ3* heteromeric channels. This would also explain the lack of a significant dominant negative effect since WT subunits could still assemble as usual.

It remains unclear why the reduced *KCNQ2* potassium current results in seizures preferentially during the neonatal period. One possibility could be that the brain is generally more likely to develop seizures in this premature state than later in life (Swann *et al*., 1993). Another explanation might be the differential expression of potassium channels during maturation, which may attribute a dominant role to *KCNQ* channels in central neurons within the first days to weeks of life. Either potassium channels of the *KCNQ* family could be upregulated during this period, or other voltage-gated potassium channels could still not have reached their full expression level. For some of the rat brain voltage-gated potassium channels such a differential expression during maturation has already been described (Beck *et al*., 1990). In electrophysiological experiments on hippocampal brain slices,

changes of potassium currents have also been reported during ontogenesis (Beck *et al*.,1992). Recently, differential expression with reduced expression of *KCNQ3* during the first days of life (Tinel *et al*., 1998) and expression of shorter *KCNQ2* splice variants during neuronal development (Smith *et al*., 2001) have been reported. Further investigations following the changes in the expression pattern of the *KCNQ* channels during maturation could provide important information about the early developmental stages of the nervous system.

7.2. FUNCTIONAL CONSEQUENCES OF THE MUTATIONS CAUSING GEFS+

The R1460H mutation shows accelerated recovery from fast inactivation, slowing of the fast inactivation time course at depolarized potentials and slightly faster activation. These findings support a gain-of-function as a disease-causing mechanism. In contrast, fast and slow inactivation are shifted in the hyperpolarizing direction, resulting in a loss-of-function. The only difference in gating between WT and T685M channels that can induce the expected hyperexcitability of the cell membrane is the observed slight acceleration of channel activation at voltages more negative than –20 mV. Much more striking and more pronounced as for R1460H is the observed stabilization of the fast and slow inactivation states by a strong shift of the steady-state availability curves for this mutant.

Hence, the common defect for both mutations is the stabilization of both fast and slow inactivation. This will decrease membrane excitability by reducing the number of sodium channels available for an action potential, a mechanism that has been already proposed to contribute to paralysis for D4/S4 mutations causing paramyotonia congenita (Lerche *et al*., 1996; Mitrovic *et al*., 1999) or more

recently for D2/S4 mutations causing hypokalemic periodic paralysis type 2 (Jurkat-Rott *et al*., 2000; Struyk *et al*., 2000; Kuzmenkin *et al*., 2002). However, in contrast to skeletal muscle fibers a decrease of excitability when occurring in inhibitory neurons may be responsible for the generation of synchronous epileptic activity in neuronal circuits and could explain the occurrence of seizures. In 1992, Ogata *et al*. showed that enhanced slow inactivation may cause selective loss of function in inhibitory neurons.

Alternatively, the R1460H mutation could cause neuronal hyperexcitability by a combination of the faster activation time course and the 3-fold acceleration of recovery from inactivation. This will shorten both the period of depolarization needed to elicit an action potential and the refractory period after an action potential. The T685M mutation also could be related to a gain-of-function by the accelerated activation kinetics. In contrast to a persistent sodium current, both mechanisms should not influence the resting membrane potential which might be fatal when occurring in neurons in contrast to skeletal or heart muscle fibers. An acceleration of sodium channel activation has not been described as a disease-causing mechanism so far. The subtle alterations in channel gating found for the two mutations are in line with two previous findings concerning sodium channel gating and epilepsy. First, the β_1-subunit mutation described by Wallace and colleagues (1998) also shows a small defect in inactivation and only causes epilepsy but no myotonia, although *SCN1B* is also expressed in skeletal muscle. Second, a transgenic mouse model with an introduced *SCN2A* mutation exhibits severe status epilepticus, although the inactivation defect was also very small compared to other known mutations (Kearny *et al*., 1998). Consistent with this hypothesis, a more severe phenotype was reported for the family carrying the D4/S4 mutation with 11 of 12 affected members suffering from epilepsy with afebrile seizures. In contrast, afebrile in addition to febrile seizures only occurred

in 5 of 12 affected individuals of the family with the D2/S4 mutation (Baulac *et al*., 1999; Moulard *et al*., 1999).

From a biophysical point of view, the results confirm those from earlier studies showing that the voltage sensor D2/S4 is more important for activation than for inactivation (Chen *et al*., 1995; Mitrovic *et al*., 1998; Cha *et al*., 1999). In particular, the results extend those by Mitrovic *et al*. (1998) that movement of the D2/S4 segment and the kinetics of activation can be influenced by mutations therein. Whereas the mutation used in their study is located at the extracellular end, T685M lies on the cytoplasmic end of the supposed S4 helix. Remarkable are the relatively large effects on slow inactivation confirming the importance of the D2/S4 and D4/S4 regions for this gating process (Cummins *et al*., 1996; Hayward *et al*., 1999; Struyk *et al*., 2000; Mitrovic *et al*., 2000).

After publication of our results (Alekov *et al.*, 2000; Alekov *et al.*, 2001), two further studies on these mutations were reported. The first report concerns investigation of both mutants, introduced in the homologous rat brain sodium channel $rNa_v1.1$, coexpressed in *Xenopus Laevis* Oocytes with the β_1-subunit and studied with the two electrode voltage clamp (TEVC) technique (Spampanato *et al*., 2000). The results of this study show complete agreement with our results concerning the effects on recovery from fast inactivation and shifts in steady-state fast and slow inactivation. The observed activation defect was not reported, but it is under the border of resolution for two-microelectrode voltage clamp recordings in oocytes. Similar results from studies using $Na_v1.1$ and $Na_v1.4$ were expected, since all functionally important regions are highly conserved among the different isoforms of voltage-gated sodium channel, as are the voltage sensors D2/S4 and D4/S4. A second study reports the investigation of both mutations and an additional mutation, introduced in the human $hNa_v1.1$ and expressed in the presence of both β_1 and β_2-subunits in tsA201 cells (Lossin *et al*., 2002). The authors report an

increased fraction of persistent current as the major pathophysiological finding which demonstrates a gain-of-function for all mutants studied. This would lead to hyperexcitability of the neuronal cell membrane. The authors did not study the effects of the mutations alone or only in the presence of the β_1 subunit, nor did they examine slow inactivation, which makes a comparison to our study and to the work of Spampanato *et al*. difficult. Therefore, a detailed evaluation of the role of the accessory β_2 subunit and the expression system on the gating of $hNa_v1.1$ is required, to resolve the discrepancies between these studies.

7.3. D4/S4-S5

7.3.1. D4/S4-S5 as a possible receptor site for the inactivation ball

Our results confirm the important role of the D4/S4-S5 loop for fast inactivation. Interestingly, activation was not affected by the mutations in D4/S4-S5 in contrast to mutations in D3/S4-S5 (Smith and Goldin, 1997), suggesting a greater specialization of D4/S4-S5. This agrees with the hypothesis that movements of the voltage sensors trigger conformational changes within the connected S4-S5 loops thereby coupling activation to inactivation. Whereas the gating charge of D4/S4 is completely immobilized by inactivation, the fraction of the charge of D3/S4 still can partially move quickly (Cha *et al*., 1999).

The introduced mutations disrupt fast inactivation, and this effect is enhanced when combined with the F1311C mutation but double mutant cycle analysis argues against a cooperative interaction between the inactivation particle and the D4/S4-S5 loop of the sodium channel but for an additive effect. The calculated values for the coupling energy are relatively small and not significant. One possible explanation could be that D4/S4-S5 interacts not directly with the

inactivation ball, but with neighboring regions. Such interactions have been demonstrated for the Shaker potassium channel, for which a similar ball and chain inactivation mechanism is proposed (Zhou *et al*., 2001).

Another possibility is that the effects of mutations in the S4-S5 loops in domains D3 and D4 on fast inactivation are not direct but are rather caused by modulation of the mobility of the voltage sensors. This hypothesis is supported by the observed cooperative effects on fast inactivation of double mutations combining changes in the S4-S5 loops in domains D3 and D4 (Popa *et al.*, 2002). Such assumption could be additionally proven by combining mutations in the voltage sensors S4 with mutations in the associated S4-S5 loops.

7.3.2. Role of the D4/S4-S5 segment in slow sodium channel inactivation

The presented results indicate an importantt role of the C-terminal end of the D4/S4-S5 loop for slow inactivation of the voltage-gated sodium channel (Alekov *et al.*, 2001b). Whereas a conclusive hypothesis can be formulated how this structure is involved in fast inactivation (Filatov *et al*., 1998; Lerche *et al*., 1997; McPhee *et al*., 1998; Mitrovic *et al*., 1996) it is difficult even to speculate upon a mechanism how the D4/S4-S5 loop contributes to slow inactivation. Most problematic is the absence of a valuated model how slow inactivation functions in general. Several regions like the pore (Balser *et al*., 1996), the voltage sensors (Mitrovic *et al*., 2000; Struyk *et al*., 2000), S4-S5 loops (Cummins *et al*., 1996; Hayward *et al*., 1997), S5 (Bendahhou *et al*., 1999) and S6 segments (Hayward *et al*., 1997, O'Reilly *et al*., 2000 and 2001) are important for regular function of SI. Complementary to these previous results, our data suggest that upon depolarization a slow structural rearrangement occurs in the region involving S4, S4-S5 and S5 segments in domain 4 contributing significantly to the formation of

the slow inactivated state. In our case L1482A had stronger effects on disruption of FI but L1482C enhanced SI more extensively. This finding contradicts the hypothesis that the changes of slow inactivation are caused by the destabilization of the fast inactivation gating. The demonstrated effects also argue against the proposed direct kinetic coupling between fast and slow inactivation gating (Nuss *et al*., 1996).

7.4. ROLE OF SEGMENT D4/S6 IN THE GATING OF SODIUM CHANNELS

The major findings of the presented study are the following:

A) Mutations in the C-terminal part strongly affect all aspects of channel gating – activation, deactivation, fast and slow inactivation, thus pointing out a central functional role of this region.

B) The accessibility of D4/S6 is modulated by closure of the slow inactivation gate.

7.4.1. D4/S6 and fast inactivation

The almost complete removal of fast inactivation described in the results section supports the idea, that the middle and C-terminal parts of D4/S6 are intimately involved in this process, for example as a receptor site for the inactivation particle. However, the accessibility of the studied double mutant (FI/CC) is not decreased during fast inactivation arguing against the idea of a receptor site. This is supported also from the previous report of McPhee *et al*. (1995) where application of a peptide containing the IFM motif restores FI in the F1764A/V1774A mutant in $rNa_v1.2a$ corresponding to our FI/AA mutation in $hNa_v1.4$. All these findings

therefore support the hypothesis that the middle and C-terminal parts of D4/S6 are involved in conformational changes which precede and are necessary for the formation of the binding site for the inactivation particle, but that the examined amino acids are not part of the receptor site itself.

Our study did not reveal any relationship between charge, size or hydrophobicity of the introduced mutations or modifying reagents and the observed effects on inactivation, since the mutations FI/AA and FI/CC modified by MTSES had the largest effects. Rather, specific steric effects of the small alanines and the large cysteines-ES are responsible for the obtained results. A possible hypothesis can be derived from findings concerning the action of Batrachotoxin (BTX) on sodium channels. BTX has been shown to bind to the cytoplasmic part of D4/S6, especially amino acid F1586 has been found to be an important molecular determinant for the action of BTX, and the effect of BTX on the sodium channel is very similar to those observed in our mutagenesis study: abolishing inactivation and slowing of the deactivation kinetics (Linford *et al*., 1998). BTX is a large aromatic molecule which binds in the middle of the conductive pathway and possibly trap channel conformation by a “foot-in-the-door” mechanism. Similar molecular mechanisms could be responsible for the effects described here. Too small or to large side chains could cause conformational changes that trap the channel in one conformation and thus prevent inactivation.

7.4.2. D4/S6 and slow inactivation gating

The introduced double mutants (especially the mutant FI/AC modified by MTSES) had a large effect on slow inactivation. There are several reports which demonstrate the importance of the S6 segments for slow inactivation (Hayward *et al*. 1996?; O’Reilly *et al*., 2000; Vedantham and Cannon 2000; Takahashi and

Cannon 2001; O'Reilly *et al*., 2001). Our results show that some mutations stabilize the slow inactivated state by shifting the half-maximal voltage of the steady-state inactivation curve to more hyperpolarized potentials and leading to a more complete slow inactivation (FI/AA and FI/AC). Other double mutations are associated with opposite effects (FI/CC+MTSES and FI/AC+MTSES). As already observed for mutations in D4/S4-S5, no correlation between the effects on fast and slow inactivation could be found (both FI/AC+MTSES and FI/AA double mutations almost completely abolish fast inactivation but FI/AC+MTSES shifts the steady state slow inactivation curve to the right and FI/AA to the left). The complex character of the observed effects prevents a precise interpretation of the results and further experiments are needed to clarify the exact function of the investigated positions in the process of slow inactivation. Possible implications concerning the position of the slow inactivation gate are discussed below.

7.4.3. Accessibility of the C-terminal part of D4/S6

The large effects on fast inactivation upon application of MTSES to cysteine mutations allowed us to measure the rates of modification at different potentials and so to examine the accessibility of this region. Both mutants, F1586C and I1596C, were accessible for modification by the permanently charged and hydrophilic MTSES reagent supporting the hypothesis that both residues face water environment – most probably the permeation pathway. The results clearly show, that the accessibility of the double mutant FI/CC is reduced in a process, which is kinetically identical with slow inactivation. Mutations at both sites (1586 and 1596) contribute to the observed abolishing of fast inactivation but the double mutant FI/AC did not show any voltage dependence of the accessibility for modification by MTSES. Thus, only the accessibility of 1586 is decreased with the onset of slow inactivation. The question remains, whether the accessibility is modulated by either conformational changes which bury both side chains in the

membrane or due to the closing of the permeation way at the bottom of the investigated region.

Similar accessibility modulation was reported for position 1583 in $rNa_v1.4$ corresponding to position 1590 in $hNa_v1.4$ (Vedantham and Cannon, 2000). Application of the small and not permanently charged MTSEA reagent blocked mutant sodium channel in a state-dependent manner. Slow inactivation prevented modification by MTSEA. From the lack of effects after application of the permanently charged and hydrophilic reagents MTSET and MTSES the authors concluded that position 1583 is facing hydrophobic environment (e.g. the membrane) and the changed accessibility is caused only by a conformational change. However, MTSEA could also first pass the membrane and then bind from the intracellular side of the membrane. Additionally, MTSET and MTSES could still bind to the engineered cysteine but this binding could not be associated with functional changes (as it is in our case with MTSEA and MTSET reagents applied on the FI/CC mutation).

In our view, the side chains of residues 1586 and 1596 are facing the pore and most likely the observed accessibility modulation of position 1586 is caused by constriction of the permeation pathway with ongoing depolarization, for example by closure of the slow inactivation gate. This hypothesis is supported by several facts:

1) MTSES is permanently negatively charged and thus highly hydrophilic and can therefore only bind to cysteines which are facing water environment.

2) The proposed model for binding of BTX predicts simultaneous attaching of the drug to more than one S6 segment in the ion conducting pathway (involving D4/S6

and in particular residue F1586) (Wang and Wang, 1998and 1999; Wang *et al.*, 2000; Wang *et al.*, 2001). Similar model have been proposed also for local anesthetic drugs. Furthermore, S6 segments are predicted to form the inner ion conducting path in cation channels (Doyle *et al.*, 1998; Lipkind and Fozzard, 2000). BTX and local anesthetic drugs are relatively small molecules and thus probably can bind to more than one S6 simultaneously only from the inner site of the pore.

3) Action of BTX requires the open channel conformation. Additionally, it exhibits a prominent voltage dependence, showing a reduced affinity of the drug to its receptor with increasing depolarization (from –30 to +60 mV) although the maximal open probability of the channels does not decrease in this voltage range (Li *et al.*, 2002). This is similar to the voltage-dependent modulation of the affinity of local anesthetics to the channel protein. The voltage dependence is usually explained by electrostatic interaction of the positively charged drugs with the local electric field in the membrane. However, this should be interpreted care because it is not supported by any experimental data which would correlate the charge of the drug with the voltage sensitivity. On the other hand we observed a similar voltage dependence of the accessibility of the same protein region (C-terminal part of D4/S6) but the reactive molecule (MTSES) has a negative charge thus opposing the local electric barrier hypothesis. Several studies propose a link of the slow inactivation process and the local anesthetic (LA) block (Balser *et al.*,1996; Kambouris *et al.*, 1998; Nuss *et al.*, 2000), but no studies have been performed to investigate the effect of slow inactivation on the voltage dependence of the block by LA drugs. This voltage dependence is very similar to the voltage dependence of slow inactivation. So the voltage dependence of action of BTX and LA could be caused by a partial protection of the binding site for these agents by the slow inactivation gate. A strong support for this hypothesis is provided by a recent study, demonstrating that lidocaine and benzocaine (which also are supposed to

bind to position F1586) are trapped during slow inactivation and cannot escape the channel permeation pathway (Li *et al.*, 2002). Such assumption would allow to restrict the possible position of the slow inactivation gate of voltage-gated sodium channels to the C-terminal part of the S6 segments.

SUMMARY

Ion channels are membrane-spanning proteins that form hydrophilic pores with a specific selectivity to particular ions. They provide the basis for excitability in nerve and muscle cells. The thesis presents the functional characterization of potassium and sodium channel mutations causing inherited epilepsies and a structure-function study about the role of two cytoplasmic protein regions of the voltage-gated sodium channel that are important for channel gating.

A mutation (2513delG) in the KCNQ2 gene encoding a neuronal voltage-gated potassium channel causes a benign familial epilepsy syndrome of neonates. Expression and and functional characterization of this mutation in Xenopus Laevis oocytesrevealed a 20-fold reduction of the resulting potassium compared to wild type (WT) channels . When coexpressed with WT KCNQ2 channels, no dominant negative effect of the mutation was observed. The reduction of potassium current impairs membrane depolarization and therefore can explain the occurrence of epileptic seizures in affected patients.

Another familial epilepsy syndrome characterized by febrile and afebrile generalized seizures in childhood was recently shown to be caused by mutations in a neuronal voltage-gated sodium channel. The first two mutations reported for this syndrome were characterized by functional expression in a mammalian cell line. Common for both mutations was a pronounced stabilization of the slow inactivated state. Additionally, mutation R1460H destabilized fast inactivation by accelerating recovery from fast inactivation by 3-fold. The reported stabilization of slow inactivation could be causative for the disease in a “loss-of-function” manner by reducing the effective number of available sodium channels in inhibitory neurons which could induce hyperexcitability of neuronal networks. In contrast, the accelerated recovery from fast inactivation causes a “gain-of-function” by shortening the refractory period of the action potential which directly increases membrane excitability in neurons. Thus both of these findings could explain the occurrence of epileptic seizures.

Voltage-gated sodium channel are responsible for the rising part of the action potentials in excitable cells. Upon depolarization they activate and with ongoing depolarization inactivate. Sodium channels have at least two kinetically distinct inactivated states called fast and slow inactivation. Fast inactivation acts on a time scale of milliseconds and slow inactivation – on the timescale of seconds. Fast inactivation is believed to function in the so-called “hinged-lid” fashion – a hydrophobic particle of three amino acids (IFM) occludes the pore from the intracellular site of the membrane. Possible binding sites for the inactivation particle are protein regions exposed to the cytoplasm that are important for fast inactivation. Such regions are the D4/S6 segment and the D4/S4-S5 interloop. Mutations in this protein regions have been shown to disrupt fast inactivation to a great extend. A conclusive hypothesis about the molecular mechanism of slow inactivation have not been developed until now, but several studies show the involvement of the S6 segments and S4-S5 loops in the modulation of this process.

In order to check for direct interactions between the D4/S4-S5 loop and the inactivation particle, mutant cycle analysis was performed by combining single

mutations from both regions which disrupt fast inactivation: F1473C and L1482C from D4/S4-S5 with F1311C, positioned in the middle of the proposed inactivation particle. The thermodynamic analysis allows one to estimate whether the effects of both mutants on fast inactivation are interdependent or not. Both double mutations exhibited only small and not significant coupling energies as derived from the effect on fast inactivation arguing against a functional cooperativity of D4/S4-S5 region and the inactivation particle in this process.

To evaluate the role of the intracellular loop D4/S4-S5 in slow inactivation of sodium channels, two mutations in this loop (L1482C/A) were expressed in cells and functionally characterized. Both mutations introduced prominent effects on slow inactivation (shifts in the steady-state voltage dependence and more complete steady-state slow inactivation at depolarizing potentials), demonstrating that D4/S4-S5 loop is involved in the regulation of slow inactivation in voltage-gated sodium channels.

To investigate in detail the role of segment D4/S6 in sodium channel inactivation, the amino acids at positions F1586, V1589, M1592 and I1596, which have been previously shown to be important for fast inactivation, were substituted by cysteines and the effects of the mutations and application of MTS reagents, covalently binding to the engineered cysteines were studied. The largest effects were observed for the double mutation F1586C/I1596C, where application of MTSES introduced more than 50% noninactivating sodium current. The reaction was voltage dependent and this voltage dependence was conferred by the slow inactivation. Combination studies with application of MTSES on the double mutations F1586C/I1596A and F1586A/I1596C revealed that only the access to position 1586 is voltage dependent. Both findings suggest that probably the slow inactivation gate of voltage-gated sodium channels is positioned in the down part of the S6 segments.

Further mutagenesis was done to better explore the molecular mechanism of the observed effects and the changes in activation, slow inactivation and deactivation were evaluated. The introduced mutations and the application of MTSES had great effect on all other aspects of channel gating: many mutations introduced big shifts (up to 20 mV) in the voltage dependence of activation, deactivation kinetics was markedly slowed for all double mutations and in addition, slow inactivation was affected in a very complex manner – some mutations greatly destabilized this process (e.g. mutation F1586A/I1596C which slowed entry into slow inactivation 3 times) but some did stabilize it (e.g. F1586A/I1596A mutation which shifted steady state slow inactivation more than 15 mV to the hyperpolarized direction). Altogether, this findings point out a central functional role of segment D4/S6 in the gating of sodium channels.

REFERENCES

ALEKOV, A., RAHMAN, M.M., MITROVIC, N., LEHMANN-HORN, F. & LERCHE, H. (2000). A sodium channel mutation causing epilepsy in man exhibits subtle defects in fast inactivation and activation in vitro. *J Physiol* **529 Pt 3**, 533-9.

ALEKOV, A.K., RAHMAN, M.M., MITROVIC, N., LEHMANN-HORN, F. & LERCHE, H. (2001a). Enhanced inactivation and acceleration of activation of the sodium channel associated with epilepsy in man. *Eur J Neurosci* **13**, 2171-6.

ALEKOV, A.K., PETER, W., MITROVIC, N., LEHMANN-HORN, F. & LERCHE, H. (2001b). Two mutations in the IV/S4-S5 segment of the human skeletal muscle Na+ channel disrupt fast and enhance slow inactivation. *Neurosci Lett* **306**, 173-6.

ARMSTRONG, C.M. & BEZANILLA, F. (1977). Inactivation of the sodium channel. II. Gating current experiments. *J Gen Physiol* **70**, 567-90.

BALSER, J.R., NUSS, H.B., CHIAMVIMONVAT, N., PEREZ-GARCIA, M.T., MARBAN, E. & TOMASELLI, G.F. (1996). External pore residue mediates slow inactivation in mu 1 rat skeletal muscle sodium channels. *J Physiol* **494 (Pt 2)**, 431-42.

BARHANIN, J., LESAGE, F., GUILLEMARE, E., FINK, M., LAZDUNSKI, M. & ROMEY, G. (1996). K_VLQT1 and lsK (minK) proteins associate to form the I(Ks) cardiac potassium current. *Nature* **384**, 78-80.

BAULAC, S., GOURFINKEL-AN, I., PICARD, F., ROSENBERG-BOURGIN, M., PRUD'HOMME, J.F., BAULAC, M., BRICE, A. & LEGUERN, E. (1999). A second locus for familial generalized epilepsy with febrile seizures plus maps to chromosome 2q21-q33. *Am J Hum Genet* **65**, 1078-85.

BEAN, B.P., COHEN, C.J. & TSIEN, R.W. (1983). Lidocaine block of cardiac sodium channels. *J Gen Physiol* **81**, 613-42.

BECK, H., FICKER, E. & HEINEMANN, U. (1992). Properties of two voltage-activated potassium currents in acutely isolated juvenile rat dentate gyrus granule cells. *J Neurophysiol* **68**, 2086-99.

BENDAHHOU, S., CUMMINS, T.R., TAWIL, R., WAXMAN, S.G. & PTACEK, L.J. (1999). Activation and inactivation of the voltage-gated sodium channel: role of segment S5 revealed by a novel hyperkalaemic periodic paralysis mutation. *J Neurosci* **19**, 4762-71.

BENITAH, J.P., CHEN, Z., BALSER, J.R., TOMASELLI, G.F. & MARBAN, E. (1999). Molecular dynamics of the sodium channel pore vary with gating: interactions between P-segment motions and inactivation. *J Neurosci* **19**, 1577-85.

BEZANILLA, F. & ARMSTRONG, C.M. (1977). Inactivation of the sodium channel. I. Sodium current experiments. *J Gen Physiol* **70**, 549-66.

BEZANILLA, F. (2000). The voltage sensor in voltage-dependent ion channels. *Physiol Rev* **80**, 555-92.

BIERVERT, C., SCHROEDER, B.C., KUBISCH, C., BERKOVIC, S.F., PROPPING, P., JENTSCH, T.J. & STEINLEIN, O.K. (1998). A potassium channel mutation in neonatal human epilepsy. *Science* **279**, 403-6.

CAHALAN, M.D. & ALMERS, W. (1979). Interactions between quaternary lidocaine, the sodium channel gates, and tetrodotoxin. *Biophys J* **27**, 39-55.

CANNON, S.C. & STRITTMATTER, S.M. (1993). Functional expression of sodium channel mutations identified in families with periodic paralysis. *Neuron* **10**, 317-26.

CARTER, P.J., WINTER, G., WILKINSON, A.J. & FERSHT, A.R. (1984). The use of double mutants to detect structural changes in the active site of the tyrosyl-tRNA synthetase (Bacillus stearothermophilus). *Cell* **38**, 835-40.

CATTERALL, W.A. (1994a). Molecular mechanisms of inactivation and modulation of sodium channels. *Ren Physiol Biochem* **17**, 121-5.

CATTERALL, W.A. (1994b). Molecular properties of a superfamily of plasma-membrane cation channels. *Curr Opin Cell Biol* **6**, 607-15.

CATTERALL, W.A. (2000). From ionic currents to molecular mechanisms: the structure and function of voltage-gated sodium channels. *Neuron* **26**, 13-25.

CHA, A., RUBEN, P.C., GEORGE, A.L. Jr, FUJIMOTO, E. & BEZANILLA, F. (1999). Voltage sensors in domains III and IV, but not I and II, are immobilized by Na+ channel fast inactivation. *Neuron* **22**, 73-87.

CHAHINE, M., GEORGE, A.L. Jr, ZHOU, M., JI, S., SUN, W., BARCHI, R.L. & HORN, R. (1994). Sodium channel mutations in paramyotonia congenita uncouple inactivation from activation. *Neuron* **12**, 281-94.

CHARLIER, C., SINGH, N.A., RYAN, S.G., LEWIS, T.B., REUS, B.E., LEACH, R.J. & LEPPERT, M. (1998). A pore mutation in a novel KQT-like potassium channel gene in an idiopathic epilepsy family. *Nat Genet* **18**, 53-5.

CHEN, L.Q., SANTARELLI, V., HORN, R. & KALLEN, R.G. (1996). A unique role for the S4 segment of domain 4 in the inactivation of sodium channels. *J Gen Physiol* **108**, 549-56.

CHOUABE, C., NEYROUD, N., GUICHENEY, P., LAZDUNSKI, M., ROMEY, G. & BARHANIN, J. (1997). Properties of KvLQT1 K^+ channel mutations in Romano-Ward and Jervell and Lange-Nielsen inherited cardiac arrhythmias. *EMBO J* **16**, 5472-9.

COLE, K.S. (1949). Dynamic electric characteristics of the squid axon mem rane. *Arch. Sci. Physiol.* **3**, 253-258.

COOPER, E.C., ALDAPE, K.D., ABOSCH, A., BARBARO, N.M., BERGER, M.S., PEACOCK, W.S., JAN, Y.N. & JAN, L.Y. (2000). Colocalization and coassembly of two human brain M-type potassium channel subunits that are mutated in epilepsy. *Proc Natl Acad Sci U S A* **97**, 4914-9.

COOPER, E.C. (2001). Potassium channels: how genetic studies of epileptic syndromes open paths to new therapeutic targets and drugs. *Epilepsia* **42 Suppl 5**, 49-54.

CUMMINS, T.R., ZHOU, J., SIGWORTH, F.J., UKOMADU, C., STEPHAN, M., PTACEK, L.J. & AGNEW, W.S. (1993). Functional consequences of a Na^+ channel mutation causing hyperkalemic periodic paralysis. *Neuron* **10**, 667-78.

CUMMINS, T.R. & SIGWORTH, F.J. (1996). Impaired slow inactivation in mutant sodium channels. *Biophys J* **71**, 227-36.

DASCAL, N. (1987). The use of Xenopus oocytes for the study of ion channels. *CRC Crit Rev Biochem* **22**, 317-87.

DESTEXHE, A. & HUGUENARD, J.R. (2000). Nonlinear thermodynamic models of voltage-dependent currents. *J Comput Neurosci* **9**, 259-70.

DOYLE, D.A., MORAIS CABRAL, J., PFUETZNER, R.A., KUO, A., GULBIS, J.M., COHEN, S.L., CHAIT, B.T. & MACKINNON, R. (1998). The structure of the potassium channel: molecular basis of K^+ conduction and selectivity. *Science* **280**, 69-77.

EAHOLTZ, G., SCHEUER, T. & CATTERALL, W.A. (1994). Restoration of inactivation and block of

open sodium channels by an inactivation gate peptide. *Neuron* **12**, 1041-8.

EAHOLTZ, G., ZAGOTTA, W.N. & CATTERALL, W.A. (1998). Kinetic analysis of block of open sodium channels by a peptide containing the isoleucine, phenylalanine, and methionine (IFM) motif from the inactivation gate. *J Gen Physiol* **111**, 75-82.

EAHOLTZ, G., COLVIN, A., LEONARD, D., TAYLOR, C. & CATTERALL, W.A. (1999). Block of brain sodium channels by peptide mimetics of the isoleucine, phenylalanine, and methionine (IFM) motif from the inactivation gate. *J Gen Physiol* **113**, 279-94.

ESCAYG, A., MACDONALD, B.T., MEISLER, M.H., BAULAC, S., HUBERFELD, G., AN-GOURFINKEL, I., BRICE, A., LEGUERN, E., MOULARD, B., CHAIGNE, D., BURESI, C. & MALAFOSSE, A. (2000). Mutations of SCN1A, encoding a neuronal sodium channel, in two families with GEFS+2. *Nat Genet* **24**, 343-5.

ESCAYG, A., HEILS, A., MACDONALD, B.T., HAUG, K., SANDER, T. & MEISLER, M.H. (2001). A novel SCN1A mutation associated with generalized epilepsy with febrile seizures plus--and prevalence of variants in patients with epilepsy. *Am J Hum Genet* **68**, 866-73.

FILATOV, G.N., NGUYEN, T.P., KRANER, S.D. & BARCHI, R.L. (1998). Inactivation and secondary structure in the D4/S4-5 region of the SkM1 sodium channel. *J Gen Physiol* **111**, 703-15.

FONTAINE, B., KHURANA, T.S., HOFFMAN, E.P., BRUNS, G.A., HAINES, J.L., TROFATTER, J.A., HANSON, M.P., RICH, J., MCFARLANE, H., YASEK, D.M. & ET, a.l. (1990). Hyperkalemic periodic paralysis and the adult muscle sodium channel alpha-subunit gene. *Science* **250**, 1000-2.

GEORGE, A.L. Jr, KOMISAROF, J., KALLEN, R.G. & BARCHI, R.L. (1992). Primary structure of the adult human skeletal muscle voltage-dependent sodium channel. *Ann Neurol* **31**, 131-7.

GOLDIN, A.L., BARCHI, R.L., CALDWELL, J.H., HOFMANN, F., HOWE, J.R., HUNTER, J.C., KALLEN, R.G., MANDEL, G., MEISLER, M.H., NETTER, Y.B., NODA, M., TAMKUN, M.M., WAXMAN, S.G., WOOD, J.N. & CATTERALL, W.A. (2000). Nomenclature of voltage-gated sodium channels. *Neuron* **28**, 365-8.

GOLDIN, A.L. (2001). Resurgence of sodium channel research. *Annu Rev Physiol* **63**, 871-94.

GRAHAM, F.L. & VAN DER EB, A.J. (1973). A new technique for the assay of infectivity of human adenovirus 5 DNA. *Virology* **52**, 456-67.

GREEN, D.S., GEORGE, A.L. Jr & CANNON, S.C. (1998). Human sodium channel gating defects caused by missense mutations in S6 segments associated with myotonia: S804F and V1293I. *J Physiol* **510 (Pt 3)**, 685-94.

GUNDERSEN, C.B., MILEDI, R. & PARKER, I. (1983). Voltage-operated channels induced by foreign messenger RNA in Xenopus oocytes. *Proc R Soc Lond B Biol Sci* **220**, 131-40.

GURDON, J.B., LANE, C.D., WOODLAND, H.R. & MARBAIX, G. (1971). Use of frog eggs and oocytes for the study of messenger RNA and its translation in living cells. *Nature* **233**, 177-82.

HAMILL, O.P., MARTY, A., NEHER, E., SAKMANN, B. & SIGWORTH, F.J. (1981). Improved patch-clamp techniques for high-resolution current recording from cells and cell-free membrane patches. *Pflugers Arch* **391**, 85-100.

HAUSER, W.A., ANNEGERS, J.F. & ROCCA, W.A. (1996). Descriptive epidemiology of epilepsy: contributions of population-based studies from Rochester, Minnesota. *Mayo Clin Proc* **71**, 576-86.

HAYWARD, L.J., BROWN, R.H. Jr & CANNON, S.C. (1997). Slow inactivation differs among mutant Na channels associated with myotonia and periodic paralysis. *Biophys J* **72**, 1204-19.

HAYWARD, L.J., SANDOVAL, G.M. & CANNON, S.C. (1999). Defective slow inactivation of sodium channels contributes to familial periodic paralysis. *Neurology* **52**, 1447-53.

HEINE, R., PIKA, U. & LEHMANN-HORN, F. (1993). A novel SCN4A mutation causing myotonia aggravated by cold and potassium. *Hum Mol Genet* **2**, 1349-53.

HILLE, B. (1966). Common mode of action of three agents that decrease the transient change in sodium permeability in nerves. *Nature* **210**, 1220-2.

HILLE, B. (1977). Local anesthetics: hydrophilic and hydrophobic pathways for the drug- receptor reaction. *J Gen Physiol* **69**, 497-515.

HOLMGREN, M., JURMAN, M.E. & YELLEN, G. (1996). N-type inactivation and the S4-S5 region of the Shaker K^+ channel. *J Gen Physiol* **108**, 195-206.

HODGKIN, A.L., A.F. HUXLEY, AND B. KATZ. (1952). Measurement of current-voltage relations in the membrane of the giant axon of *Loligo*. *J. Physiol. (Lond)* **116**, 424-448.

HOSHI, T., ZAGOTTA, W.N. & ALDRICH, R.W. (1990). Biophysical and molecular mechanisms of Shaker potassium channel inactivation. *Science* **250**, 533-8.

ISACOFF, E.Y., JAN, Y.N. & JAN, L.Y. (1991). Putative receptor for the cytoplasmic inactivation gate in the Shaker K^+ channel. *Nature* **353**, 86-90.

ISOM, L.L., DE JONGH, K.S. & CATTERALL, W.A. (1994). Auxiliary subunits of voltage-gated ion channels. *Neuron* **12**, 1183-94.

ISOM, L.L. (2001). Sodium channel beta subunits: anything but auxiliary. *Neuroscientist* **7**, 42-54.

JENTSCH, T.J. (2000). Neuronal KCNQ potassium channels: physiology and role in disease. *Nat Rev Neurosci* **1**, 21-30.

JURKAT-ROTT, K., MITROVIC, N., HANG, C., KOUZMEKINE, A., IAIZZO, P., HERZOG, J., LERCHE, H., NICOLE, S., VALE-SANTOS, J., CHAUVEAU, D., FONTAINE, B. & LEHMANN-HORN, F. (2000). Voltage-sensor sodium channel mutations cause hypokalemic periodic paralysis type 2 by enhanced inactivation and reduced current. *Proc Natl Acad Sci U S A* **97**, 9549-54.

KAMBOURIS, N.G., HASTINGS, L.A., STEPANOVIC, S., MARBAN, E., TOMASELLI, G.F. & BALSER, J.R. (1998). Mechanistic link between lidocaine block and inactivation probed by outer pore mutations in the rat micro1 skeletal muscle sodium channel. *J Physiol* **512 (Pt 3)**, 693-705.

KEARNEY, J.A., PLUMMER, N.W., SMITH, M.R., KAPUR, J., CUMMINS, T.R., WAXMAN, S.G., GOLDIN, A.L. & MEISLER, M.H. (2001). A gain-of-function mutation in the sodium channel gene Scn2a results in seizures and behavioral abnormalities. *Neuroscience* **102**, 307-17.

KELLENBERGER, S., WEST, J.W., CATTERALL, W.A. & SCHEUER, T. (1997a). Molecular analysis of potential hinge residues in the inactivation gate of brain type IIA Na^+ channels. *J Gen Physiol* **109**, 607-17.

KELLENBERGER, S., WEST, J.W., SCHEUER, T. & CATTERALL, W.A. (1997b). Molecular analysis of the putative inactivation particle in the inactivation gate of brain type IIA Na^+ channels. *J Gen Physiol* **109**, 589-605.

KONTIS, K.J. & GOLDIN, A.L. (1997). Sodium channel inactivation is altered by substitution of voltage sensor positive charges. *J Gen Physiol* **110**, 403-13.

KUBISCH, C., SCHROEDER, B.C., FRIEDRICH, T., LUTJOHANN, B., EL-AMRAOUI, A., MARLIN, S., PETIT, C. & JENTSCH, T.J. (1999). KCNQ4, a novel potassium channel expressed in sensory outer hair cells, is mutated in dominant deafness. *Cell* **96**, 437-46.

KUHN, F.J. & GREEFF, N.G. (1999). Movement of voltage sensor S4 in domain 4 is tightly coupled to sodium channel fast inactivation and gating charge immobilization. *J Gen Physiol* **114**, 167-83.

KUZMENKIN, A., MUNCAN, V., JURKAT-ROTT, K., HANG, C., LERCHE, H., LEHMANN-HORN, F. & MITROVIC, N. (2002). Enhanced inactivation and pH sensitivity of Na(+) channel mutations causing hypokalaemic periodic paralysis type II. *Brain* **125** , 835-43.

LEHMANN-HORN, F. & JURKAT-ROTT, K. (1999). Voltage-gated ion channels and hereditary disease. *Physiol Rev* **79**, 1317-72.

LERCHE, H., MITROVIC, N., DUBOWITZ, V. & LEHMANN-HORN, F. (1996). Paramyotonia congenita: the R1448P Na^+ channel mutation in adult human skeletal muscle. *Ann Neurol* **39**, 599-608.

LERCHE, H., PETER, W., FLEISCHHAUER, R., PIKA-HARTLAUB, U., MALINA, T., MITROVIC, N. & LEHMANN-HORN, F. (1997). Role in fast inactivation of the IV/S4-S5 loop of the human muscle Na^+ channel probed by cysteine mutagenesis. *J Physiol* **505 (Pt 2)**, 345-52.

LERCHE, H., JURKAT-ROTT, K. & LEHMANN-HORN, F. (2001). Ion channels and epilepsy. *Am J Med Genet* **106**, 146-59.

LI, H.L., HADID, D. & RAGSDALE, D.S. (2002). The batrachotoxin receptor on the voltage-gated sodium channel is guarded by the channel activation gate. *Mol Pharmacol* **61**, 905-12.

LINFORD, N.J., CANTRELL, A.R., QU, Y., SCHEUER, T. & CATTERALL, W.A. (1998). Interaction of batrachotoxin with the local anesthetic receptor site in transmembrane segment IVS6 of the voltage-gated sodium channel. *Proc Natl Acad Sci U S A* **95**, 13947-52.

LIPKIND, G.M. & FOZZARD, H.A. (2000). KcsA crystal structure as framework for a molecular model of the Na(+) channel pore. *Biochemistry* **39**, 8161-70.

LIU, Y., JURMAN, M.E. & YELLEN, G. (1996). Dynamic rearrangement of the outer mouth of a K^+ channel during gating. *Neuron* **16**, 859-67.

LOOTS, E. & ISACOFF, E.Y. (1998). Protein rearrangements underlying slow inactivation of the Shaker K^+ channel. *J Gen Physiol* **112**, 377-89.

LOSSIN, C., WANG, D.W., RHODES, T.H., VANOYE, C.G. & GEORGE, A.L. Jr (2002). Molecular basis of an inherited epilepsy. *Neuron* **34**, 877-84.

MACKINNON, R., COHEN, S.L., KUO, A., LEE, A. & CHAIT, B.T. (1998). Structural conservation in prokaryotic and eukaryotic potassium channels. *Science* **280** , 106-9.

MALO, M.S., BLANCHARD, B.J., ANDRESEN, J.M., SRIVASTAVA, K., CHEN, X.N., LI, X., JABS, E.W., KORENBERG, J.R. & INGRAM, V.M. (1994). Localization of a putative human brain sodium channel gene (SCN1A) to chromosome band 2q24. *Cytogenet Cell Genet* **67**, 178-86.

MASUI, Y. (1967). Relative roles of the pituitary, follicle cells, and progesterone in the induction of oocyte maturation in Rana pipiens. *J Exp Zool* **166**, 365-75.

MCPHEE, J.C., RAGSDALE, D.S., SCHEUER, T. & CATTERALL, W.A. (1994). A mutation in segment IVS6 disrupts fast inactivation of sodium channels. *Proc Natl Acad Sci U S A* **91**, 12346-50.

MCPHEE, J.C., RAGSDALE, D.S., SCHEUER, T. & CATTERALL, W.A. (1995). A critical role for

transmembrane segment IVS6 of the sodium channel alpha subunit in fast inactivation. *J Biol Chem* **270**, 12025-34.

MCPHEE, J.C., RAGSDALE, D.S., SCHEUER, T. & CATTERALL, W.A. (1998). A critical role for the S4-S5 intracellular loop in domain IV of the sodium channel alpha-subunit in fast inactivation. *J Biol Chem* **273**, 1121-9.

MEISLER, M.H., KEARNEY, J., OTTMAN, R. & ESCAYG, A. (2001). Identification of epilepsy genes in human and mouse. *Annu Rev Genet* **35**, 567-88.

MINOR, D.L. Jr, MASSELING, S.J., JAN, Y.N. & JAN, L.Y. (1999). Transmembrane structure of an inwardly rectifying potassium channel. *Cell* **96**, 879-91.

MITROVIC, N., LERCHE, H., HEINE, R., FLEISCHHAUER, R., PIKA-HARTLAUB, U., HARTLAUB, U., GEORGE, A.L. Jr & LEHMANN-HORN, F. (1996). Role in fast inactivation of conserved amino acids in the IV/S4-S5 loop of the human muscle Na^+ channel. *Neurosci Lett* **214**, 9-12.

MITROVIC, N., GEORGE, A.L. Jr & HORN, R. (1998). Independent versus coupled inactivation in sodium channels. Role of the domain 2 S4 segment. *J Gen Physiol* **111**, 451-62.

MITROVIC, N., GEORGE, A.L. Jr, RUDEL, R., LEHMANN-HORN, F. & LERCHE, H. (1999). Mutant channels contribute <50% to Na^+ current in paramyotonia congenita muscle. *Brain* **122 (Pt 6)**, 1085-92.

MITROVIC, N., GEORGE, A.L. Jr & HORN, R. (2000). Role of domain 4 in sodium channel slow inactivation. *J Gen Physiol* **115**, 707-18.

MOULARD, B., GUIPPONI, M., CHAIGNE, D., MOUTHON, D., BURESI, C. & MALAFOSSE, A. (1999). Identification of a new locus for generalized epilepsy with febrile seizures plus (GEFS+) on chromosome 2q24-q33. *Am J Hum Genet* **65**, 1396-400.

NEHER, E. & SAKMANN, B. (1976). Single-channel currents recorded from membrane of denervated frog muscle fibres. *Nature* **260**, 799-802.

NUSS, H.B., BALSER, J.R., ORIAS, D.W., LAWRENCE, J.H., TOMASELLI, G.F. & MARBAN, E. (1996). Coupling between fast and slow inactivation revealed by analysis of a point mutation (F1304Q) in mu 1 rat skeletal muscle sodium channels. *J Physiol* **494 (Pt 2)**, 411-29.

NUSS, H.B., KAMBOURIS, N.G., MARBAN, E., TOMASELLI, G.F. & BALSER, J.R. (2000). Isoform-specific lidocaine block of sodium channels explained by differences in gating. *Biophys J* **78**, 200-10.

O'REILLY, J.P., WANG, S.Y. & WANG, G.K. (2000). A point mutation in domain 4-segment 6 of the skeletal muscle sodium channel produces an atypical inactivation state. *Biophys J* **78**, 773-84.

O'REILLY, J.P., WANG, S.Y. & WANG, G.K. (2001). Residue-specific effects on slow inactivation at V787 in D2-S6 of Na(v)1.4 sodium channels. *Biophys J* **81**, 2100-11.

OGATA, N. & TATEBAYASHI, H. (1992). Slow inactivation of tetrodotoxin-insensitive Na^+ channels in neurons of rat dorsal root ganglia. *J Membr Biol* **129**, 71-80.

PATTON, D.E., WEST, J.W., CATTERALL, W.A. & GOLDIN, A.L. (1992). Amino acid residues required for fast Na(+)-channel inactivation: charge neutralizations and deletions in the III-IV linker. *Proc Natl Acad Sci U S A* **89**, 10905-9.

RAGSDALE, D.S., MCPHEE, J.C., SCHEUER, T. & CATTERALL, W.A. (1994). Molecular determinants of state-dependent block of Na^+ channels by local anesthetics. *Science* **265**, 1724-8.

RAGSDALE, D.S., MCPHEE, J.C., SCHEUER, T. & CATTERALL, W.A. (1996). Common molecular determinants of local anesthetic, antiarrhythmic, and anticonvulsant block of voltage-gated Na^+ channels. *Proc Natl Acad Sci U S A* **93**, 9270-5.

RUDEL, R., RICKER, K. & LEHMANN-HORN, F. (1993). Genotype-phenotype correlations in human skeletal muscle sodium channel diseases. *Arch Neurol* **50**, 1241-8.

RUTECKI, P.A., LEBEDA, F.J. & JOHNSTON, D. (1987). 4-Aminopyridine produces epileptiform activity in hippocampus and enhances synaptic excitation and inhibition. *J Neurophysiol* **57**, 1911-24.

RUTECKI, P.A., LEBEDA, F.J. & JOHNSTON, D. (1990). Epileptiform activity in the hippocampus produced by tetraethylammonium. *J Neurophysiol* **64**, 1077-88.

SAMBROOK, J., FRITSCH, E. F. AND MANIATIS, T. (1989) *Molecular Cloning: A Laboratory Manual.* 2nd Edn., Cold Spring Harbor Laboratory Press, Cold Spring Harbor, New York, NY.

SANGUINETTI, M.C. & ZOU, A. (1997). Molecular physiology of cardiac delayed rectifier K^+ channels. *Heart Vessels* **Suppl 12**, 170-2.

SATO, C., UENO, Y., ASAI, K., TAKAHASHI, K., SATO, M., ENGEL, A. & FUJIYOSHI, Y. (2001). The voltage-sensitive sodium channel is a bell-shaped molecule with several cavities. *Nature* **409**, 1047-51.

SCHEFFER, I.E. & BERKOVIC, S.F. (1997). Generalized epilepsy with febrile seizures plus. A genetic disorder with heterogeneous clinical phenotypes. *Brain* **120 (Pt 3)**, 479-90.

SCHMITT, N., SCHWARZ, M., PERETZ, A., ABITBOL, I., ATTALI, B. & PONGS, O. (2000). A recessive C-terminal Jervell and Lange-Nielsen mutation of the KCNQ1 channel impairs subunit assembly. *EMBO J* **19**, 332-40.

SCHROEDER, B.C., KUBISCH, C., STEIN, V. & JENTSCH, T.J. (1998). Moderate loss of function of cyclic-AMP-modulated KCNQ2/KCNQ3 K^+ channels causes epilepsy. *Nature* **396**, 687-90.

SCHWAKE, M., PUSCH, M., KHARKOVETS, T. & JENTSCH, T.J. (2000). Surface expression and single channel properties of KCNQ2/KCNQ3, M-type K^+ channels involved in epilepsy. *J Biol Chem* **275**, 13343-8.

SHEETS, M.F., KYLE, J.W., KALLEN, R.G. & HANCK, D.A. (1999). The Na channel voltage sensor associated with inactivation is localized to the external charged residues of domain IV, S4. *Biophys J* **77**, 747-57.

SINGH, N.A., CHARLIER, C., STAUFFER, D., DUPONT, B.R., LEACH, R.J., MELIS, R., RONEN, G.M., BJERRE, I., QUATTLEBAUM, T., MURPHY, J.V., MCHARG, M.L., GAGNON, D., ROSALES, T.O., PEIFFER, A., ANDERSON, V.E. & LEPPERT, M. (1998). A novel potassium channel gene, KCNQ2, is mutated in an inherited epilepsy of newborns. *Nat Genet* **18**, 25-9.

SINGH, R., SCHEFFER, I.E., CROSSLAND, K. & BERKOVIC, S.F. (1999). Generalized epilepsy with febrile seizures plus: a common childhood- onset genetic epilepsy syndrome. *Ann Neurol* **45**, 75-81.

SMITH, J.S., IANNOTTI, C.A., DARGIS, P., CHRISTIAN, E.P. & AIYAR, J. (2001). Differential expression of kcnq2 splice variants: implications to m current function during neuronal development. *J Neurosci* **21**, 1096-103.

SMITH, M.R. & GOLDIN, A.L. (1997). Interaction between the sodium channel inactivation linker and domain III S4-S5. *Biophys J* **73**, 1885-95.

SPAMPANATO, J., ESCAYG, A., MEISLER, M.H. & GOLDIN, A.L. (2001). Functional effects of two voltage-gated sodium channel mutations that cause generalized epilepsy with febrile seizures plus type 2. *J Neurosci* **21**, 7481-90.

STRUYK, A.F., SCOGGAN, K.A., BULMAN, D.E. & CANNON, S.C. (2000). The human skeletal muscle Na channel mutation R669H associated with hypokalemic periodic paralysis enhances slow inactivation. *J Neurosci* **20**, 8610-7.

STUHMER, W., CONTI, F., SUZUKI, H., WANG, X.D., NODA, M., YAHAGI, N., KUBO, H. & NUMA, S. (1989). Structural parts involved in activation and inactivation of the sodium channel. *Nature* **339**, 597-603.

SWANN, J.W., SMITH, K.L. & BRADY, R.J. (1993). Localized excitatory synaptic interactions mediate the sustained depolarization of electrographic seizures in developing hippocampus. *J Neurosci* **13**, 4680-9.

TAKAHASHI, M.P. & CANNON, S.C. (2001). Mexiletine block of disease-associated mutations in S6 segments of the human skeletal muscle Na(+) channel. *J Physiol* **537**, 701-14.

TANG, L., CHEHAB, N., WIELAND, S.J. & KALLEN, R.G. (1998). Glutamine substitution at alanine1649 in the S4-S5 cytoplasmic loop of domain 4 removes the voltage sensitivity of fast inactivation in the human heart sodium channel. *J Gen Physiol* **111**, 639-52.

TINEL, N., LAURITZEN, I., CHOUABE, C., LAZDUNSKI, M. & BORSOTTO, M. (1998). The KCNQ2 potassium channel: splice variants, functional and developmental expression. Brain localization and comparison with KCNQ3. *FEBS Lett* **438**, 171-6.

TOWNSEND, C. & HORN, R. (1997). Effect of alkali metal cations on slow inactivation of cardiac Na^+ channels. *J Gen Physiol* **110**, 23-33.

VASSILEV, P., SCHEUER, T. & CATTERALL, W.A. (1989). Inhibition of inactivation of single sodium channels by a site-directed antibody. *Proc Natl Acad Sci U S A* **86**, 8147-51.

VASSILEV, P.M., SCHEUER, T. & CATTERALL, W.A. (1988). Identification of an intracellular peptide segment involved in sodium channel inactivation. *Science* **241**, 1658-61.

VEDANTHAM, V. & CANNON, S.C. (2000). Rapid and slow voltage-dependent conformational changes in segment IVS6 of voltage-gated Na(+) channels. *Biophys J* **78**, 2943-58.

VELLUTI, J.C., CAPUTI, A. & MACADAR, O. (1987). Limbic epilepsy induced in the rat by dendrotoxin, a polypeptide isolated from the green mamba (Dendroaspis angusticeps) venom. *Toxicon* **25**, 649-57.

WALLACE, R.H., WANG, D.W., SINGH, R., SCHEFFER, I.E., GEORGE, A.L. Jr, PHILLIPS, H.A., SAAR, K., REIS, A., JOHNSON, E.W., SUTHERLAND, G.R., BERKOVIC, S.F. & MULLEY, J.C. (1998). Febrile seizures and generalized epilepsy associated with a mutation in the Na^{+-}channel beta1 subunit gene SCN1B. *Nat Genet* **19**, 366-70.

WANG, D.W., YAZAWA, K., MAKITA, N., GEORGE, A.L. Jr & BENNETT, P.B. (1997). Pharmacological targeting of long QT mutant sodium channels. *J Clin Invest* **99**, 1714-20.

WANG, D.W., VANDECARR, D., RUBEN, P.C., GEORGE, A.L. Jr & BENNETT, P.B. (1999). Functional consequences of a domain 1/S6 segment sodium channel mutation associated with painful congenital myotonia. *FEBS Lett* **448**, 231-4.

WANG, H.S., PAN, Z., SHI, W., BROWN, B.S., WYMORE, R.S., COHEN, I.S., DIXON, J.E. & MCKINNON, D. (1998). KCNQ2 and KCNQ3 potassium channel subunits: molecular correlates of the M-channel. *Science* **282**, 1890-3.

WANG, J.Z., ROJAS, C.V., ZHOU, J.H., SCHWARTZ, L.S., NICHOLAS, H. & HOFFMAN, E.P. (1992). Sequence and genomic structure of the human adult skeletal muscle sodium

channel alpha subunit gene on 17q. *Biochem Biophys Res Commun* **182**, 794-801.

WANG, Q., LI, Z., SHEN, J. & KEATING, M.T. (1996). Genomic organization of the human SCN5A gene encoding the cardiac sodium channel. *Genomics* **34**, 9-16.

WANG, S.Y. & WANG, G.K. (1997). A mutation in segment I-S6 alters slow inactivation of sodium channels. *Biophys J* **72**, 1633-40.

WANG, S.Y. & WANG, G.K. (1998). Point mutations in segment I-S6 render voltage-gated Na^+ channels resistant to batrachotoxin. *Proc Natl Acad Sci U S A* **95**, 2653-8.

WANG, S.Y. & WANG, G.K. (1999). Batrachotoxin-resistant Na^+ channels derived from point mutations in transmembrane segment D4-S6. *Biophys J* **76**, 3141-9.

WANG, S.Y., NAU, C. & WANG, G.K. (2000). Residues in Na(+) channel D3-S6 segment modulate both batrachotoxin and local anesthetic affinities. *Biophys J* **79**, 1379-87.

WANG, S.Y., BARILE, M. & WANG, G.K. (2001). Disparate role of Na(+) channel D2-S6 residues in batrachotoxin and local anesthetic action. *Mol Pharmacol* **59**, 1100-7.

WEST, J.W., PATTON, D.E., SCHEUER, T., WANG, Y., GOLDIN, A.L. & CATTERALL, W.A. (1992). A cluster of hydrophobic amino acid residues required for fast Na(+)- channel inactivation. *Proc Natl Acad Sci U S A* **89**, 10910-4.

WIGLER, M., PELLICER, A., SILVERSTEIN, S. & AXEL, R. (1978). Biochemical transfer of single-copy eucaryotic genes using total cellular DNA as donor. *Cell* **14**, 725-31.

WOLLNIK, B., SCHROEDER, B.C., KUBISCH, C., ESPERER, H.D., WIEACKER, P. & JENTSCH, T.J. (1997). Pathophysiological mechanisms of dominant and recessive KVLQT1 K^+ channel mutations found in inherited cardiac arrhythmias. *Hum Mol Genet* **6**, 1943-9.

YANG, N., GEORGE, A.L. Jr & HORN, R. (1996). Molecular basis of charge movement in voltage-gated sodium channels. *Neuron* **16**, 113-22.

YANG, N., GEORGE, A.L. Jr & HORN, R. (1997). Probing the outer vestibule of a sodium channel voltage sensor. *Biophys J* **73**, 2260-8.

YANG, W.P., LEVESQUE, P.C., LITTLE, W.A., CONDER, M.L., RAMAKRISHNAN, P., NEUBAUER, M.G. & BLANAR, M.A. (1998). Functional expression of two KvLQT1-related potassium channels responsible for an inherited idiopathic epilepsy. *J Biol Chem* **273**, 19419-23.

ZHOU, M., MORAIS-CABRAL, J.H., MANN, S. & MACKINNON, R. (2001a). Potassium channel receptor site for the inactivation gate and quaternary amine inhibitors. *Nature* **411**, 657-61.

ZHOU, Y., MORAIS-CABRAL, J.H., KAUFMAN, A. & MACKINNON, R. (2001b). Chemistry of ion coordination and hydration revealed by a K^+ channel- Fab complex at 2.0 A resolution. *Nature* **414**, 43-8.